Università degli Studi di Milano

Department of Pharmacological and Biomolecular Sciences

PhD program in

Pharmacological Biomolecular Sciences, Experimental and Clinical

XXXV Cycle

Proprotein convertase subtilisin/kexin type 9, Atherosclerosis and Extracellular Vesicles – experimental and clinical evidence

SSD MED/04

Main supervisor: Prof. Massimiliano Ruscica
Coordinator: Prof. Giuseppe Danilo Norata

PhD student: Maria Francesca Greco
R12575

Academic Year: 2021/2022

INDEX

1. Abbreviations

ACS, acute coronary syndrome

ACTA2, actin alpha-2

AFM, atomic force microscopy

Alix, ALG-2-interacting protein X

ASCVD, atherosclerotic cardiovascular disease

BMI, body mass index

BSA, bovine serum albumin

CCL, C-C Motif Chemokine Ligand

CFSE, 5(6)-carboxyfluorescein diacetate N-succinimidyl ester

CD, cluster of differentiation

CVD, cardiovascular disease

CXCL1, C-X-C motif chemokine ligand 1

DMEM, Dulbecco's Modified Eagle's Medium

dpf, day post fertilization

ECs, endothelial cells

EGF-A, epidermal growth factor repeat A

ELISA, enzyme-linked immunosorbent assay

eNOS, endothelial nitric oxide synthase

ERK, extracellular-regulated kinase

ERS1, oestrogen receptor 1

ESCRT, endosomal sorting complex required for transport

EVs, extracellular vesicles

FBS, foetal bovine serum

FC, flow cytometry

FCCP, carbonyl cyanide p-trifluoromethoxy-phenyldydrazone

glycoPER, glycolytic proton efflux rate

GO, gene ontology

HDL, high density lipoprotein

HOMA-IR, homeostasis model assessment-insulin resistance

hpi, hours post injection

hpf, hours post fertilization

hs-CRP, high-sensitivity C-reactive protein

HSP70, heat-shock 70 kDa proteins

ICAM-1, intercellular adhesion molecule-1

IL-, interleukin-

ILVs, intraluminal vesicles

IRR, incidence rate ratio

ISEV, international society for extracellular vesicles

LBPA, lysobisphosphatidic acid

LC-MSE, label-free mass spectrometry analysis

LDL, low density lipoprotein

LDL-C, low density lipoprotein-cholesterol

LDLR, low density lipoprotein receptor

LOX-1, lectin-like oxidized LDL receptor 1

LRP5, LDL receptor related protein 5

MACE, major adverse cardiovascular events

MISEV, minimal information for studies of extracellular vesicles

mRNA, messenger RNA

miRNA, microRNA

MYH11, smooth muscle cell myosin heavy chain

MVBs, multivesicular bodies

NARC1, neural apoptosis-regulated convertase-1

NO, nitric oxide

NLRP3, NLR family pyrin domain containing 3

NTA, nanoparticle tracking analysis

OCR, oxygen consumption rate

oxLDL, oxidized low density lipoprotein

PBS, Dulbecco's Phosphate Buffered Saline

PCSK9, proprotein convertase subtilisin/kexin type 9

PM, particulate matter

PMA, phorbol 12-myristate 13-acetate

pSTAT, phosphorilated-signal transducer and activator of transcription

QUICKI, quantitative insulin sensitivity check index

RPMI, Gibco Roswell Park Memorial Institute 1640

rRNA, ribosomial RNA

SM22α/tagln, 22-kDa SMC lineage-restricted protein

SOCS3, suppressor of cytokine signaling-3

SRs, scavenger receptors

SR-A1, scavenger receptor-A1

SREBP-1/2, sterol regulatory element binding protein family 1/2

STEMI, ST-elevation myocardial infarction

TC, total cholesterol

TEM, transmission electron microscopy

TG, triglyceride

TLR4, toll-like receptor 4

tRNA, transfer RNA

TNFα, tumour necrosis factor alpha

TSG101, tumour susceptibility gene 101

VCAM-1, vascular cell adhesion molecule-1

VPS4, Vacuolar protein sorting-associated protein 4

VSMCs, vascular smooth muscles cells

VTA1, Vesicle Trafficking 1

2. Abstract italiano

Background: Le vescicole extracellulari (EV) sono particelle costituite da un doppio strato fosfolipidico secrete all'interno dello spazio extracellulare da diversi tipi cellulari. Le EV trasportano proteine, lipidi e acidi nucleici e per questo sono coinvolti nella comunicazione intercellulare, in particolare giocano un ruolo importante nello sviluppo della malattia cardiovascolare aterosclerotica. L'aterosclerosi è una malattia infiammatoria cronica caratterizzata dalla formazione di placche lipidiche nella parete arteriosa. Oltre alle cellule endoteliali, monociti e macrofagi, un altro gruppo di cellule con un ruolo molto importante in tutte le fasi dello sviluppo della placca aterosclerotica è rappresentato dalle cellule muscolari lisce vascolari (VSMC). Nella patofisiologia della malattia cardiovascolare aterosclerotica anche la proproteina convertasi subtilisina/kexina di tipo 9 (PCSK9) gioca un ruolo importante, infatti PCSK9 influenza la differenziazione, la migrazione e la proliferazione delle VSMC. **Obiettivo:** L'obiettivo del mio progetto di dottorato è stato quello di valutare l'effetto di PCSK9 sul contenuto delle EV isolate da un modello *in vitro* di VSMC e di valutare la funzione di queste EV sulle componenti cellulari dell'ateroma quali cellule endoteliali (EA.hy926), monociti (THP-1), macrofagi (derivati da THP-1 e J774), e in un modello *in vivo* di embrione di zebrafish (Danio rerio). Inoltre, l'associazione di PCSK9 e il contenuto delle EV è stato confermato in una coorte di 936 individui. **Metodi:** Le EV sono state isolate dal terreno di coltura delle VSMC sovraesprimenti o non PCSK9 ($VSMC^{PCSK9}$-EV e $VSMC^{WT}$-EV, rispettivamente) tramite ultracentrifugazione e dal sangue di 936 individui sovrappeso/obesi. L'espressione di marcatori specifici di EV (Alix, β1-Integrin, CD9 e CD63) è stata valutata tramite Western Blot e analisi citofluorimetrica; la concentrazione e la dimensione delle EV è stata misurata tramite Nanoparticle Tracking Analysis (NTA) e la morfologia tramite microscopia a trasmissione elettronica (TEM). Per valutarne il contenuto proteico, le EV sono state sottoposte a cromatografia

liquida/spettrometria di massa e per l'analisi dei miRNA è stata usata la combinazione miRNeasy kit e RNeasy Cleanup Kit. L'espressione genica e proteica è stata analizzata tramite qPCR e Western Blot. L'effetto delle EV sulla capacità migratoria di monociti e macrofagi è stata studiata tramite transwell con membrana di policarbonato. L' uptake lipoproteine a bassa densità ossidate (oxLDL) è stata misurata fluorometricamente usando Amplex Red Cholesterol Assay Kit. L'attività mitocondriale è stata valutata tramite Agilent Seahorse XF Cell Mito Stress Test. La migrazione di macrofagi nel sito di iniezione dell'embrione di zebrafish è stato valutato tramite colorazione in immunofluorescenza. **Risultati:** Sia le $VSMC^{WT}$-EV che le $VSMC^{PCSK9}$-EV esprimono le tetraspanine (CD9, CD63), Alix and β1-Integrin. La sovraespressione di PCSK9 nelle VSMC non influenza la concentrazione (625.17±235.23/mL/cell count vs 926.17±815.26/mL/cell count), la dimensione (235.78±29.78 nm vs 233.16±16.3 nm) e la morfologia delle $VSMC^{PCSK9}$-EV comparate alle $VSMC^{WT}$-EV. Le $VSMC^{PCSK9}$-EV trasportano un differente contenuto di proteine (n= 14) e di miRNA (n= 6) comparato alle $VSMC^{WT}$-EV. La Gene Ontology analisi ha rivelato un arricchimento in particolare nelle componenti della matrice extracellulare, i quali sono coinvolti in tutti gli aspetti della patobiologia vascolare. I miRNA trasportati dalle EV isolate dalle VSMC sovraesprimenti PCSK9 hanno come target 54 geni che sono associati sia con l'aterosclerosi che con l'infiammazione. Questo gruppo di EV attiva le cellule endoteliali, incrementando l'espressione di molecole di adesione e di marker pro-infiammatori. Nei monociti THP-1 e nei macrofagi derivati da THP-1, l'esposizione per 24 ore alle $VSMC^{PCSK9}$-EV ha determinato un'aumentata espressione genica del ligando della chemochina 2 (CCL2), e dell'interleuchina (IL)-1α, IL-1β, IL-6, and IL-8. Inoltre, l'esposizione a queste EV aumenta la fosforilazione della proteina trasduttore di segnale e attivatore della trascrizione-3 (STAT3) e diminuisce quella della proteina soppressore della segnalazione delle citochine-3 (SOCS3). Le $VSMC^{PCSK9}$-EV hanno influenzato anche la

capacità migratoria e l'attività mitocondriale di monociti THP-1 così come l'uptake di oxLDL da parte dei macrofagi derivati dalle THP-1. L'ipotesi che le VSMC^{PCSK9}-EV abbiano un fenotipo pro-infiammatorio è stato confermato iniettando le EV in embrioni di zebrafish, in seguito alla quale aumenta l'espressione genica delle citochine IL-1β e IL-8 e la migrazione dei macrofagi nel sito di iniezione. L'assiociazione tra PCSK9 e EV è stata valutata anche in 936 individui sovrappeso/obesi, in cui è stata vista una associazione negativa in particolare con le EV derivate da cellule endoteliali, macrofagi e neutrofili. Inoltre, in questi individui i livelli di PCSK9 risultano associare con miRNA, trasportati da queste EV, che hanno come target i geni del recettore LDL (LDLR), del recettore toll-like 4 (TLR4) e del recettore estrogenico (ER1). **Conclusioni:** La sovraespressione di PCSK9 nelle cellule donatrici (VSMC) influenza il contenuto delle EV favorendo un ambiente pro-infiammatorio nelle cellule accettrici (cellule endoteliali, monociti e macrofagi), evidenza confermata anche negli embrioni di zebrafish. Nell'uomo, il ruolo pro-infiammatorio di PCSK9 è stato confermato dall'associazione con specifici miRNA che regolano TLR4. In conclusione, questi dati supportano l'evidenza che PCSK9 possa giocare un ruolo infiammatorio nel contesto della formazione dell'ateroma.

3. English abstract

Background. Extracellular vesicles (EVs) are membrane-bound vesicles secreted into the extracellular space by several cell types. EVs contain and carry proteins, lipids and nucleic acids. EVs play a significant role in the process of atherosclerotic cardiovascular disease (ASCVD), actively participating in each step of atherosclerosis onset and progression. Atherosclerosis is a chronic inflammatory disease characterized by formation of lipid-laden plaques in the arterial wall. Besides endothelial cells (ECs), monocytes and macrophages, a major cell type present at all stages of atherosclerotic plaque development is represented by vascular smooth muscle cells (VSMCs). In the pathophysiology of ASCVD, proprotein convertase subtilisin/kexin type 9 (PCSK9) appears to play a crucial role, *e.g.*, PCSK9 influences VSMCs differentiation, migration and proliferation. **Aim**. The goals of my PhD project have been three-fold: first, to unveil the impact of PCSK9 on the cargo of EVs derived from human VSMCs; second, to evaluate the impact of these EVs on the component of the atheroma by using *in vitro* models of ECs (EA.hy926), monocytes (THP-1), and macrophages (THP-1-derived macrophages and J774) and an *in vivo* model of Danio rerio; third, to confirm the association of PCSK9 and EVs content in a human cohort of 936 individuals. **Methods**. EVs were isolated, by ultracentrifugation technique, from cell culture media of VSMCs overexpressing or not PCSK9 ($VSMC^{PCSK9}$-EVs and $VSMC^{WT}$-EVs) and from blood of a human cohort of 936 individuals with overweight/obesity. A multistep approach was used to characterize the phenotypic pattern of EVs: 1) The expression of specific markers for EVs was assessed by Western blot (WB) analysis (Alix and β1-Integrin) and by high-resolution flow cytometry (FC) analysis (CD9 and CD63); 2) Number and size of EVs were measured by Nanoparticle Tracking Analysis (NTA); 3) Morphology and size of EVs were evaluated also by transmission electron microscopy (TEM); 4) To characterize the protein cargo, EVs were subjected to liquid chromatography-mass spectrometry

analysis; 5) To characterize miRNA content of EVs, the combination of miRNeasy kit and RNeasy Cleanup Kit to isolate them was used. Gene and protein expressions were assessed by qPCR and WB analyses. The effect of EVs on cell migratory capacity of monocytes and macrophages was evaluated by using a transwell chamber with polycarbonate membrane. The uptake of oxidized low-density lipoprotein (oxLDL) was measured fluorometrically by using the Amplex Red Cholesterol Assay Kit. Mitochondrial activity was measured by the Agilent Seahorse XF Cell Mito Stress Test. Macrophages recruitment at the injection site of zebrafish embryos was evaluated by immunofluorescence staining. **Results**. $VSMC^{WT}$-EVs and $VSMC^{PCSK9}$-EVs express tetraspanins (CD9, CD63), Alix and β1-Integrin. The overexpression of PCSK9 in VSMCs did not affect EVs' concentrations (625.17±235.23/mL/cell count and 926.17±815.26/mL/cell count, respectively), size (235.78±29.78 nm and 233.16±16.3 nm, respectively) and morphology. $VSMC^{PCSK9}$-EVs carried a different cargo of proteins (n= 14) and miRNAs (n= 6) compared to $VSMC^{WT}$-EVs. Gene ontology analysis found an enrichment in extracellular matrix structural constituent that is involved in all aspects of vascular pathobiology. $VSMC^{PCSK9}$-EV-miRNAs targeted 54 genes which were associated with both atherosclerosis and inflammation.

$VSMC^{PCSK9}$-EVs activate ECs, by increasing the expression of adhesion molecules and pro-inflammatory markers. In THP-1 monocytes and macrophages, 24-h exposure to $VSMC^{PCSK9}$-EVs raised the gene expression of C-C Motif Chemokine Ligand 2 (CCL2), interleukin (IL)-1α, IL-1β, IL-6, and IL-8. Furthermore, the exposure to $VSMC^{PCSK9}$-EVs raised the phosphorylation of signal transducer and activator of transcription (STAT)3 and decreased that of suppressor of cytokine signaling-3 (SOCS3). In addition, $VSMC^{PCSK9}$-EVs impacted on migratory capacity and mitochondrial activity of THP-1 cells as well as on the uptake of oxLDL by THP-1-derived macrophages. The hypothesis that $VSMC^{PCSK9}$-EVs

carried a pro-inflammatory phenotype was verified by the EVs injection in zebrafish embryos, which also raised the gene expression of IL-1β and IL-8 and increased the local recruitment of macrophages into the site of injection. When the liaison between PCSK9 and EVs was tested in humans, a negative association was found with EVs derived from endothelium, macrophages and neutrophils. In addition, PCSK9 levels were associated with EV-derived miRNA targeting LDL receptor (LDLR), toll-like receptor (TLR) 4 and oestrogen receptor (ER1). **Conclusions**: The overexpression of PCSK9 in donor cells (at least in VSMCs) impacts on the cargo of EVs favouring a proinflammatory milieu in recipient cells (ECs, monocytes, and macrophages), evidence confirmed in embryos of zebrafish. Pertaining human studies, the pro-inflammatory feature of PCSK9 was confirmed by the association with EVs-derived miRNAs regulating TLR4. Therefore, these data support the evidence that PCSK9 may play a feed-forward inflammatory loop in the context of atheroma formation.

4. Introduction

The field of extracellular vesicles (EVs) is gaining a growing interest owing to their role in cell-to-cell communication in both the healthy state and during pathophysiological stress; they transport proteins, lipids, and nucleic acids. Referred to as ‘‘platelet dust’’ by Wolf in 1967 [1], EVs are now known to play a major role in cell maintenance, tissue repair, blood coagulation, angiogenesis, immune regulation, cellular growth, development, differentiation, migration, and other physiological processes. EVs are associated with the pathophysiology of stroke, Alzheimer’s disease, Parkinson’s disease, cancer, obesity, cardiovascular disease, and rheumatoid arthritis. EVs can be released by all cell types, including endothelial cells (ECs), pericytes, vascular smooth muscle cells (VSMCs), as well as central nervous system parenchymal cells, and are found in biological fluids such as cerebrospinal fluid, plasma, serum, semen, saliva, and urine.

Due to their role in intercellular communication, disease pathogenesis and diagnosis, the investigation of their potential to serve as biomarkers to follow the progression of various pathological states as well as therapeutic vehicle is increased[2].

Pertaining the topic of the present thesis, EVs have been related to all phases of the atherosclerotic process from initiation to unforeseen thrombotic complications. In fact, human atherosclerotic plaques, from initial lesions to advanced stages, contain EVs expressing markers from vascular and blood cells (leukocytes, red blood cells and particularly from white blood cells, supporting the idea of an inflammatory milieu), VSMCs, and ECs). Therefore, it seems plausible that EVs released from most cell types of the cardiovascular system participate in the atherosclerotic process as biomarkers and effectors [3].

4.1. Extracellular vesicles: definition and biogenesis

According to minimal information for studies of extracellular vesicles (MISEV), EVs is an umbrella term for particles naturally released from the cell that are delimited by a lipid bilayer and cannot replicate, namely, they do not contain a functional nucleus. EVs are small membrane vesicles containing cytosol from the secreting cells enclosed in a lipid bilayer. They are secreted from cells of different organisms, including both prokaryotic and eukaryotic cells into the extracellular space [4]. Each cell type, depending on its physiological state, releases extracellular vesicles of different size and subcellular origins and with a particular lipid, protein, and nucleic acid compositions that account for their specific fates and functions. They have been isolated from diverse body fluids, including blood, urine, saliva, breast milk and according to their size and biogenesis they are commonly classified into three major subtypes: exosomes, microvesicles and apoptotic bodies. Exosomes are derived from the endolysosomal pathway and represent the smallest subgroups ranging from 30 to 100 nm; microvesicles are generated by an outward budding from the plasma membrane and range from 200 nm to 1000 nm; apoptotic bodies (1-4μm) are released as blebs of cells undergoing apoptosis. (Fig. 1)

4.1.1 Mechanisms of exosome biogenesis

Different specific machineries are involved in the biogenesis of exosomes and microvesicles. Exosomes are generated as intraluminal vesicles (ILVs) within the lumen of endosomes during their maturation into multivesicular bodies (MVBs) and secreted during the fusion of MVBs with the cell surface. First, lipids and membrane-associated proteins are clustered in membrane microdomains of the limiting membrane of the MVBs. In turn, such microdomains participate in the recruitment of soluble components, such as cytosolic

proteins and RNA species, that are fated for sorting in extracellular vesicles. Both the formation of these clustered microdomains and the additional machineries promote inward membrane budding followed by a fission process at the limiting membrane of the MVB towards the lumen of the MVB with the following formation of small membrane vesicles containing sequestered cytosol [5].

Among the machineries involved in the biogenesis of exosomes, the mechanism driven by the ESCRT (endosomal sorting complex required for transport) represents a driver of membrane shaping and scission. ESCRT has four protein complexes termed ESCRT–0, –I, –II and –III, assembled from ~20 proteins and their cognate proteins VPS4 (Vacuolar protein sorting-associated protein 4), VTA1 (Vesicle Trafficking 1) and Alix (ALG-2-interacting protein X). ESCRT controls the sorting of ubiquitinated proteins into ILVs via recognition of ubiquitin molecule (~8.5 kDa) tagged in the protein's lysine residue/s. Briefly, the ESCRT-0 and ESCRT-I subunits cluster ubiquitylated transmembrane cargoes on microdomains of the limiting membrane of MVBs and through the ESCRT-II subunit recruit the ESCRT-III subcomplexes that is responsible for the budding and the fission of this microdomain. In particular, the ESCRT-III is recruited by Alix to drive vesicle scission. Although, the ESCRT-III subcomplexes are required for the scission of the ILVs into the MVB lumen, cargo clustering and membrane budding can occur by either ESCRT-dependent or ESCRT-independent mechanisms. The formation of EVs can occur also in an ESCRT independent manner, for instance the generation of ceramide determines the formation of membrane subdomains and, as a consequence, the membranes undergo through a spontaneous negative curvature. Notwithstanding, other proteins regulate the sorting of cargoes to EVs, such as the proteins belonging to the tetraspanin family (CD63, CD81 and CD9). In the absence of all the ESCRT complexes, exosome biogenesis depends on lipids such as ceramide, lysobisphosphatidic acid (LBPA) and tetraspanins (CD63, CD9, CD81)

that are crucial for membrane remodeling, budding and protection from hydrolases in the extracellular environment [6].

4.1.2 Mechanisms of microvesicle biogenesis

A similar process is involved in the formation of microvesicles, but in this case the formation of microdomains occurs at the level of the plasma membrane and, after outward membrane budding, the fission process is at the plasma membrane towards the extracellular medium. First there is a molecular rearrangement within the plasma membrane, including changes in lipid components and protein composition: upon nucleation of plasma membrane the interaction between cytoskeletal proteins and the plasma membrane is lost and consequently calcium accumulates inducing disassembly and degradation of cytoskeletal components and the externalization of phospholipid phosphatidylserine. These events determine a membrane asymmetry that favours membrane budding and microvesicle formation [7]. Some molecular machineries that act at the different steps of EV biogenesis are partly common to exosomes and microvesicles. Microvesicles exocytosis relies on calcium- or lipid-mediated mechanisms. Increase in intracellular calcium is followed by plasma membrane and cytoskeletal changes. Calcium-sensitive proteins such as gelsolin and calpain alter microvesicles actin cytoskeleton, leading to their detachment from plasma membrane and initiation of plasma membrane blebbing and vesiculation. Modulation of aminophospholipid translocase, flippase and lipid scramblase functions via elevated calcium signalling, lead to a loss of plasma membrane asymmetry, destabilization of plasma membrane-cytoskeleton contact and exposure of phosphatidylserine [6].

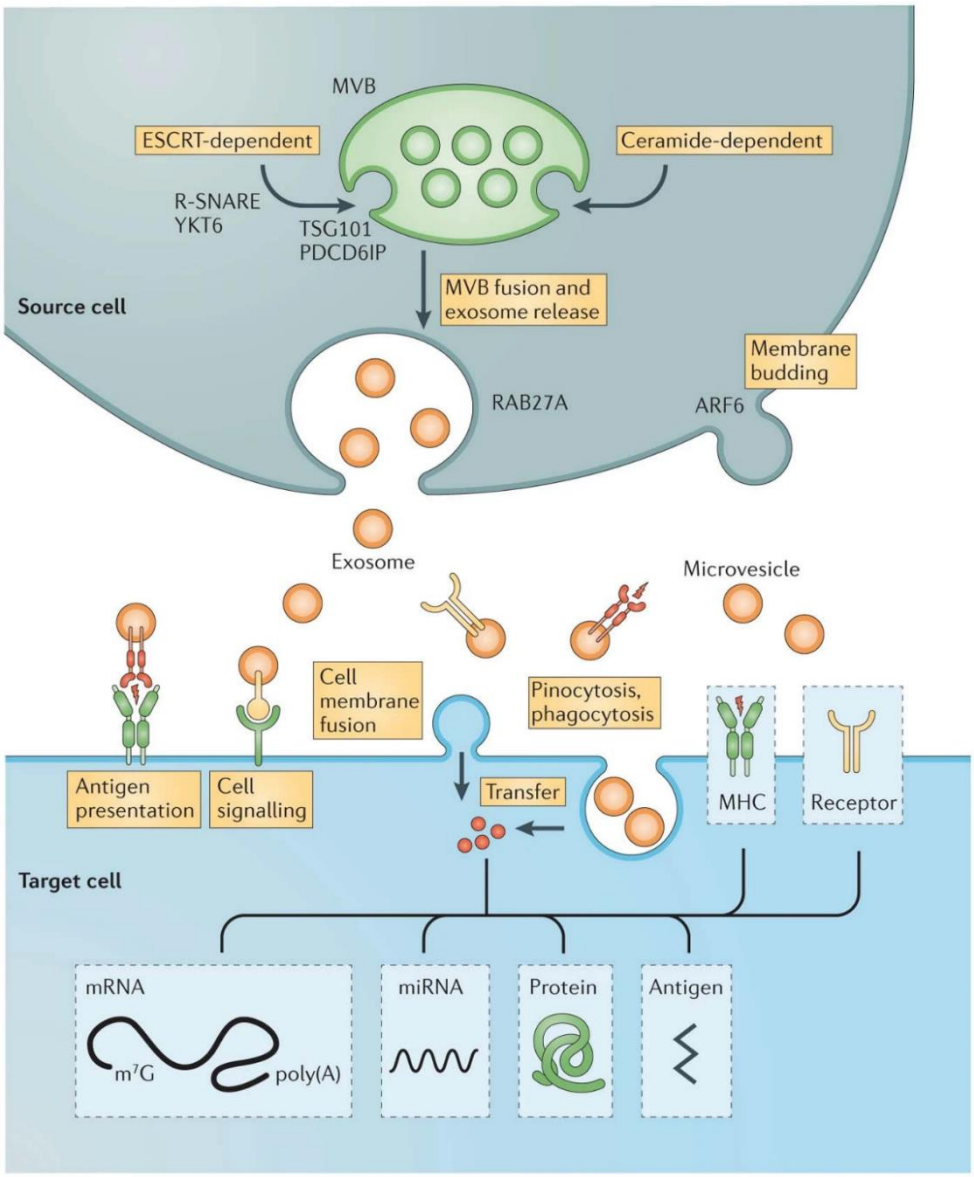

Figure 1. Schematic representation of EVs biogenesis and interaction with target cells. *Exosomes generate by the inward budding of the MVBs that in turn fuse with the cell membrane and this process is regulated by the ESCRT. Other ESCRT-independent mechanism, that contribute to exosome generation, require the lipid ceramide and neutral sphingomyelinase. Whereas microvesicles generate by the outward budding and fission of the cell membrane, that is regulated by membrane lipid microdomains. EVs are involved in cell-to-cell communication. Different mechanisms of interaction between EVs and target cells exist. For instance, they can bind surface receptors present on the target cell or deliver lipids, proteins and nucleic acids to recipient cells. MVB= multivesicular body; ESCRT= endosomal sorting complex required for transport; EVs= extracellular vesicles.* [117].

4.1.3 Mechanisms of EVs secretion and uptake

Microvesicles and exosomes are released into the extracellular space by means of two different pathways: once the microvesicles are generated, they are directly released, separating from the plasma membrane. By contrast, the release of exosomes requires two additional steps: the transport and the fusion of MVBs to the plasma membrane.

Into the extracellular space, EVs reach their recipient cells and bind to the cell surface by both specific interaction among proteins localized on their surface and receptors located on the plasma membrane. EVs can remain at the plasma membrane and exchange proteins or lipids with the recipient cells or they can be internalized by endocytosis and deliver the contents in the cytoplasm of recipient cell. Both direct fusion of EVs with the membrane of recipient cells and vesicle internalization activate different responses and processes that impact on the physiological or pathological status of the target cell.

Clearance of EVs from circulation is caused by organ uptake, as shown in a biodistribution study with red blood cell-derived EVs, in which they have been absorbed by liver (44.9%), bone (22.5%), skin (9.7%), muscle (5.8%), spleen (3.4%), kidney (2.7%) and lung (1.8%). In general, EVs half-life in circulation is very short: when purified exogenous EVs have been introduced into circulation, their clearance is more 90% after 30 min, except for human platelet concentrate-derived EVs that remain in the circulation with a half-life of 5.5 hour.

Currently, there are no specific markers to distinguish among these populations of EVs due to the lack of standardization of both isolation procedures, that usually do not purify specific types of vesicles, and methods for their characterization. Furthermore, some cell types may secrete different EVs depending on their state or the stimuli that activate them. Thus, the term of EVs is referred to both microvesicles and exosomes.

Once EVs are released from the donor cells, they can interact with the target cells by different mechanisms on the basis of the type of recipient cells. Indeed, the uptake of EVs by target cells depends on the type of recipient cells. Although the most common mechanism of the uptake of EVs is phagocytosis, EVs can interact with membrane receptors present on the target cells or their uptake can occur by the direct fusion of EVs with the plasma [8].

In particular, the fusion of membranes occurs at acidic pH conditions and when there is similar fluidity between the 2 fusing membranes, as in the case of EVs and plasma membranes that display the same fluidity at pH 5.0 but not at neutral pH (which makes the membrane more rigid) [8]. EVs can interact with target cells through a ligand-to-receptor interaction. Although differences in the lipid composition of EVs derived from different sources have been already demonstrated, EVs are generally enriched in sphingomyelin, cholesterol, phosphatidylserine and glycosphingolipids compared to their parent cells. Therefore, a functional molecule is delivered by EVs it may be more active than in its soluble form.

4.1.4 EV content

The luminal cargo of EVs mimics their cellular origin; EVs derived from cancer cells, virus-infected cells, stem cells and myocytes carry distinctly different cargo. Interestingly, the same cells can excrete morphologically different EVs with varying nucleic acid, lipid and protein content (Fig. 2). Databases of proteins, lipids and RNAs detected in EVs from different cell sources are found in ExoCarta (www.exocarta.org) [9], in Vesiclepedia (www.microvesicles.org/) [10] and EVpedia (www.evpedia.info) [11]. Therefore, the heterogeneity in composition and function among EVs depends on the cell type and their maturation stage, that can be influenced by other signals and pathological stimuli, which in

turn determines the recruitment of a different sorting machinery. It is worth mentioning that EVs do not synthesize proteins but are rich in cytoskeletal-, cytosolic-, heat shock-, plasma membrane proteins and in those involved in vesicle trafficking. Conversely, intracellular organelle proteins, *e.g.*, those from the nucleus, mitochondria, endoplasmic reticulum, and the Golgi complex, are less abundant or absent. Site of vesicle formation and the pathway involved (ESCRT- dependent or -independent) affect the protein composition of EVs. In addition, EVs also carry soluble mediators, such as cytokines, and RNA, in particular messenger RNA (mRNA) and microRNA (miRNA). RNA loading into EVs is also regulated by specific sorting mechanisms and the incorporation of miRNAs in EVs allows those miRNAs to circulate in the blood while avoiding degradation from blood RNAse activity. Of these different RNA species, miRNAs have attracted the most attention, due to their regulatory roles in gene expression [6].

The molecular composition of exosomes may also be closer to the composition of endosomes than to the composition of the plasma membrane, whereas the opposite may apply for plasma membrane-derived EVs [4]. For example, exosomes contain typically membrane transport and fusion proteins, such as annexins, flotillin, HSP70 (heat-shock 70 kDa proteins), tetraspanins (CD9, CD63, CD81) and protein members in ESCRT complex (Alix and TSG101 (Tumour susceptibility gene 101)) [12]. Microvesicles contain a diverse population of proteins, like matrix metalloproteinases, glycoproteins and integrins [13].

EVs also contain lipid, including cholesterol, eicosanoids, ceramide, sphingomyelin, glycosphingolipid, phosphatidylserine, and other bioactive lipids captured from the cytosol during EV formation or synthesized by EV metabolizing enzymes. and nucleic acids, including mRNA, miRNA, transfer RNA (tRNA) and ribosomal RNA (rRNA) [11].

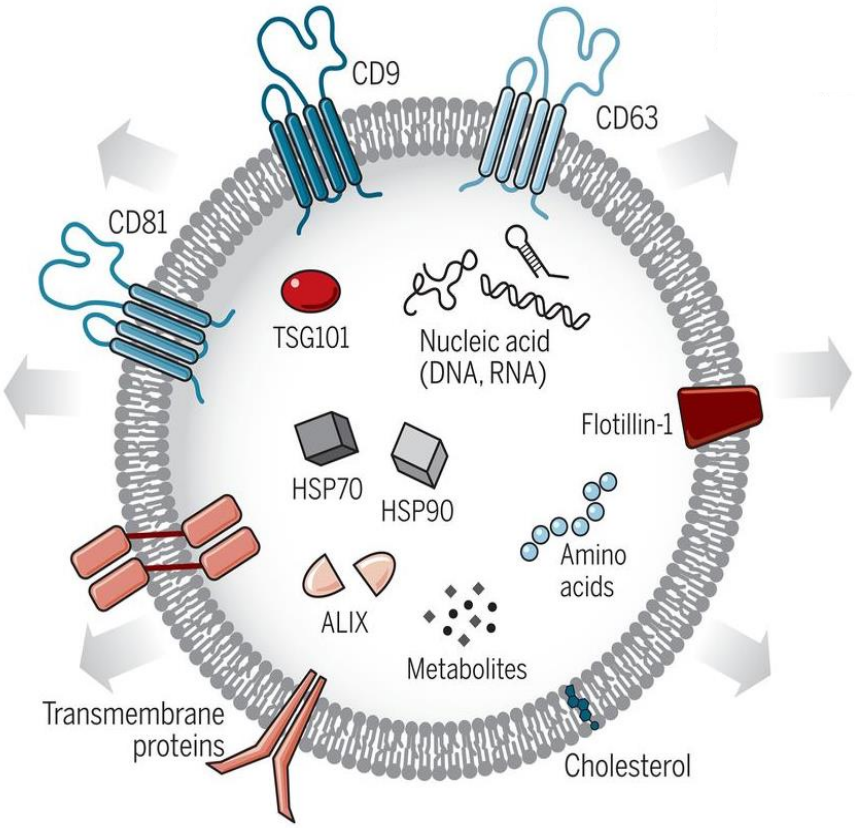

Figure 2: Composition of EVs. *EVs carry various cargoes, including proteins, lipids and nucleic acids. Their composition is different between the cell of origin and the condition. Common proteins found in EVs are Alix, TSG101, HSP70, Integrins and the tetraspanins CD9, CD63, CD81. ALIX= ALG-2 interacting protein; TSG101= tumour susceptibility gene 101 protein; HSP70= heat shock 70 kDa protein; CD= cluster of differentiations* [118].

4.1.5 EV characterization methods

Because of the heterogeneity in EVs, there are no standardized techniques and this represents an important drawback. To overcome these limitations, a guideline called minimal information for studies of extracellular vesicles (MISEV) was created by the International Society for Extracellular Vesicles (ISEV) for EV studies [14]. Indeed, various techniques such as identification of molecular biomarkers or signatures and development of better isolation protocols aid in EV classification and characterization.

Many methods exist to enrich EVs from biological samples, and these include ultracentrifugation, ultrafiltration, immunoprecipitation, microfluidic technologies, and commercially available kits.

Several techniques are available to characterize their size, concentration, and composition, such as flow cytometry (FC), resistive pulse sensing, Nanoparticle Tracking Analysis (NTA), and small-angle x-ray scattering. Optical methods have also been employed to assess the size, concentration, morphology, biochemical composition, and cellular origin of single EVs.

According to the ISEV Guidelines [14], complementary techniques should be used to characterize EVs. Among these techniques, Dynamic Light Scattering, by using a photon detector, calculate the velocity distribution of particle in suspension caused by Brownian motion, then yields the particle size, and density by analysing the fluctuations in scattered light using Stokes–Einstein equation. It does not directly visualize the EVs but evaluates the entire sample, for this reason the analysis of heterogeneous EV populations is limited with this technique; NTA, by using a camera as the detector, can determine the size and concentration of EVs in liquid suspension. This technique can measure EV sizes ranging from 60 to 1000 nm. NTA alone is unable to distinguish EVs from other particles; FC enables detection and characterization of the cytoplasmic or surface proteins, allowing the measurement of relatively large-sized EVs (≥300 nm); Transmission Electron microscopy (TEM) is considered as the gold standard for visualization of single EVs allowing the determination of size and morphology. Atomic force microscopy (AFM) allows topographical imaging at sub-nanometer resolutions and can be used to measure the relative size distribution of EVs; Western blotting (WB) is commonly used to detect the presence of specific proteins. There are no single protein or combination of proteins that is an universal EV marker, but according to MISEV2018 it is recommended that at least one transmembrane

protein (e.g., CD9, CD63, and CD81) and one cytosolic protein (e.g., TSG101, ALIX, and syntenin) is detected for positive identification of EVs in a preparation [2].

4.2 Pathophysiology of atherosclerosis

Atherosclerotic cardiovascular disease (ASCVD) remains a leading cause of vascular disease worldwide. Specifically, atherosclerosis is a coronary artery disease, characterized by accumulation of lipids, inflammatory cells, VSMCs and necrotic cell debris in the intimal space, that can lead to clinical complications such as myocardial infarction and stroke. Risk factors implicated causally in atherogenesis include hypertension, hypercholesterolemia, tobacco use and the components of the metabolic syndrome cluster [15]. The pathogenesis of atherosclerosis occurs in three phases: initiation, progression, and complications (Fig. 3).

4.2.1 LDL modification and retention

The cumulative exposure of an artery to low-density lipoprotein-cholesterol (LDL-C) over years remains a principal determinant of disease initiation and progression. The observation that patients with familial hypercholesterolaemia achieve this cumulative LDL-C burden threshold at early ages and develop premature ASCVD supports a causal role of LDL in atherosclerosis. LDL-C can deposit in the arterial wall owing to impaired barrier function of the endothelium and is retained within the intimal layer by extracellular matrix macromolecules. Once in the sub-intimal space of the vessel, LDL particles undergo modifications becoming aggregated and/or oxidized, resulting in the formation of relatively large lipidic complexes. This retention of lipids favours the endothelial dysfunction, which stimulates leukocyte recruitment to the plaques, also known as lesion sites. Although lipids

undoubtedly contribute causally to atherosclerosis, many studies have demonstrated that in the pathophysiology of atherosclerosis are involved multiple cellular components that are crucial for its development.

4.2.2 Endothelial dysfunction

The initial events of this inflammatory disease consist of endothelial cell dysfunction and subsequent leucocyte recruitment. Endothelial dysfunction has been defined by Hunt and Jurd as an event characterized by the loss of vascular integrity, the increased expression of adhesion molecules and the production of cytokines, a pro-thrombotic phenotype, and the upregulation of human leucocyte antigen molecules [16]. In the presence of damaging stimuli, the endothelium responds by upregulating the transcriptional messenger NF-kB and releasing a series of substances that enhance leukocyte adhesion on the endothelium such as E-selectin, vascular and inter-cellular adhesion molecules (VCAM-1 and ICAM-1), as well as endothelin and angiotensin II, and pro-coagulant factors [17]. Increased permeability and decreased nitric oxide (NO) production are recognised as defining events in endothelial activation and dysfunction within the context of atherogenesis [18]. Endothelial dysfunction has an impact on VSMCs, by impairing NO-dependent vasodilation, and is accompanied by activation of pro-inflammatory pathways. This activation is mainly due to the presence within vascular regions, that are prone to atherosclerotic lesion formation, of pro-inflammatory agonists (*e.g.,* interleukin-1 (IL-1) and tumour necrosis factor (TNF)), oxidized lipoproteins (oxLDL), advanced glycation end products, and biomechanical stimuli like altered blood flow [19]. In addition to expression of adhesion molecules, other endothelial behaviours can contribute to early atherogenesis.

4.2.3 Recruitment of monocytes and macrophage differentiation

Under inflammatory conditions, the increased permeability of the endothelium, due to the increased expression of VCAM-1, ICAM-1, and other pro-inflammatory chemokines, induces the recruitment, and eventual adherence of monocytes and lymphocytes from the blood circulation into the intima. As they enter the subendothelial space, monocytes differentiate into macrophages and engulf modified LDL. Specifically, macrophages can act to either promote inflammation or resolve it during wound and tissue repair. Indeed, macrophages can be classified as M1, contributing to tissue destruction secreting pro-inflammatory factors including high levels of IL-1β, IL-6, and TNF-α, and M2 with anti-inflammatory properties, secreting anti-inflammatory factors such as the IL-1 receptor agonist, IL-10, and collagen. In human lesions both M1 and M2 macrophages are present, although M1 macrophages are predominant [20].

When macrophages take up more lipoprotein-derived cholesterol than they excrete, the intracellular free cholesterol is esterified into cholesteryl ester for storage in lipid droplets and results in the foam cell morphology. In turn, the formation of foam cells induce cytokine (IL-1, IL-6 and TNF-α) and chemokine (C-C Motif Chemokine Ligand (CCL2 and CCL5) and C-X-C motif chemokine ligand 1 (CXCL1)) production and the additional recruitment of others circulating immune cells, triggering the inflammatory response [21]. Moreover, activated macrophages display increased matrix metalloproteinase enzyme production, which degrade the interstitial collagen present within the intima, supporting the fibrous cap. Macrophages that gather in atherosclerotic plaques seem to have a diminished capacity to migrate, which contributes to their inability to resolve inflammation and to the progression of these lesions to more advanced, complex plaques in which other immune cell types (T cells and B cells) and VSMCs further aggravate the inflammatory state of the plaque[21].

Foam cells undergo apoptosis or necrosis determining a necrotic core, consisting of cholesterol esters, cholesterol crystals and cell debris, increasing the risk of lesion rupture [22].

Although macrophages can clear normal LDL via the low-density lipoprotein receptor (LDLR), the expression of this receptor is downregulated during the early stages of foam cell formation due to elevated cholesterol levels [21]. On the contrary, monocyte-derived macrophages begin to express multiple scavenger receptors (SRs), that are macrophage receptor with collagenous structure (MARCO), on their surface with which they can engulf oxLDL at very early stages of atherogenesis. The activation of SRs, particularly CD36, by modified cholesterol engages innate immune responses downstream of the toll-like receptor pathway. Others SRs are scavenger receptor A1 (SR-A1) and lectin-like oxidized LDL receptor 1 (LOX1), all of which enable the accumulation of oxidized LDLs [21]. *Apoe*$^{-/-}$ mice deficient in SR-A or CD36 in all tissues are largely protected from atherosclerosis. Moreover, SR-A and CD36 affect atherosclerosis process beyond their role in promoting lipid uptake. Indeed, SR-A seems implicated in mediating proliferation of lesional macrophages and CD36 in inhibiting migration and in promoting macrophage attachment. Both SR-A and CD36 are involved in promoting apoptosis, lesion necrotic core expansion, and inflammatory gene expression [23].

Furthermore, cholesterol crystals induce the activation of the NLRP3 inflammasome in the cytoplasm of the macrophages in the arterial intima. NLRP3 is a protein complex that cleaves proIL-1β and IL-18 that are then secreted as activated cytokines [24]. IL-1α is secreted in response to SRs activation by modified cholesterol. In the extracellular space, IL-1β, IL-1α and IL-18 interact with their receptors and cause the release of reactive oxygen species, matrix degrading enzymes, activation and proliferation of T-cells and the further production of cytokines.

In advanced lesions, macrophage apoptosis, necrosis, and reduced efferocytosis contribute to expanding necrotic cores, which make the lesion unstable leading to its rupture.

4.2.4 Vascular smooth muscle cells

VSMCs present in the media layer of the artery express markers such as smooth muscle cell myosinheavy chain (MYH11), 22-kDa SMC lineage-restricted protein (SM22α/tagln), ACTA2, smoothelin, and calponin. When exposed to modified cholesterol, cytokines, and growth factors, VSMCs become activated, with a reduced expression of these markers, and acquire proliferative capacity, a migratory capacity, and they secrete various extracellular matrix proteins and cytokines populating the arterial intima. These cells can migrate into the intima from the tunica media, contributing to the accumulation within the developing plaque[15]. Particularly, proliferative VSMCs produce extracellular matrix molecules, such as collagen and elastin, contributing to the thickening of the intimal layer and formation of the fibrous cap, hence stabilizing the plaque [25]. This phenotypic switch was considered a reversible process at the basis of vascular repair. However, the continuous exposure to phenotypic switching-inducing stimuli during atherosclerosis, do not allow VSMCs retain in their contractile status.

Although, the contribution of VSMCs to lesion formation seemed be limited to these steps, to date many studies have demonstrated that VSMCs contribute directly to the inflammatory events within the plaque. In fact, VSMCs can take up modified lipids, acquiring a ‘macrophage-like’ phenotype, expressing macrophage markers on their surface and develop phagocytic activity. This phenotypic switching is considered of fundamental importance to atherosclerosis, because VSMCs assume a phenotype that is proatherogenic [26]. Indeed, up to 50% of the cells in an atherosclerotic plaque that appear to be macrophages may be

derived from an VSMC lineage [27]. In addition, recent studies showed that 40% of foam cells within advanced human coronary artery lesions express both the SMC marker ACTA2 and the macrophage marker CD68 [26]. However, macrophage-like VSMCs are not efficient in phagocytosis and do not express abundant levels of cholesterol export machinery compared with macrophages. Indeed, the gene expression of VSMC-derived macrophage-like cells is significantly different from the one that found in classical monocytes and macrophages. The reduced phagocytosis exerted by VSMC-derived macrophage-like cells may exacerbate inflammation within the atherosclerotic lesion, by not being able to remove accumulated lipoproteins, dying cells and necrotic debris. These cells could be held partially responsible for the formation of the necrotic core of the plaque, due to their impaired clearance of apoptotic macrophages and smooth muscle cells, along with other dying cells [26]. The presence of a high number of intimal VSMCs has been taken as evidence that VSMC migration from the media plays a crucial role in atherosclerosis. In addition, since the stability of the atherosclerotic plaque depends on the thickness of the fibrous cap and the degree of cap inflammation, VSMCs could affect the late state of the disease, contributing to plaque rupture. Indeed, plaque rupture is increased by cap thinning promoted by death of VSMCs and breakdown of collagen and extracellular matrix, which may subsequently lead to myocardial infarction or stroke.

In general, VSMCs in a healthy vessel wall have a low turnover and cell proliferation increases during early atherogenesis and on vascular injury. The migration of VSMCs from the media plays an important role in atherogenesis because of this event is a difficult process to be quantified; there are no specific markers available, and human arteries also contain intimal VSMCs. The balance of cell proliferation and migration versus cell death and cell senescence determines the population of VSMCs within the atherosclerotic plaque and the regulation of these processes is crucial to both atherogenesis and plaque stability [26].

However, it is not still clear whether the migration depends upon contractile-synthetic dedifferentiation and whether the migration of VSMCs occurs before proliferation or the two or processes occur simultaneously [28].

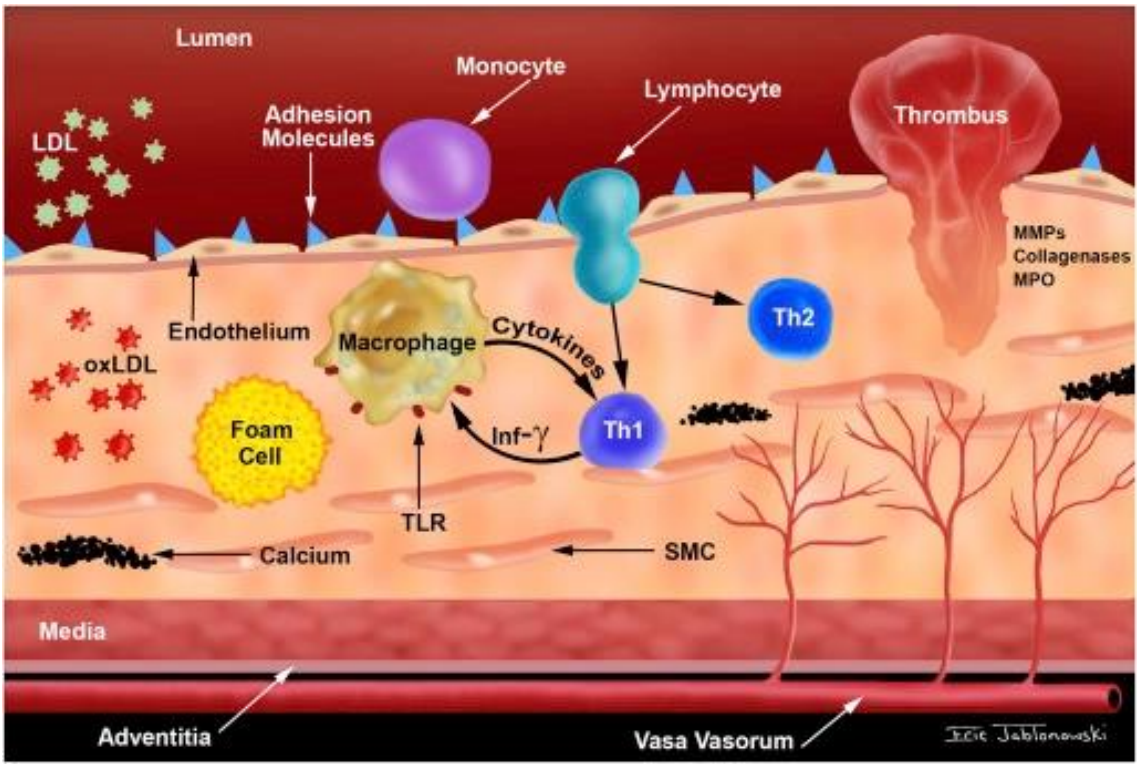

Figure 3. Representation of atherosclerosis initiation and progression. *LDL accumulation and modification (oxLDL) represent a key events in the atherosclerotic plaque formation. In particular, the early phases of atherosclerosis are characterized by endothelial dysfunction that determines a higher expression of adhesion molecules that in turn recruit monocytes into the subendothelial space. Monocytes can differentiate in macrophages that can engulf oxLDL becoming foam cells. VSMCs can also switch from a contractile to a synthetic phenotype, consisting in higher proliferation rate and higher migratory capacity. LDL= low density lipoproteins; oxLDL= oxidized-LDL; VSMCs= vascular smooth muscle cells* [17].

4.2.5 Role of PCSK9 in atherosclerosis development

Despite the main player in atherosclerosis is the retention of modified lipoprotein in the arterial wall, many studies have shown that proprotein convertase subtilisin/kexin type 9 (PCSK9) is directly implicated in plaque development.

PCSK9 was initially discovered as neural apoptosis-regulated convertase-1 (NARC1), an uncharacterized brain subtilase [29] and in 2003 Abifadel et al. found out two gain-of-function mutations in PCSK9 gene that were associated with autosomal dominant hypercholesterolemia [30].

PCSK9 belongs to the proprotein convertase family and its 3D structure is characterized by a signal peptide, a prodomain, a subtilisin-like catalytic domain and a variable C-terminal domain (Fig. 4A). The mature form (60 kDa) is generated in the endoplasmic reticulum after autocatalysis of the precursor of PCSK9 (74 kDa). Differently from the other PCSKs, mature PCSK9 remains associated to its prodomain. Once secreted at the cell surface, the catalytic subunit of PCSK9 binds the epidermal growth factor repeat A domain (EGF-A) of the LDLR. The complex LDLR-PCSK9 undergoes endocytosis and lysosomal degradation into hepatocytes, preventing LDLR recycling to the cell surface and thus increasing LDL-C levels (Fig. 4B). Indeed, PCSK9 is primarily synthesized in the hepatocytes and its gene is regulated by the sterol regulatory element binding protein family (SREBP-1 and SREBP-2), providing evidence that PCSK9 is a cholesterol-regulated gene and its promoter activity is induced by cellular cholesterol depletion [31]. In addition of liver, PCSK9 is also expressed in other tissues such as small intestine, lung, pancreas, kidney, and brain. Emerging evidence has also found that PCSK9 is expressed in ECs, VSMCs and macrophages, supporting the direct role of PCSK9 on vascular homeostasis and atherosclerotic plaque development. PCSK9 may be involved in the development of atherosclerotic plaque through inflammation-mediated process beyond its effect on LDL-C catabolism. Indeed, the expression of PCSK9 in ECs and VSMCs is mainly regulated by pro-inflammatory stimulation such as ox-LDL, TNF-α and IL-1β [32]. Moreover, PCSK9 expression in VSMCs is also regulated by reactive oxygen species and shear stress [31]**.** Interestingly, Liu S. et al. have demonstrated that low-flow state at arterial branch points increased the gene

and protein expression of PCSK9 compared with normal flow [33]. ATHEROREMO-IVUS study [34] showed the correlation between the increased PCSK9 levels with volume of inflammatory plaque and necrotic core tissue in coronary atherosclerosis. Furthermore, PCSK9 levels associate also with inflammatory markers, including pro-inflammatory cytokines (IL-6, IL-1β, TNF) and high-sensitivity C-reactive protein (hs-CRP). *In vivo*, the loss of PCSK9 expression in mouse determines ~3-fold higher LDLR levels in the liver and consequently a reduction in LDL-C levels [35]. Moreover, in a model of PCSK9$^{-/-}$ mouse, neointima formation in atherosclerotic plaques is reduced. On the contrary, PCSK9 overexpression results in increased size of atherosclerotic plaques. In addition of LDLR, other members of the LDLR superfamily such as LRP5 (LDL receptor related protein 5) may also be a target of PCSK9 (Fig. 5).

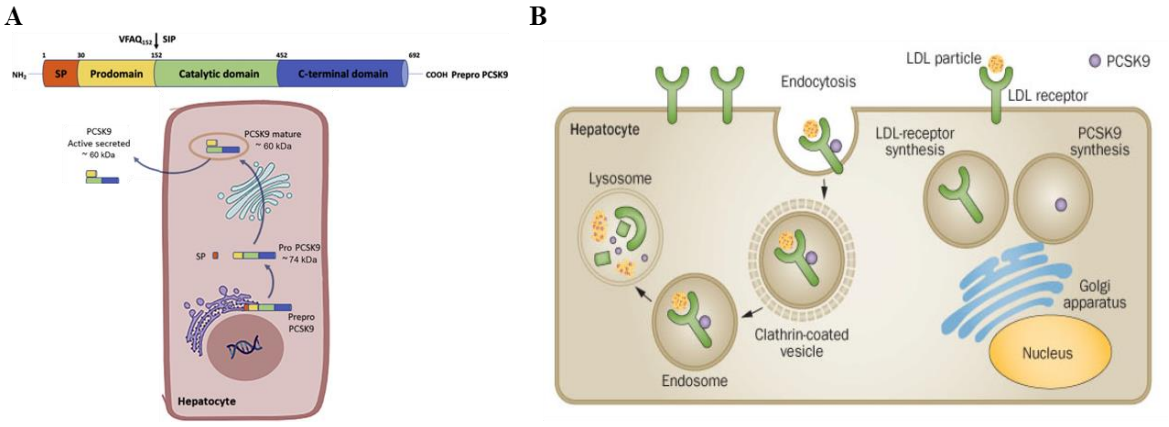

Figure 4. Structure and function of PCSK9. A) *PCSK9, mainly expressed in the liver, consists of a signal peptide, a prodomain, a catalytic domain and a C-terminal domain. The mature form is synthesized in the endoplasmic reticulum after autocatalysis of the precursor.* **B)** *PCSK9 binds LDLR determining its degradation in the lysosome. PCSK9= proprotein convertase subtilisin kexin type 9; LDLR= low density lipoprotein receptor* [119], [120].

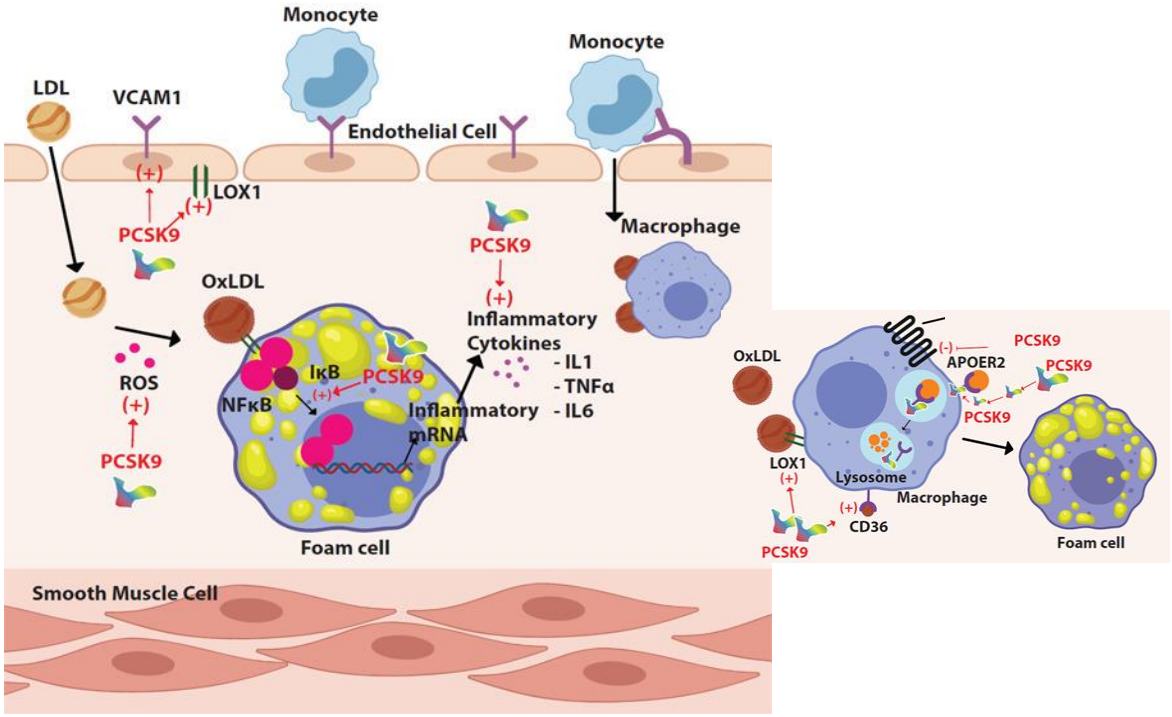

Figure 5. Beyond the role of PCSK9 on LDL metabolism. *PCSK9 can promote inflammation by inducing cell adhesion molecule expression and the release of inflammatory cytokines. PCSK9 can also affect foam cell formation inducing the expression of scavenger such as CD36. CD36= cluster of differentiation 36* [121].

4.3 Extracellular vesicles in cardiovascular biology

EVs, carrying lipids, proteins, and nucleic acids, are involved in both physiological and pathological conditions. In particular, EVs are involved in all phases of atherosclerosis development. Indeed, EVs from ECs, VSMCs, leucocytes, are present in human atherosclerotic plaques.

Under inflammatory stimuli, such as oxLDL, hypertension and visceral adipose tissue, or in patients with CVD, EVs affect the EC function, determining vasorelaxation and disturbing their barrier function. Monocyte-derived EVs contribute to the atherothrombotic event since they express high levels of tissue factor. Specifically, they can stimulate monocytes themselves in producing inflammatory cytokines. They can also stimulate endothelial cells determining high expression of cell adhesion molecules as well as the expression of ICAM-

1, TNF-α, IL-6, thus promoting leucocytes recruitment [36]. Another study showed that in ST-elevation myocardial infarction (STEMI) patients, platelet-derived EVs contributed to endothelial inflammatory phenotype within 48 hours from ischemic events [37].

Furthermore, EVs mediate vascular inflammation, exporting and transferring miRNA to target cells, for instance miRNA-155 and miRNA-92a [38]. During foam cell formation, macrophages release EVs carrying miRNA-146a that decrease the migratory capacity in naïve macrophages that in turn are entrapped in the atherosclerotic plaque [39].

In addition, macrophages into the atherosclerotic lesions affect VSMCs proliferation and migration via EVs. As shown in another study, EVs isolated from macrophages of atherosclerotic patients, compared to those isolated from healthy donors, induce a switching in the phenotype of VSMCs by transferring integrins (receptors for fibronectin) to the cell surface of VSMCs and thus activating the extracellular-regulated kinase (ERK) and Akt pathways [40]. Even EVs derived from ECs has been demonstrated to promote angiogenesis transferring of miR-126-3p and pSTAT into the recipient EC leading to ERK1/2 activation. They can also induce eNOS dysfunction in hearts of hypercholesterolemic mice, inhibiting angiogenesis in the heart [41]. EVs isolated from patients with myocardial infarction have a pro-inflammatory effect because they increase IL-8 secretion in vitro in primary monocytes and THP-1 macrophages [42].

Beyond the direct role in atherosclerotic process, EV can be used for diagnosis and prognosis in cardiovascular disease. Levels of circulating EVs are detectable in plasma of healthy subjects and are elevated in patients with cardiovascular risk factors like hypertension, dyslipidaemia and smoking [37]. Both EV counts and EV content are of potential interest for the use as disease-specific biomarkers for CVDs. The plasma EV content responds to environmental changes and can regulate pro-inflammatory and innate immune responses, coagulation pathways, and atherogenic interactions. For instance, in patients with acute

coronary syndrome or coronary artery disease, levels of EVs that are released, in particular, from leucocytes and ECs are higher [43],[44]. As similar evidence has been noted, in patients with familial hypercholesterolemia carrying subclinical atherosclerotic plaques [45]. EVs can be also used as biomarkers to predict plaque vulnerability and the occurrence of ischemic events [46],[47] In accordance with another study in which Camera et al. showed that microvesicles derived from platelets are predictive of reocclusion in patients with cardiovascular artery disease that undergo elective coronary artery bypass surgery [48]. Therefore, beyond their potential use as a diagnostic tool, EVs can be used to predict major adverse cardiovascular events (MACE).

In obese individuals, it has been shown an association between EVs secreted by monocytes expressing CD14 and atherosclerotic plaque formation. Under inflammatory conditions, the levels of circulating microvesicles and apoptotic bodies are highly elevated. In patients with ASCVD and acute coronary syndrome (ACS), EVs isolated from platelet seem to induce apoptosis of ECs and cardiomyocytes, thus determining vascular and cardiac dysfunction as well as coagulation. Circulating EVs also associate with the Framingham Risk Score (used to predict CVD risk) [49]. The authors demonstrated that EVs carried miRNA-199a and miRNA-126, that were associated with MACE. As mentioned above, EVs associate with both early and late phases of atherosclerosis. For instance, EVs released from ECs, VSMCs, and macrophages are also involved in the calcification process and in thrombus formation [41]

In the clinical setting, EVs can be used as therapeutic delivery of specific drugs, proteins, miRNA, to treat or block ASCVD. Different loading methods have been developed to incorporate a therapeutic agent such as electroporation, sonication and room temperature incubation [50]. Furthermore, EVs have the advantages to be stable in the bloodstream, to

be biodegradable, to have low immunogenicity and to have the ability to cross the biological barriers [51].

5. Aim

EVs have attracted rising interests in the cardiovascular field since they serve as serological markers and they participate in pathophysiological processes including ASCVD [52]. EVs contribute in multifaceted and environment-dependent fashion toward endothelial function and/or dysfunction, endothelial permeability, apoptosis, endothelial-immune cellular crosstalk, pro- and anti-inflammatory signalling, leukocyte transmigration and lipid accumulation, VSMCs proliferation and migration, intravascular calcification, and extracellular matrix remodelling and plaque rupture [53]. In line with this knowledge, epidemiological studies showed that circulating levels of EVs associate with the occurrence of major adverse cardiac events (stroke, angina and myocardial infarction) and are raised in patients with ASCVD risk, such as hypercholesterolemia, hypertension or metabolic syndrome [48], [54].

In the context of the pathophysiology of ASCVD, PCSK9 appears to play a crucial role. PCSK9 is not only the key-player in the regulation of LDL-C but plays pleiotropic effects on atherosclerosis [31]. PCSK9 is expressed in cultured human ECs, in macrophages and mostly in VSMCs. Furthermore, PCSK9 positively influences VSMCs differentiation, migration and proliferation [55].

Overall, the aim of the present three-year project was to evaluate the impact of PCSK9 on the cellular components of the atheroma. Specifically, the cargo of EVs released by human VSMCs overexpressing PCSK9 was characterized and the functionality of these EVs tested in *in vitro* and *in vivo* models.

6. Materials and methods

In vitro studies

6.1 Cell cultures. VSMCs (A617 from human femoral artery) were maintained in Dulbecco's Modified Eagle's Medium (DMEM, Thermo Fisher Scientific, Milan, Italy) High Glucose supplemented by 10% Fetal Bovine Serum (FBS), penicillin/streptomycin solution (10,000 U/mL and 10 mg/mL, respectively), l-glutamine and sodium pyruvate (Merck, Milan, Italy) and maintained in humidified incubators at 37°C and 5% CO_2. Overexpressing human PCSK9 ($VSMCs^{PCSK9}$) were generated by the means of HEK293-Phoenix (φNX-A) cells as previously described [56], using empty pBMN-IRES-puromycin vector or the same vector carrying human PCSK9 coding sequence to generate, respectively, $VSMCs^{PURO}$ ($VSMCs^{WT}$) and $VSMCs^{PCSK9}$. For cell morphology evaluation, VSMCs were seeded in 35x10 mm polystyrene non-pyrogenic Petri dish at a cell density of 0.4M cells/dish in DMEM supplemented with 10% FBS. Cell culture medium was replaced twice, at day 3 and day 5, and the morphology was evaluated on day 7.

THP-1 monocyte cells were cultured in Gibco Roswell Park Memorial Institute 1640 (RPMI, Thermo Fisher Scientific, Milan, Italy) supplemented with 10% FBS and penicillin (10,000 U/mL), streptomycin (10 mg/mL) and β-mercaptoethanol 0.05 mM (Merk, Milan, Italy). THP-1-derived macrophages were obtained by treating THP-1 monocytes with phorbol 12-myristate 13-acetate (PMA; 10 ng/mL, Merk, Milan, Italy) for 72 h. J774 macrophages were cultured in DMEM High glucose supplemented with 10% FBS and penicillin (10,000 U/mL), streptomycin (10 mg/mL), L-glutamine and maintained in humidified incubators at 37 °C and 5% CO2. J774 macrophages were cultured in DMEM High glucose supplemented with 10% FBS and penicillin (10,000 U/mL), streptomycin (10 mg/mL), L-glutamine and maintained in humidified incubators at 37 °C and 5% CO_2. The

EC line EA.hy926 was cultured in DMEM supplemented with penicillin (10,000 U/mL), streptomycin (10 mg/mL), non-essential amino acids, tricine buffer (Merk, Milan, Italy), HAT (Merk, Milan, Italy), HEPES (Euroclone, Milan, Italy) and 10% FBS on gelatin-coated 6-well plates.

6.2 Interaction between EVs and target cells. EVs were labelled using lipophilic dye PKH67 Fluorescent Cell Linker Kit (Merk, Milan, Italy). 1 μL of the PKH67 ethanolic dye solution was added to 250 μL of Diluent C and incubated with the EVs pellet for 5 minutes. The labelling reaction was stopped by adding an equal volume of 1% bovine serum albumin (BSA) (AppliChem, Darmstadt, Germany), which was incubated for 1 minute to allow the binding of excess dye. EVs were ultracentrifuged at 110,000 x g for 2 hours to remove the free dye. The supernatant was discarded, and the EVs pellet was resuspended in 500 μl of Dulbecco's Phosphate Buffered Saline without calcium chloride and magnesium chloride (PBS, Merck, Milan, Italy) triple-filtered through a 0.10 μm pore-size polyethersulfone filter. THP-1 monocytes were seeded at a cell density of $2x10^6$/well in a 6-well plate and exposed to labelled EVs for 24 hours. Cells were then collected and centrifuged to remove unincorporated EVs and fluorescence (λex 490 nm; λem 502 nm) was analyzed by high-resolution flow cytometry (NovoCyte Flow Cytometer, Agilent, Santa Clara, United States).

6.3 Cell treatment with EVs. Relative to treatments with isolated EVs, all cell lines were starved overnight in the appropriate medium (RPMI or DMEM supplemented with BSA 0.1%). After starvation, the cell viability was measured by Dead Cell Apoptosis Kits with Annexin V (Invitrogen, ThermoFisher Scientific).

Media were replaced with fresh medium (RPMI or DMEM + BSA 0.1%), THP-1 monocytes, THP-1-derived macrophages, ECs and J774 macrophages were seeded at a cell density of $2x10^6$/well, $4x10^6$/well and $3x10^6$/well, respectively, in a 6-well plate and treated with $5x10^8$ EVs/mL for 24 hours. After treatment, mRNA and proteins were extracted from all cell lines.

6.4 Extracellular vesicles isolation. According to the most recent MISEV Guidelines [14], to isolate EVs, $VSMCs^{WT}$ and $VSMCs^{PCSK9}$ were grown in flasks 75 cm^2 (Euroclone, Milan, Italy) until 80% of confluence. Then, the cell medium was replaced with 12 mL of serum-free DMEM [57], [58]. The cell viability was measured by Dead Cell Apoptosis Kits with Annexin V (Invitrogen, ThermoFisher Scientific).

After 24 hours, the conditioned medium was collected, cells harvested and counted. The medium was centrifuged at 1000, 2000, and 3000 × g for 15 min at 4 °C, and the pellet from each centrifugation was discarded to remove cells and debris. Supernatant was transferred to 10.4 mL polypropylene ultracentrifuge tubes (Beckman Coulter, CA, USA), and ultracentrifuged at 110,000 × g for 4 hours at 4°C. To minimize the background contribution of interfering particles, three pellets from the same cell line were resuspended in 500 μL of PBS triple-filtered. All ultracentrifugation steps were performed on an Optima MAX-XP ultracentrifuge (Beckman Coulter, California, United States) with a type 55-MLA Rotor (Beckman Coulter).

6.5 Nanoparticle Tracking Analysis (NTA). The number and dimension of EVs were assessed by NTA by using the NanoSight NS300 system (Malvern Panalytical, Malvern, UK), which measures the Brownian motion of particles suspended in fluid and displays them

in real-time through a high sensitivity CCD camera. For NTA analysis, PBS-resuspended EVs were properly diluted in order to reach a number of particles per frame between 20–120 and bringing the final volume at 500 μL using triple-filtered PBS. To carry the sample on syringe pump, a 1 mL insulin syringe was used. The acquisition for each sample was performed at camera level 13 and at infusion rate 30 to have the same constant flow for all samples. Five videos of 30 seconds were recorded for each sample and data were analysed with NTA software (Malvern, Panalytical), which provided high-resolution particle-size distribution profiles as well as measurements of the EVs concentration.

6.6 Transmission electron microscopy (TEM). After isolation, EVs resuspended in PBS and properly diluted, were incubated for 5 min onto carbon-coated copper grids, 200 mesh (Electron Microscopy Sciences, Hatfield, PA, USA) at room temperature. Once adsorbed on the grids, EVs were fixed with 2% glutaraldehyde in PBS (Electron Microscopy Sciences, Hatfield, PA, USA) for 10 min then washed 3 times in Milli-Q water; negative staining was performed with 2% phosphotungstic acid; finally, the grids were air dried and observed using a Microscope Zeiss GEMINI 500.

6.7 Flow cytometry (FC). EVs were characterized by high-resolution FC (MACSQuant, Miltenyi Biotec, Bergisch Gladbach, Germany), according to a previous protocol. Briefly, sample acquisition was performed at the minimum speed flow (25 μl/min) using a MACSQuant Analyzer (Miltemyi Biotec). Sheath fluid was filtered through 0.1 μm pore size filter to further improve the signal-to-noise ratio. The fluorescent beads Fluoresbrite® YG Carboxylate Microspheres Size Range Kit I (0.1, 0.2, 0.5, 0.75, and 1 μm; Polysciences Inc, Warrington, Pennsylvania) were used to set the calibration gate in the FSC/FL1 and

FSC/SSC dot plots. Using a side scatter (SSC) threshold of 10 arbitrary units, the lower sensitivity of the instrument was determined and the SSC and FITC voltages were set up. An overlap in the 100 nm beads population and the background noise were observed. In this way, it was possible to gate the EVs ≥ 200 nm diameter. A total of 30 µL of sample was acquired on the MACSQuant Analyzer. Event numbers, analysed at a low flow rate and below 10,000 events/second of equal sample volumes were counted. To assess the integrity of isolated EVs, 60 µL of sample were stained with 0.2 µM 5(6)-carboxyfluorescein diacetate N-succinimidyl ester (CFSE, Thermo Fisher Scientific) at 37 °C for 20 minutes. The immunophenotyping of EVs was analyzed by means of tetraspanins family antibodies, purchased from Miltenyi Biotec and used according to the product manufacturers: CD9-APC (clone REA1071), CD63-APC (clone REA1055). The CFSE stained samples were incubated with 6 µL of CD9 and CD63 antibodies previously diluted 1:5 for 30 minutes in the dark at 4 °C. Each antibody aliquot was previously centrifuged at 17,000× g for 30 minutes at 4 °C to eliminate aggregates. To detect the autofluorescence of each antibody, 60 µL of triple 0.10 µm pore size membrane-filtered PBS (control sample) were stained with CFSE, CD9 and CD63. Quantitative multiparameter analysis of flow cytometry data was carried out using FlowJo Software (OR, USA).

6.8 qPCR. Total mRNA was extracted by using spin column (Qiagen, Milan, Italy) according to the manufacturer's instructions. Reverse transcription-polymerase first-strand cDNA synthesis was performed by using the Maxima First Strand cDNA synthesis kit (Thermo Fisher Scientific). Quantitative PCR was then performed by using the Thermo SYBR Green/ROX qPCR Master Mix kit (Thermo Fisher Scientific) and specific primers for selected genes. The analyses were performed with the 9600 Bio-Rad Real-Time PCR Detection Systems (Bio-Rad Laboratories). PCR cycling conditions were as follows: 95 °C

for 10 minutes, 40 cycles at 95 °C for 15 seconds, and 55 °C for 1 minute. Data were expressed as Ct values and used for the relative quantification of targets with the $2^{-\Delta\Delta Ct}$ calculation. In the case of ECs, THP-1 and THP-1-derived macrophages, 18S and 36B4 were used, respectively, as housekeeping genes. Primer sequences used for qRT-PCR analysis are shown in Table 1.

Table 1. List of primers sequences used for qRT-PCR analysis.

	Forward(5'-3')	***Reverse(5'-3')***
	Cell culture	
IL-1α	GTAGCAACCAACGGGAAGGT	AAGGTGCTGACCTAGGCTTG
IL-1β	TACCTGTCCTGCGTGTTGAA	TCTTTGGGTAATTTTTGGGATCT
IL-6	ACCCCCAGGAGAAGATTCCA	GGTTGTTTTCTGCCAGTGCC
CCL2	AGCCACCTTCATTCCCCAAG	CTCCTTGGCCACAATGGTCT
IL-8	GAGCACTCCATAAGGCACAAA	ATGGTTCCTTCCGGTGGT
ET-1	AGAGTGTGTCTACTTCTGCCA	CTTCCAAGTCCATACGGAACAA
ICAM-1	CTCCAATGTGCCAGGCTTG	CAGTGGGAAAGTGCCATCCT
VCAM-1	TTCCCTAGAGATCCAGAAATCGAG	CTTGCAGCTTACAGTGACAGAGC
18S	CGGCTACCACATCCAAGGAA	CCTGTATTGTTATTTTTCGTCACTACCT
36B4	CCACGCTGCTGAACATGC	TCGAACACCTGCTGATGAC
	Zebrafish	
Rpl8	CTCCGTCTTCAAAGCCCATGT	TCCTTCACGATCCCCTTGATG
β-actin	GCACGAGAGATCTTCACTCC	GCAGCGATTTCCTCATCCAT
IL-16	TGGACTTCGCAGCACAAAATG	CGTTCACTTCACGCTCTTGGATG
CXCL8	CGACGCATTGGAAAACACAT	TGTCATCAAGGTGGCAATGA

***IL-1α**= Interleukin-1α; **IL-1β**= Interleukin-1β; **IL-6**= Interleukin-6; **CCL2**= C-C motif chemokine ligand 2; **IL-8**= Interleukin-8; **ET-1**= Endothelin 1; **ICAM-1**= Intercellular adhesion molecule 1; **VCAM-1**= Vascular cell adhesion molecule 1; **Rpl8**= 60S ribosomal protein L8; **IL-16**= Interleukin-16; **CXCL8**= C-X-C Motif Chemokine Ligand 8.*

Relative to zebrafish, total RNA was extracted from at least 20 systemically EVs-treated embryos at 20 hours post-injection (hpi) using NucleoZOL reagent (Macherey-Nagel, Düren, Germany) according to the producer's instructions. The concentration and purity of

RNA were measured using NTA. To avoid possible genomic contamination, RNA was treated with RQ1 RNase-free DNase (Promega, Madison, Wisconsin, USA). 1 μg of DNase-treated RNA was reverse-transcribed with GoScript Reverse Transcription Kit (Promega, Madison, Wisconsin USA), using a mixture of random primers and oligo(dT), following the manufacturer's instructions. qPCR analyses were performed with the GoTaq qPCR Master Mix (Promega), in the QuantStudio 5 Real-Time PCR System (Applied Biosystems, ThermoFisher Scientific), following the manufacturer's guidelines. The calculation of gene expression was based on the $2^{-\Delta\Delta Ct}$ method[59]. *rpl8* and β-*actin* were used as the internal reference genes, for normalization purposes. Primers sequences used for qRT-PCR analysis are shown in Table 1.

6.9 Western Blot (WB). Total cytosolic protein extracts of EVs were obtained by resuspending EVs pellet in 50 μL of RIPA buffer (0.05M Tris-HCl pH 7.7, 0.15 M NaCl, 0.8% TritonX-100, 0.8% sodium deoxycholate, and 0.08% SDS, 10 mM EDTA, 100 μM sodium vanadate, 50 mM NaF, 5 mM Iodoacetic acid) containing a cocktail of protease and phosphatase inhibitors (Roche Diagnostics, Switzerland). After 1 hour on ice, EV lysates were centrifuged at 14,000 x g for 10 minutes. Total cytosolic protein extracts of THP-1 and THP-1-derived macrophages were obtained by collecting cells in 70 μL of Mammalian Protein Extraction Reagents (Thermo Fisher Scientific) containing a cocktail of protease and phosphatase inhibitors (Roche Diagnostics). Protein concentration was determined by the Pierce BCA protein assay (Thermo Fisher Scientific) according to the manufacturer's instructions. Twenty micrograms of proteins and a molecular mass marker (Novex Sharp Protein Standard, Invitrogen; Thermo Fisher Scientific) were separated on a 10% SDS-PAGE gel under denaturing and reducing conditions. Proteins were then transferred to a

nitrocellulose membrane at 200 mA for 120 minutes. The membranes were washed with Tris-buffered saline-Tween 20, and nonspecific binding sites were blocked in Tris-buffered saline-Tween 20 containing 5% BSA (Sigma-Aldrich) for 90 minutes at room temperature. The blots were incubated overnight at 4°C with a diluted solution (5% BSA or nonfat dry milk) of the human primary antibodies that are shown in Table 2. Membranes were washed with Tris-buffered saline-Tween 20 and then exposed for 90 minutes at room temperature to a diluted solution (5% nonfat dry milk) of the secondary antibodies (anti-mouse and anti-rabbit peroxidase-conjugated secondary antibodies; New England Biolabs, MA). Immunoreactive bands were detected by exposing the membranes to Clarity Western ECL chemiluminescent substrates (Bio-Rad Laboratories) for 5 minutes, and images were acquired with a ChemiDoc XRS System (Bio-Rad Laboratories). Densitometric readings were evaluated using the ImageLab software version 6.0.1 (Bio-Rad Laboratories).

Table 2. List of primary antibodies used for western blot and immunofluorescence analyses.

Primary antibodies	***Dilution***
Alix (Abcam, Cambridge, UK)	1:1,000
β1-Integrin (Abcam, Cambridge, UK)	1:1,000
β-Actin (Santa Cruz Biotechnology, Santa Cruz, CA)	1:1,000
CD36 (Proteintech, Manchester, UK)	1:2,000
PCSK9 (Genetex, Irvine, CA)	1:1,000
pSTAT3 (Abcam, Cambridge, UK)	1:10,000
SOCS3 (Proteintech, Manchester, UK)	1:1,000
Vinculin (Genetex, Irvine, CA)	1:1,000
LCP1 (Genetex, Irvine, CA)	1:200

CD36*= Cluster of differentiation 36;* ***PCSK9=*** *Proprotein convertase subtilisin/kexin type 9;* ***pSTAT3=*** *phospho-Signal Transducer And Activator Of Transcription 3;* ***SOCS3=*** *Suppressor of Cytokine Signaling 3;* ***LCP1=*** *L-Plastin.*

6.10 Migration assay. Cell migration of THP-1 monocytes and J774 macrophages was assessed by using a 24-transwell support of 5 μm and 8 μm pore size, respectively (Costar, Cambridge, MA). THP-1 and J774 cells were seeded in 6-well plates at a density of $1.2x10^6$ cells/well in RPMI + 0.1% BSA and $3x10^5$ cells/well in DMEM + 0.1% BSA and were treated with $5x10^8$ EVs/mL isolated from both $VSMCs^{WT}$ and $VSMCs^{PCSK9}$ for 24 hours. After 24h, cells were collected, resuspended in fresh medium and seeded in the insert of 24-transwell. The lower chamber was filled with 600 μL of RPMI containing CCL2 at a concentration of 10 ng/mL. Plates were incubated at 37 °C with 5% CO_2 for 10 hours (THP-1) and 24 hours (J774). At the end of the assay, cells migrated in the lower chamber were counted using a microscope.

6.11 Preparation of oxLDL. Chemical oxidation of human LDL (Sigma Aldrich) was performed under sterile condition as previously described [60], by incubating LDL at 37°C for 24 hours, at 0.2 mg protein/mL phosphate buffer saline (PBS) + 20μM $CuSO_4$. Oxidation was blocked in ice, with the addition of 40 μM butylhydroxytoluene (BHT). Modification of lipoproteins was verified by the change in the electrophoretic mobility tested by non-denaturing gel electrophoresis as compared to native LDL [61].

6.11.1 Lipoprotein-induced cholesterol accumulation. Human THP-1 monocytes were grown in RPMI containing 10% FBS (Euroclone, Milano, Italy) in the presence of antibiotics (penicillin–streptomycin, Thermo Fisher Scientific, USA). Cells were plated in the presence of 10 ng/mL PMA (Sigma-Aldrich, Milano, Italy) for 72 h to allow differentiation into macrophages. After overnight starvation in RPMI + 0.1% BSA, cells were incubated for 24 hours with $5x10^8$ EVs/mL isolated from $VSMCs^{PCSK9}$ and from

VSMCs^{WT}. Cells were then incubated for additional 24 hours with RPMI + 1% FBS in the absence or presence of 50 μg/ml of native LDL or oxLDL. At the end of the incubation, cell monolayers were lysed in 1% sodium cholate solution (Sigma-Aldrich) and supplemented with 10 U/mL DNase (Sigma-Aldrich). Cholesterol was then measured fluorometrically using the Amplex Red Cholesterol Assay Kit (Molecular Probes, Eugene, OR, US) following manufacturer's instructions. An aliquot of cell lysates was used to measure cell proteins by the BCA assay (Thermo Fisher Scientific). Intracellular cholesterol content was expressed as micrograms of cholesterol/milligram of protein.

6.12 Mitochondrial bioenergetic evaluation. Mitochondrial activity was measured by the Agilent Seahorse XF Cell Mito Stress Test which measures key parameters of mitochondrial function by directly measuring the oxygen consumption rate (OCR) of cells. OCR was measured at baseline to determine basal respiration and after injection of optimised doses of specific mitochondrial activators and inhibitors to determine non-mitochondrial respiration, maximal respiration and spare respiratory capacity. Briefly, after 24 hour-treatment with EVs, THP-1 cells were plated on a pre-coated Seahorse XF24-well microplate at a density of $4x10^5$ cells/well in 100 μL of Seahorse XF DMEM, supplemented with glucose, pyruvate and glutamine. The plate was centrifuged at 200 x g for 5 minutes and filled to 500 μL with Seahorse XF DMEM. The plate was incubated at 37 °C in a non-CO_2 incubator for 30 minutes. The oxygen consumption rate was measured using the XFe24 analyzer, with 3 baseline measurements recorded before and after adding Oligomycin (ATP synthase inhibitor; 1 μM), carbonyl cyanide p-trifluoromethoxy-phenyldydrazone (FCCP, an uncoupling agent, 1 μM), and a mix of Rotenone and Antimycin A (complex I and III inhibitors, respectively; 0.5 μM).

To further shed light on THP-1 glycolysis, Seahorse XF Glycolytic Rate Assay was used. Rates at basal level as well as after injections of Rotenone plus antimycin A (1 μM) and 2-deoxy-D-glucose (50 mM) were recorded.

6.13 Mass spectrometry analysis. For proteomic analysis, samples were dissolved in 25 mmol/L NH_4HCO_3 containing 0.1% RapiGest (Waters Corporation, Mildford, USA), sonicated, and centrifuged at 13,000 x g for 10 minutes. 50 μg of protein were incubated 15 minutes at 80 °C and reduced with 5 mmol/L DTT at 60 °C for 15 minutes, followed by carbamidomethylation with 10 mmol/L iodoacetamide for 30 minutes at room temperature in the darkness. Then, 2.5 μg of sequencing grade trypsin (Promega) was added to each sample and incubated overnight at 37 °C. After digestion, 2% trifluoroacetic acid (TFA) was added to hydrolyze RapiGest and to inactivate trypsin. Proteomic analysis of secretome samples was performed as described above after desalting, concentration and digestion as previously described [62]. Label-free mass spectrometry analysis (LC-MSE) was performed on a hybrid quadrupole-time of flight mass spectrometer (Synapt XS, Waters corporation, Milford, USA) coupled with a UPLC Mclass system and equipped with a nanosource (Waters Corporation, Milford USA). Samples were injected into a Symmetry C18 nanoACQUITY trap column, 100 Å, 5 μm, 180 μm×2 cm (Waters Corporation, Milford, MA, USA) and subsequently directed to the analytical column HSS T3 C18, 100 Å, 1.7 μm, 75 μm×150 mm (Waters Corporation, Milford, MA, USA), for elution at a flow rate of 300 nL/min by increasing the organic solvent B concentration from 3 to 40 % over 90 minutes, using 0.1%v/v formic acid in water as reversed phase solvent A, and 0.1 %v/v formic acid in acetonitrile as reversed phase solvent B. All of the analyses were made in triplicate and analysed by LC-MSE as previously detailed [61], with the introduction of an ion mobility-enhanced data-independent acquisition (IMS-DIA). The spectral acquisition time in each

mode was 0.5 s, with a 0.1 s inter-scan delay. In the low-energy MS mode, the data were collected at constant collision energy of 6 eV; in high energy mode, fragmentation was obtained by applying drift time-specific collision energies [63]. The software Progenesis QI for proteomics (Version 4.0, http://www.nonlinear.com) was used for the quantitative analysis of peptide features and protein identification, as previously described.

6.14 Gene Ontology (GO) analysis. Proteomics data were analysed with the Search Tool for the Retrieval of Interacting Genes/Proteins (STRING 10.5) database to identify enriched gene ontology (GO) terms in the biological process, molecular function or cellular component categories. In particular, the enrichment function of STRING that calculates an enrichment P-value based on the Hypergeometric test using the method of Benjamini and Hochberg for correction of multiple testing (P value cut-off of <0.05) was used.

6.15 EVs-miRNA Isolation and Analysis. To prepare the EV pellets for miRNA extraction, supernatant was ultracentrifuged (BeckmanCoulter Optima-MAX-XP) at 110,000 x g for 4 hours at 4 °C and decanted. The EV pellet was stored at -80°C until use. Isolation of miRNAs from EVs was performed with the combination of miRNeasy kit and RNeasy Cleanup Kit (Qiagen), according to the manufacturer's protocol. miRNAs were eluted in 20 μL of Nuclease-Free Water and stored at -80 °C, until use. miRNAs reverse transcription (RT) and preamplification reactions, followed by real-time RT-PCR analysis with the QuantStudio™ 12K Flex OpenArray® Platform (Applied Biosystems), were previously described. Gene Expression Suite Software 13 (Applied Biosystems) was used to process miRNA expression data from the "TaqMan™ OpenArray™ Human MicroRNA panel" (ThermoFisher) analysis.

To elucidate the possible role of the EV-miRNAs, we performed a miRNA target analysis using SpidermiR by R software (v 4.0.4). Then, we compared genes obtained by the miRNA target analysis, with genes associated with atherosclerosis and inflammation downloaded from DisGeNET v 7.0. In addition, for each miRNA, we performed an enrichment analysis [64].

In vivo study

6.16 Zebrafish husbandry. Zebrafish (*Danio rerio*) were maintained at the Università degli Studi di Milano according to international (EU Directive 2010/63/EU) and national guidelines (Italian decree No 26 of the 4th of March 2014). Embryonic ages are expressed in hours post fertilization (hpf) and days post fertilization (dpf). Embryos were collected by natural spawning, staged according to Kimmel *et al*. [65] and raised at 28.5°C in fish water (Instant Ocean, 0,1% Methylene Blue) in Petri dishes, according to established techniques. After 24 hpf, to prevent pigmentation 0.003% 1-phenyl-2-thiourea (PTU, Sigma-Aldrich, Saint Louis, MO) was added to the fish water. Embryos were washed, dechorionated and anaesthetized, with 0.016% tricaine (Ethyl 3-aminobenzoate methanesulfonate salt, Sigma-Aldrich) before observations and microinjection.

6.17 Microinjection of zebrafish embryos and immunostaining analysis. Two or 3 dpf embryos were microinjected systemically or locally with $VSMC^{PCSK9}$- or $VSMC^{WT}$-derived EVs suspensions. Before being injected, aliquots of EVs suspension were stained with 0.2μM CFSE. For immune response experiments, 2 nL of a suspension of EVs was systematically microinjected into embryos at 2 dpf [66]. At least 20 embryos were injected

for each treatment, and each experiment was repeated at least twice. For macrophage recruitment experiments, 72 hpf embryos were injected with 2 nL of a suspension of EVs in the hindbrain ventricle and intramuscularly, as previously described [67]. For intra-muscle injection, EVs suspension was delivered among the second and the fifth somite before the yolk extension. Embryos were raised at 28.5°C until their use for analysis.

6.18 Immunostaining analysis of embryos. Evaluation of macrophages recruitment at the injection site was performed by immunofluorescence staining of zebrafish embryos as described in [68] with some modifications. Embryos were fixed at the indicated developmental stage for 2 hours in 4% paraformaldehyde (PFA; Merck) in PBS overnight at 4 °C, then rinsed in PBS and washed in PBS + 1% Tween-20 (PBT). Embryo permeabilization was performed in cold acetone for 25 min at room temperature. Embryos were then blocked for 3 hours at room temperature (RT) in a solution of PBT plus 5% BSA. Subsequently, embryos were incubated with the primary antibody in blocking solution overnight at 4 °C with agitation. Successively, embryos were washed in PBT over 2 hours at RT and then incubated in blocking solution for 2 hours at RT. Embryos were then incubated with the secondary antibody in blocking solution, at 4 °C with agitation. Fluorescent images were sequentially acquired using an epi-fluorescence stereomicroscope (M205FA, Leica, Wetzlar, Germany) mounting TRITC and GFP filters (excitation of 542 and 469 nm). When necessary, images were processed using the Adobe software. Macrophages count/quantification was measured in an indicated dashed line box, by means of ImageJ software (Developer: W. Rasband).

6.19 Statistical analysis. Data are given as means ± standard deviation (SD) of three independent experiments. When possible, p values were determined by t-test or Mann-Whitney. Otherwise, differences between treatment groups were evaluated by one-way analysis of variance. A probability value of $p < 0.05$ was considered statistically significant. Statistical analysis was performed using the Prism statistical analysis package version 8.0 (GraphPad Software, San Diego, CA). Concerning EVs, descriptive statistics were performed on all variables. Linear regressions analyses were applied to evaluate the association between mean EV size produced by $VSMCs^{WT}$ and $VSMCs^{PCSK9}$. EV size showed a skewed distribution and was naturally log-transformed to achieve normal distribution. We reported geometric means with 95% CI. Negative binomial linear regression models were applied to evaluate the association between EV total average number produced by $VSMCs^{WT}$ and $VSMCs^{PCSK9}$. We tested over-dispersion by the likelihood ratio test, and based on its results, we decided to apply the negative binomial models instead of Poisson regression. We reported marginal means with 95% CI and p-values. For each EV size, we estimated EV mean concentration and 95% CI by $VSMC^{PCSK9}$-EVs, with negative binomial linear regression models. Due to the high number of comparisons, we used a multiple comparison method based on Benjamini-Hochberg False Discovery Rate (FDR) to calculate the FDR p-value. To display results of the analyses we used a series graph for EVs mean concentrations of each group and a vertical bar charts to represent FDR p-values and p-values. For the two graphs X axis was the size of EVs. Statistical analyses were performed with SAS 9.4 software (SAS Institute Inc., Cary, NC).

In human studies

6.20 Study design and participants. Nine hundred and thirty-six individuals of the cross-sectional Susceptibility to Particle Health Effects, miRNAs and Exosomes (SPHERE) study were randomly selected [69]. These individuals were recruited at the Center for Obesity and Work-Activity (Fondazione IRCCS Ca' Granda Ospedale Maggiore Policlinico in Milan, Lombardy, Italy). The eligibility criteria of the SPHERE study were: (a) older than 18 years at enrolment; (b) overweight/obese according to body mass index (BMI): overweight, BMI between 25 and 30 kg/m2; obese: BMI of 30 kg/m2 or more; (c) resident in the Lombardy Region at the time of recruitment. Exclusion criteria were: previous diagnosis of cancer, heart diseases, stroke, other chronic diseases, or known diagnosis of diabetes. The study was conformed to the Declaration of Helsinki and each participant provided written informed consent which was approved by the Ethics Committee of Fondazione IRCCS Cà Granda Ospedale Maggiore Policlinico (approval number 1425). Fasting blood drawing was all performed at 9 a.m. in order to avoid circadian variations and processed within 2h. Blood was collected in two EDTA vacutainers (7.5mL) and in one PAX gene (2.5mL). See STROBE statement [70].

6.21 Clinical and laboratory measurements. Body weight and height were determined on a standard scale; BMI and weight-to-height ratio were also calculated. Systolic and diastolic blood pressures (SBP and DBP, respectively) were taken on the left arm using a mercury sphygmomanometer (mean of two measurements taken after 5min of rest). Plasma lipids/lipoproteins and glucose were determined by established methodologies, as carried out in the laboratory of the Institution. hs-CRP and liver function tests (ALT, AST, and GGT), as well as a full haematological profile (red blood cells, haematocrit, and leukocyte

formula), were determined. HbA1c was measured by ion-exchange high-performance liquid chromatography on a VARIANT II Turbo Instrument (Glyco Hb Control, Menarini Diagnostics, Firenze, Italy); insulin by electrochemiluminescence immunoassay (ECLIA) on the Modular P automated analyser (Roche, Basel, Switzerland).

Homeostasis model assessment-insulin resistance (HOMA-IR) was computed as fasting plasma glucose (mg/dl) times fasting serum insulin (mU/L) divided by 405; quantitative insulin sensitivity check index (QUICKI) was given by 1/[Log (Fasting Insulin, μU/mL) + Log (Fasting Glucose, mg/dL)].

6.22 Enzyme-Linked immunosorbent assay. Plasma PCSK9 concentrations were measured by a commercial ELISA kit (R&D Systems, MN). Samples were diluted at 1:20 and incubated onto a microplate pre-coated with a monoclonal human-PCSK9-specific antibody. Sample concentrations were obtained by a four-parameter logistic curve-fit, with a minimum detectable PCSK9 concentration of 0.219 ng/mL.

6.23 EV isolation and characterization. Isolation, purification, and characterization of EVs were performed by following MISEV 2018 Guidelines [14]. Briefly, EDTA-blood was centrifuged 1,200 × g for 15min at RT to obtain platelet-free blood plasma. Plasma was further centrifuged at 1,000, 2,000, and 3,000 × g for 15min at 4◦C, discarding the pellet to clean the cell debris. To prepare EV pellet for Nanosight and FC, 1.5mL of fresh plasma was transferred into an ultracentrifuge tube (Quick-Seal R -Round-Top, Polypropylene, 13.5mL-Beckman Coulter, Inc.) and filled up with PBS, filtered with 0.10μm pore size membrane to minimalize the background contribution of interfering particles. Plasma was then ultracentrifuged at 110,000 x g for 75min at 4◦C, to obtain an extracellular vesicles-

rich pellet. The pellet was re-suspended with 500 μL triple 0.10μm pore size membrane-filtered PBS. To prepare the EV pellet for miRNA extraction, 1.5mL of fresh plasma was transferred into an ultracentrifuge tube (Centrifuge bottles polycarbonate, 10.4 mL-Beckman Coulter) and filled up with PBS. Plasma was then ultracentrifuged (BeckmanCoulter Optima-MAX-XP) at 110,000 x g for 75min at 4◦C, decanted, and the EV pellet was kept at −80◦C until miRNA extraction.

The number and the size of EVs were measured by NTA and cell origin was evaluated by flow cytometry as previously described (Section 2.5 and 2.7). Samples were incubated with the following antibodies: CD14-APC (Clone TÜK4), CD105-APC (clone:43A4E1), CD326 (EpCAM)-APC (clone: HEA-125), CD66b-FITC (clone: TET2), and CD61-APC (clone: Y2/51). All of them were purchased from Miltenyi Biotec.

6.24 EV-miRNA analysis. Isolation of miRNAs from EVs was performed with the combination of miRNeasy kit and RNeasy Cleanup Kit (Qiagen) as previously described (section 5.15).

To elucidate the possible mechanisms connecting EVs-miRNA content and the biological processes related to atherosclerosis a three-step analysis has been performed. First, Disgenet2r R package was used to find genes related to atherosclerosis [71]. Second, a miRNA-target interactions analysis was performed on miRWalk for each miRNA associated with PCSK9. As bona-fide miRNA-target interactions was considered only those predicted by at least 2 algorithms among miRWalk, RNA22, miRanda, and Targetscan (in the version provided by miRWalk 2.0) [72]. Finally, the miRNA-target interactions analysis data were imported on R software and the genes matching with atherosclerosis-related genes were

selected. The gene network and the Venn Diagram were drawn by using R software and GIMP-2.10.

6.25 Statistical analysis. Descriptive statistics were performed on all variables. Continuous data were expressed as the mean ± SD or as the median and interquartile range (Q1–Q3), as appropriate. Categorical data were presented as frequencies and percentages. We applied multivariable negative binomial regression models for over-dispersed count observations to evaluate the relationship between circulating PCSK9 levels and EV count (total count from NTA, $CD66^+$, $CD14^+$, $CD61^+$, $CD105^+$, and $EPCAM^+$). We tested the presence of over-dispersion basing upon the Lagrange Multiplier (LM) test. The regression models were adjusted for age, gender, BMI, smoking habit, use of statin medication, particulate matter (PM)10, and apparent temperature measured the day before the blood draw. In the model with the dependent variable $CD61^+$ EVs, we adjusted also for platelets concentration, in the $CD14^+$ EVs model we adjusted also for monocytes percentage, and in the $CD66^+$ EVs model we corrected also for neutrophils percentage. Estimated effects were described as a percentage of variation associated with an increase of 10 ng/mL in PCSK9 concentration. The percentage of variation was defined as (1-incidence rate ratio (IRR))$*$100. For each EV size, we estimated IRR and 95% CI of total count EV for each 10 ng/mL increment in PCSK9 levels, with negative binomial regression models. Due to the high number of comparisons, we used a multiple comparison method based on Benjamini–Hochberg False Discovery Rate (FDR) to calculate the FDR P-value. To display the results of the analyses we used a series graph for IRR and 95% CI and vertical bar charts to represent FDR p-values and p-values. For the two graphs, X-axis reported the size of EVs (30 to 700 nm). We applied multivariable negative binomial regression models for over-dispersed count observations to evaluate the relationship between circulating PCSK9 levels and EV count. We tested over-

dispersion by the likelihood ratio test, and based on its results, we decided to apply the negative binomial regression model. To examine the potential effect modification of cell percentages and cytokines on EV concentration, we tested the interaction term PCSK9∗cell percentage/cytokine to the multivariable selected model. The reported results are the ones showing a statistically significant interaction: (a) effect of PCSK9 on $CD61^+$ EVs concentration depending on platelets levels; (b) effect of PCSK9 on $CD14^+$ EVs concentration depending on monocyte percentage; (c) effect of PCSK9 on $EPCAM^+$ and $CD105^+$ EVs depending on IL-8 plasmatic concentration. Multivariable linear regression models were applied to verify the association between PCSK9 and miRNA expression. miRNA expression values were log2-transformed to achieve a normal distribution. The regression models were adjusted for age, gender, BMI, smoking habit, use of statin medication, PM10, and apparent temperature measured the day before the blood draw. Due to the high number of comparisons, we applied multiple comparison correction methods based on the Benjamini-Hochberg False Discovery Rate (FDR) to calculate the FDR p-value. A volcano plot of 1% vs. –log10 Pvalues was used to display results. All statistical analyses were performed with SAS software (version 9.4; SAS Institute Inc., Cary, North Carolina, USA). A two-sided p-value of 0.05 was considered statistically significant.

7. Results

In vitro

7.1 Characterization of VSMC overexpressing PCSK9. The first step was to assess whether VSMCs transfected with a vector carrying human PCSK9 efficiently overexpressed PCSK9 compared to cells transfected with a mock plasmid. Since PCSK9 was FLAG-tagged (Asp-Tyr-Lys-Asp-Asp-Asp-Asp-Lys), we detected the presence of this short sequence by WB analysis (Fig. 6).

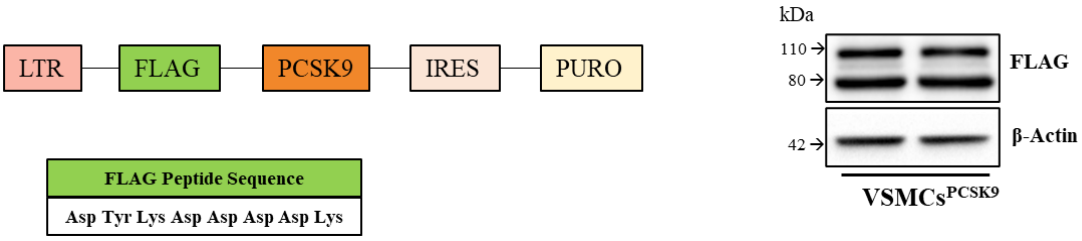

Figure 6. *Protein expression of FLAG was assessed by WB analysis. β-actin was used as a housekeeping protein.*

The overexpression of PCSK9 was demonstrated by gene (Fig.7A), protein expression (Fig. 7B) and ELISA (Fig. 7C), and confirmed, by proteomic analysis change of 1.65 compared to VSMCs^{WT} (Table 3).

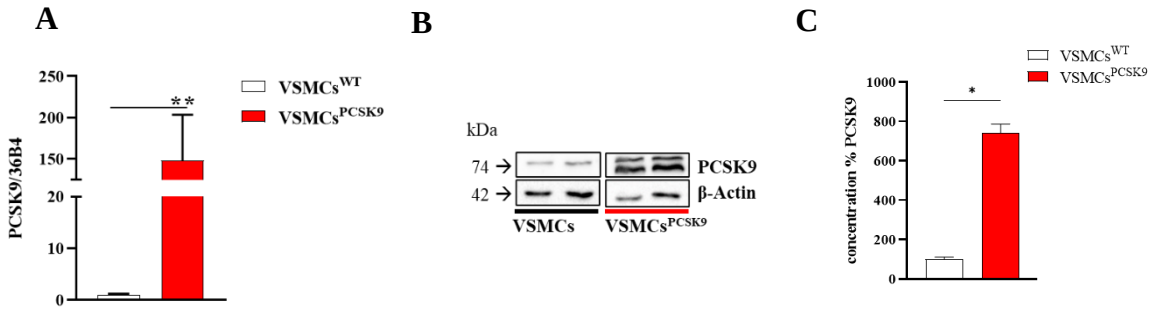

Figure 7. *Gene and protein expression of PCSK9 in VSMCs. 36B4 was used as a reference gene and β-Actin was used as housekeeping proteins. Red bar represents VSMCs^{PCSK9} and white bar represents VSMCs^{WT}. Results are expressed relative to the normal control and represent the means of 3 independent experiments ± SD. Differences between groups have been assessed by t-test. *p<0.05, **p < 0.01 vs control.*

Since our group previously demonstrated that VSMCs freshly isolated from Pcsk9$^{-/-}$ mice have a slower proliferation rate compared to those isolated from their counterpart (Pcsk9$^{+/+}$) [73], we investigated if the overexpression of PCSK9 in human VSMCs could have affected this feature. Cell count analysis showed that the proliferation rate of human VSMCs^{PCSK9} was faster than that of control cells (VSMCs^{WT}) with a stepwise increment at 24-, 48- and 72 hours (Fig. 8A). Based on this evidence, we also tested a possible switch towards a synthetic phenotype. VSMCs^{PCSK9} displayed a more rounded shape, while VSMCs^{WT} exhibited an elongated and spindle-shape phenotype (Fig. 8B). Moreover, the gene expression of smooth muscle markers, such as Acta2 and Calponin, were downregulated in VSMCs^{PCSK9}, further highlighting the switch from a contractile to a synthetic phenotype (Fig. 8C).

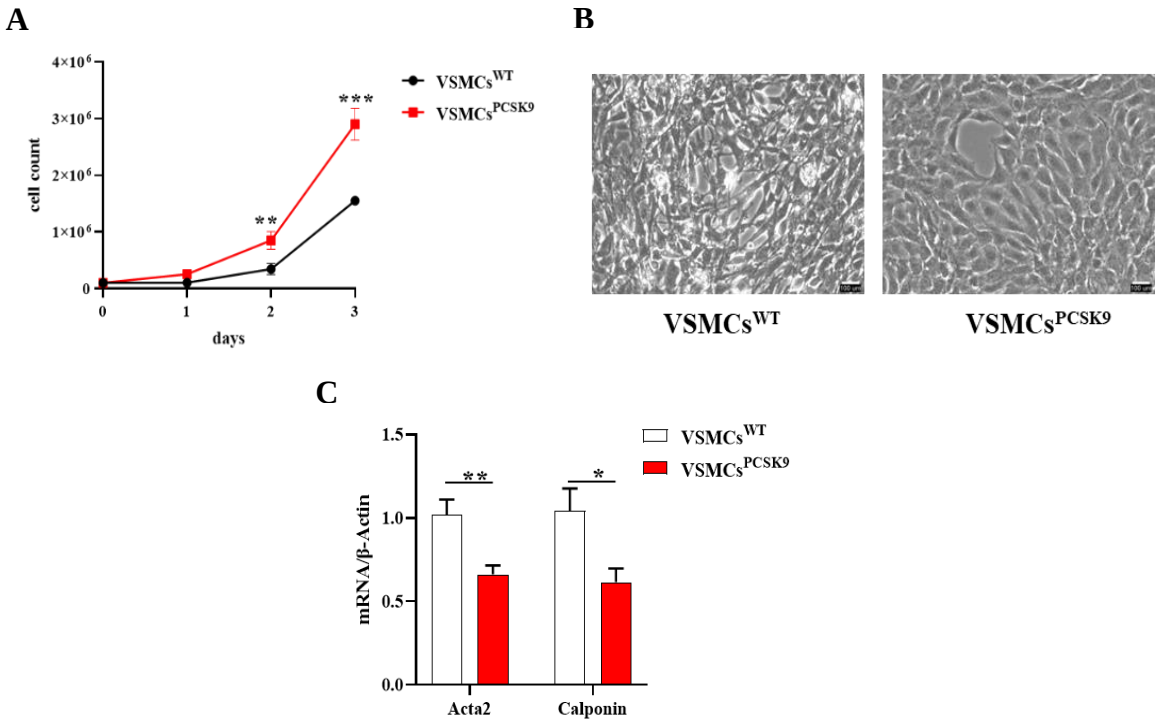

Figure 8. (A) *Proliferative assay of VSMCs (cell counting).* **(B)** *Morphology of VSMCs.* **(C)** *Gene expression of VSMCs markers Acta2 and Calponin. β-Actin was used as a reference gene. Red bar represents VSMCs^{PCSK9} and white bar represents VSMCs^{WT}. Results are expressed relative to the normal control and represent the means of 3 independent experiments ± SD. Differences between groups have been assessed by t-test. *p < 0.05, **p < 0.01, ***p < 0.001 vs control.*

These findings were further corroborated by GO enrichment analysis conducted on the 33 proteins which were highly expressed in VSMCs^{PCSK9} compared to VSMCs^{WT} (Table 3). A significant enrichment (FDR < 0.05) was found in the categories pertaining cell differentiation and regulation of cell morphogenesis involved in differentiation (Fig. 9).

Table 3. List of proteins significantly more abundant in VSMCs^{PCSK9}

Accession	*Description*	*Peptide count*	*Unique peptides*	*Confidence score*	*p value*	*Max fold change*
P20592; P20591	Interferon-induced GTP-binding protein Mx2	2	2	10.9191	2.88E-05	3.57
P13807	Glycogen [starch] synthase_ muscle	4	4	23.7127	1.83E-13	2.95
P68036; A0A1B0GUS4	Ubiquitin-conjugating enzyme E2 L3	5	5	53.6754	1.97E-13	2.72
Q02750; P36507	Dual specificity mitogen-activated protein kinase kinase 1	6	2	36.9708	4.70E-07	2.64
P17302	Gap junction alpha-1 protein	2	2	13.0282	9.33E-08	2.36
P04075; P05062	Fructose-bisphosphate aldolase A	15	7	154.9503	1.12E-13	2.19
Q13228	Methanethiol oxidase	3	3	17.1796	3.04E-08	2.07
Q96HE7	ERO1-like protein alpha	6	3	37.1017	1.39E-10	2.03
P00338	L-lactate dehydrogenase A chain	17	10	149.7567	2.92E-12	2.01
P00558	Phosphoglycerate kinase 1	17	11	169.714	3.76E-11	1.87
P30044	Peroxiredoxin-5_ mitochondrial	4	4	39.6043	2.53E-08	1.84
Q9Y6B6	GTP-binding protein SAR1b	4	2	34.8882	0.000135	1.81
O00499	Myc box-dependent-interacting protein 1	4	3	20.6274	1.42E-09	1.75
Q9BVA1	Tubulin beta-2B chain	20	3	179.1295	0.001302	1.74
Q12797	Aspartyl/asparaginyl beta-hydroxylase	4	3	19.8442	2.91E-11	1.71
Q10471	Polypeptide N-acetylgalactosaminyltransferase 2	5	2	27.7374	6.82E-08	1.69
Q12840	Kinesin heavy chain isoform 5A	14	4	86.3094	4.71E-07	1.66
Q8NBP7	**Proprotein convertase subtilisin/kexin type 9**	6	5	39.041	2.34E-06	**1.65**
P43490	Nicotinamide phosphoribosyltransferase	7	4	40.7607	1.29E-08	1.64

P23381	Tryptophan--tRNA ligase_ cytoplasmic	5	4	33.1145	3.90E-10	1.64
P48059	LIM and senescent cell antigen-like-containing domain protein 1	2	2	11.0741	4.80E-05	1.63
Q15050	Ribosome biogenesis regulatory protein homolog	2	2	11.5261	2.63E-06	1.61
O95379	Tumor necrosis factor alpha-induced protein 8	2	2	11.9457	0.000177	1.60
P07948	Tyrosine-protein kinase Lyn	3	2	19.5759	7.27E-09	1.58
P31150	Rab GDP dissociation inhibitor alpha	12	4	99.4649	1.58E-07	1.57
P14854	Cytochrome c oxidase subunit 6B1	3	3	17.7228	1.91E-13	1.56
Q06330	Recombining binding protein suppressor of hairless	5	4	27.0163	1.45E-08	1.56
P60174	Triosephosphate isomerase	12	7	99.9492	2.06E-08	1.55
Q9HC10	Otoferlin	4	2	20.1364	3.29E-08	1.54
P68366	Tubulin alpha-4A chain	18	2	187.6321	3.90E-08	1.53
P46108	Adapter molecule crk	4	4	25.5171	3.67E-06	1.53
P58546	Myotrophin	3	2	18.9137	4.77E-05	1.52
Q9BQE3	Tubulin alpha-1C chain	22	2	232.7934	5.32E-07	1.50

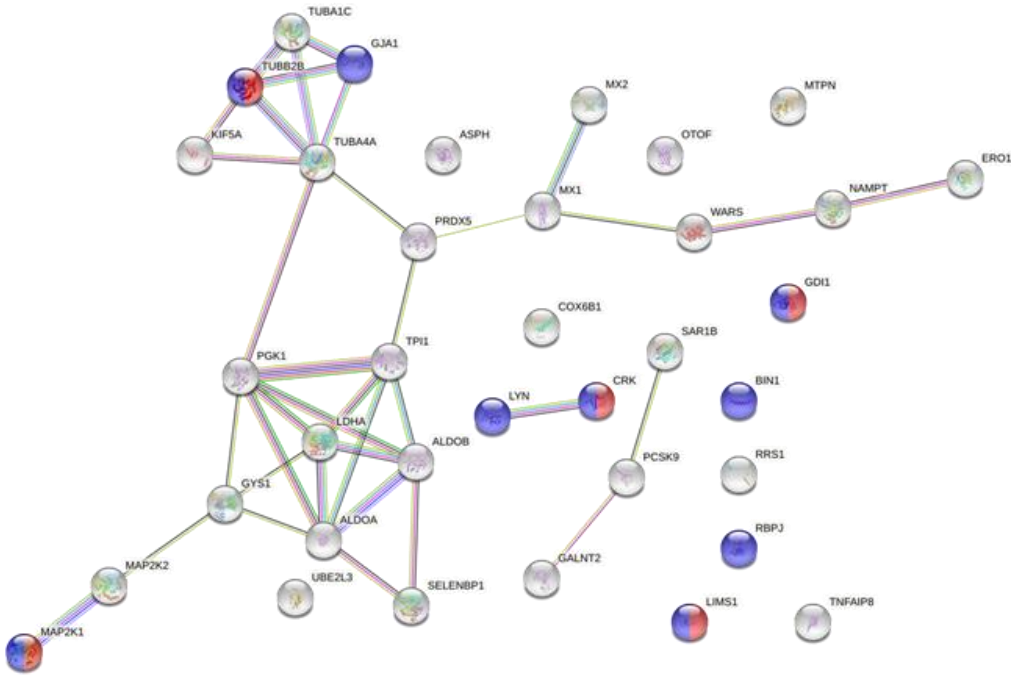

Figure 9. *Gene ontology enrichment analysis relative to proteins with a significant higher expression in VSMCs*^{PCSK9}.

7.2 Phenotypic characterization of EVs. EVs were harvested from VSMCs cultured in medium without serum. Since EVs change their cargo according to the physiological state of the donor cell, to avoid collecting also apoptotic bodies (that fall within the same size and density of EVs), we evaluated the cell viability of donor cells by FITC annexin V and propidium iodide staining. Any significant difference in the percentage of live cells between those cultured for 24 hours in 10% FBS or 0.1% BSA was found (Fig. 10).

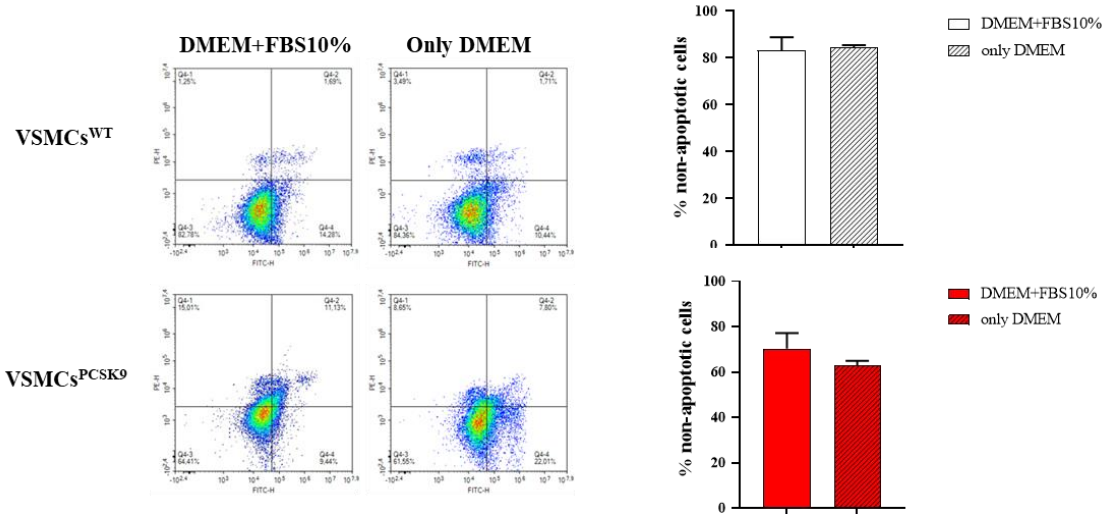

Figure 10. *Cell viability of VSMCs supplemented or not with FBS was assessed by Annexin V/propidium iodide double staining.*

We have conducted a time-point experiment to assess when the highest release of EVs occurs. By means of a time-course experiment, we set 24 hours as the best time point to collect the highest amount of EVs. After 48 hours the concentration was decreased (Fig. 11).

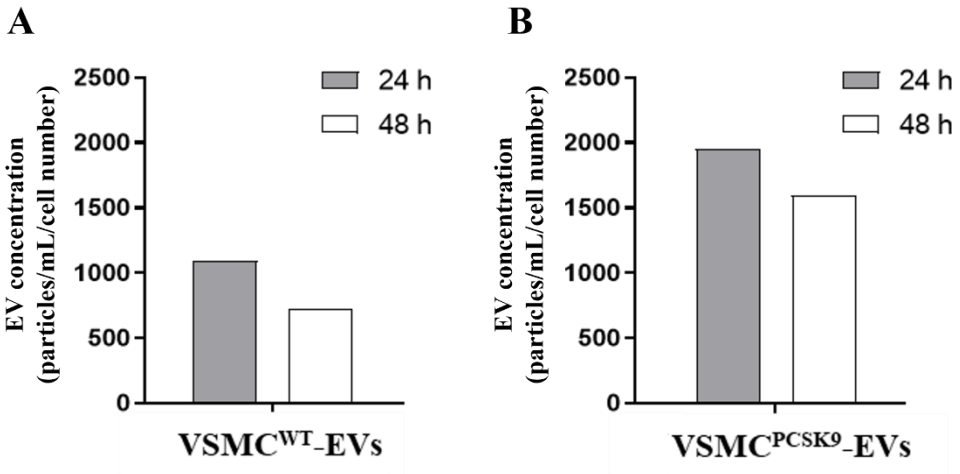

Figure 11. *Time course experiment to assess optimal conditions for EVs isolation. VSMCs were maintained in DMEM. EVs were isolated from the conditioned medium of VSMC^{WT}-EVs **(A)** and VSMC^{PCSK9}-EVs **(B)** after 24 and 48 hours and then the concentration was assessed by NTA.*

In particular, we evaluated whether the overexpression of PCSK9 in the donor cells (VSMCs) could have affected EVs concentration, size, and shape. NTA analysis showed that there were no differences in the concentration and size between EVs released by VSMCs^{PCSK9} (from now on VSMC^{PCSK9}-EVs) and those released from VSMCs^{WT} (from now on VSMC^{WT}-EVs). After normalization for cell count, mean concentrations were 926.17±815.26/ml/cell count and 625.17±235.23/ml/cell count, respectively, whereas mean sizes were 233.16±16.3 nm and 235.78±29.78 nm, respectively. We further analysed the effect of the overexpression of PCSK9 in terms of distribution of vesicle concentrations for each EV size. In Figure 12 A, the mean concentration for all EV sizes (*i.e.*, from 30 to 700 nm) is depicted. The comparisons among the EV sizes are shown in Figure 12B, where the two p-values obtained, comparing VSMC^{WT}-EVs vs VSMC^{PCSK9}-EVs (negative binomial linear regression models at each size), showed no significant differences.

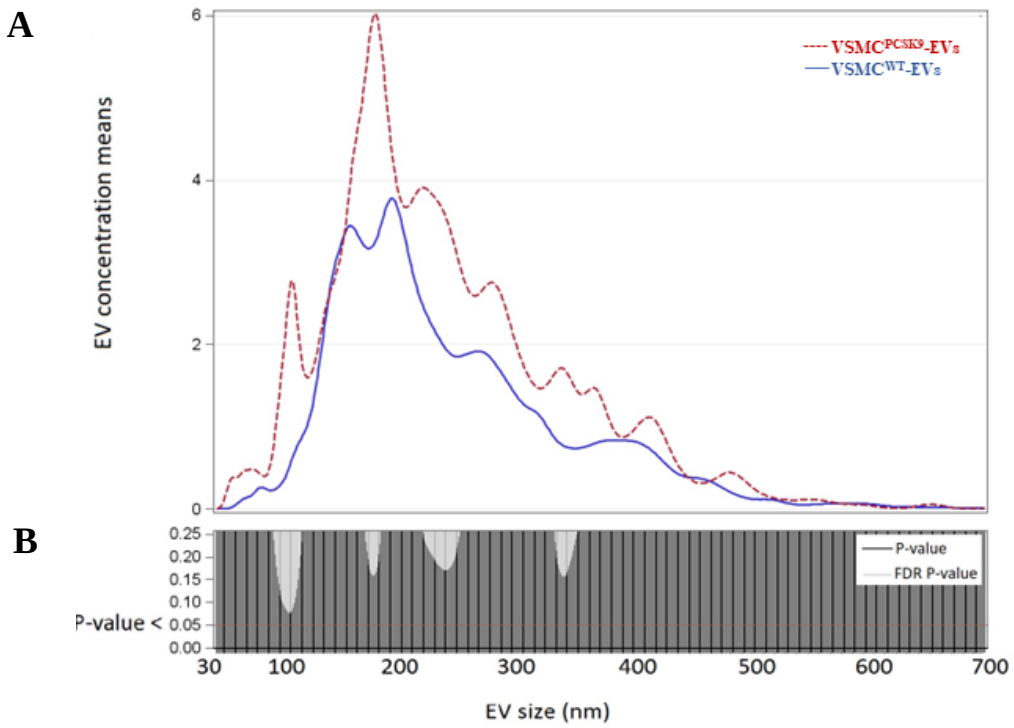

Figure 12. (A) *EV concentrations are expressed as means for each size for the VSMC^{PCSK9}-EVs (dashed line) and VSMC^{WT}-EVs (solid line). EV concentrations were calculated as marginal means from negative binomial regression models.* **(B)** *p-value and False Discovery Rate p-value of the comparisons of each size EV for the entire 30-700 nm size range are reported.*

No differences were found also in the case of their shape as assessed by ultrastructural morphology (Fig. 13). TEM analysis showed the presence of typical rounded, whole and undamaged large EVs and small EVs in both cell lines. The EVs integrity was confirmed by the presence of an unbroken bilayer membrane, visible as a thin white filament surrounding the electron-dense EV content.

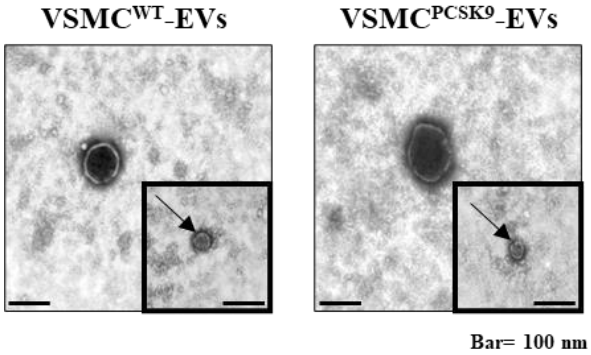

Figure 13. *Representative ultrastructural images of EVs by TEM. Scale bar= 100 nm.*

We evaluated the presence of specific biomarkers for exosomes and microvesicles and both VSMC^{WT}-EVs vs VSMC^{PCSK9}-EVs were positive for CD9 and CD63 tetraspanins as well as for β1-integrin and Alix (Fig. 14).

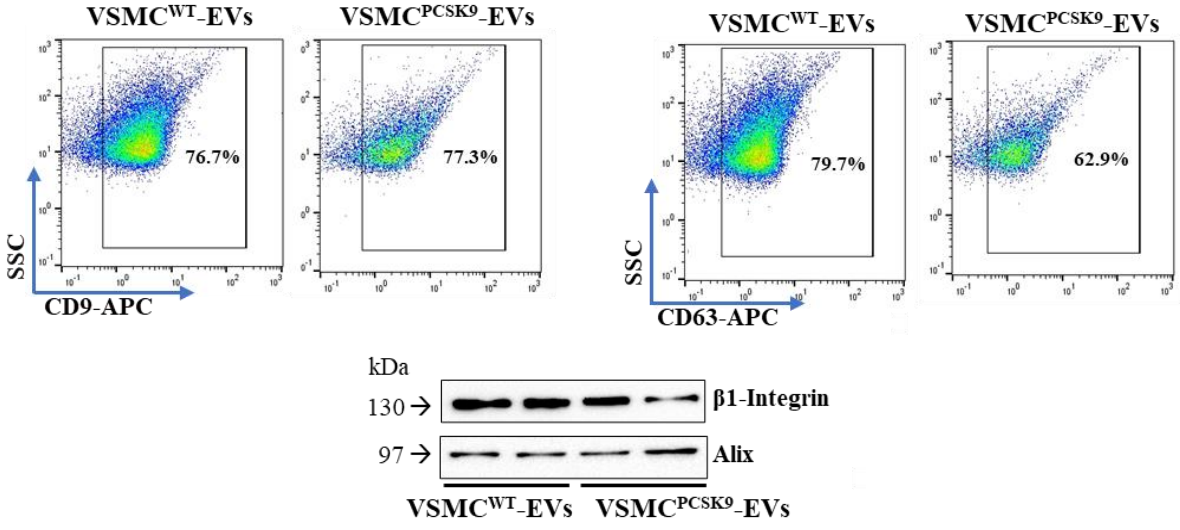

Figure 14. *Evaluation of CD9 and CD63 tetraspanins expression by flow cytometry analysis and protein expression of β1-Integrin and Alix by WB in EVs.*

In addition, immunoblotting analysis showed that VSMC^{PCSK9}-EVs carried a higher amount of PCSK9 compared to VSMC^{WT}-EVs (Fig. 15). Further, untargeted proteomic analysis identified 14 proteins significantly more abundant in VSMC^{PCSK9}-EVs (Table 4).

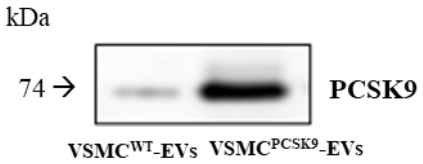

Figure 15. *PCSK9 expression in VSMC^{PCSK9}-EVs and VSMC^{WT}-EVs through WB analysis.*

Table 4. List of proteins significantly more abundant in VSMC^{PCSK9}-EVs

Accession	*Description*	*Peptide count*	*Unique peptides*	*Confidence score*	*p value*	*Max fold change*
Q8NBP7	*Proprotein convertase subtilisin/kexin type 9*	12	12	105.04	8.05E-05	7.10
O95967	*EGF-containing fibulin-like extracellular matrix protein 2*	7	7	64.03	2.27E-04	4.30
Q9Y6C2	*EMILIN-1*	12	12	92.98	8.26E-05	3.42
P04908	*Histone H2A type 1-B/E*	3	3	23.21	1.21E-03	2.90
P62805	*Histone H4*	5	5	38.37	3.81E-04	2.76
P35442	*Thrombospondin-2*	10	9	61.02	4.07E-04	2.61
P01024	*Complement C3*	7	7	44.15	3.35E-04	2.40
Q14112	*Nidogen-2*	10	9	64.07	1.09E-05	2.29
P17987	*T-complex protein 1 subunit alpha*	3	3	16.69	4.26E-03	2.25
Q9UQP3	*Tenascin-N*	4	4	22.53	2.15E-03	2.08
P98160	*Basement membrane-specific heparan sulfate proteoglycan core protein*	40	40	264.35	2.40E-04	2.01
O60814	*Histone H2B type 1-K*	5	5	36.96	5.82E-03	1.83
Q8WUM4	*Programmed cell death 6-interacting protein*	15	15	97.41	2.69E-03	1.55
P78509	*Reelin*	7	7	37.44	8.13E-03	1.55

A GO analysis performed with STRING on the panel of proteins more abundant in VSMC^{PCSK9}-EVs showed significant enrichment in the following categories: lipoprotein extracellular matrix structural constituent, lipoprotein particle receptor binding, very-low-density lipoprotein particle receptor binding, and signalling receptor binding (Fig. 16).

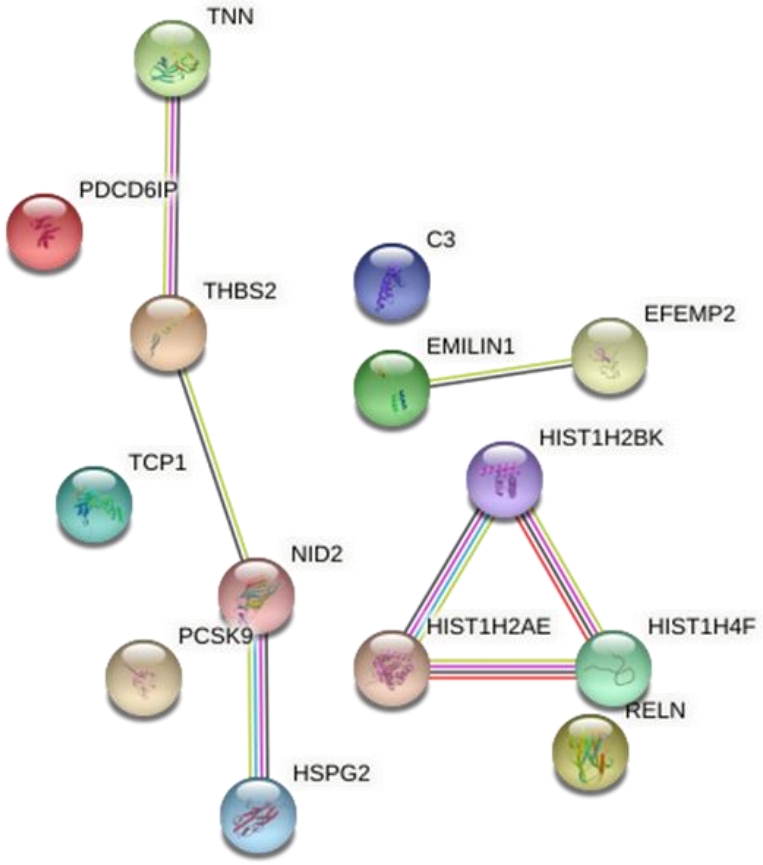

Figure 16. *GO enrichment analysis relative to proteins with a significant higher expression in VSMC^{PCSK9}-EVs.*

Concerning EV-miRNA content, compared to those isolated from VSMC^{WT}-EVs, VSMC^{PCSK9}-EVs differently express 6 miRNAs: hsa-miR-34c, hsa-miR-29, hsa-miR-148b, hsa-miR-221 and hsa-miR-125b were down regulated; hsa-miR-49 was up regulated (Fig. 17A). Thus, the genes targeted by these miRNAs were compared with genes associated with atherosclerosis (N= 20,445) and inflammation (N=467) downloaded from DisGeNET v 7.0.

The Venn Diagram shows that 54 genes were associated with atherosclerosis and inflammation (Fig. 17B and Table 5).

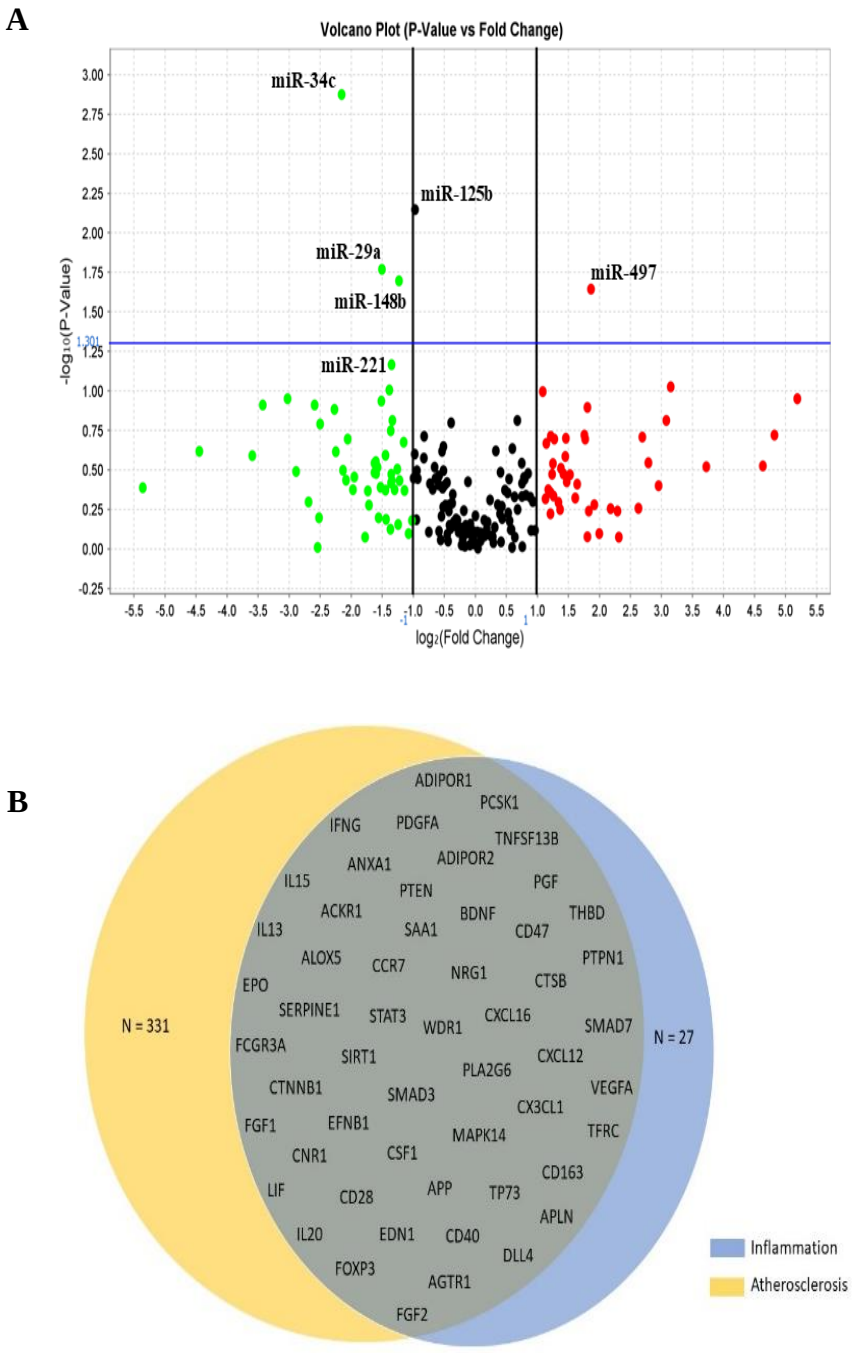

Figure 17. **(A)** *Volcano plot of miRNA with a significant different expression between VSMC^{PCSK9}-EVs and VSMC^{WT}-EVs.* **(B)** *Venn diagram of miRNAs targets. All predicted genes for the differentially expressed miRNAs (B) were filtered according to their relationship with atherosclerosis and inflammation and were selected for checking gene targets overlap. Results show the miRNAs target common genes.*

Table 5. Gene target associated with inflammation and atherosclerosis.

Gene	***miRNA***
ACKR1	hsa-miR-34c-5p
ADIPOR1	hsa-miR-221-3p
ADIPOR2	hsa-miR-34c-5p
AGTR1	hsa-miR-34c-5p
ALOX5	hsa-miR-29a-5p
ANXA1	hsa-miR-221-3p
APLN	hsa-miR-497-5p
APP	hsa-miR-497-5p
BDNF	hsa-miR-497-5p
CCR7	hsa-miR-125b-5p
CD163	hsa-miR-497-5p
CD28	hsa-miR-497-5p
CD40	hsa-miR-497-5p
CD47	hsa-miR-497-5p, hsa-miR-34c-5p
CNR1	hsa-miR-221-3p
CSF1	hsa-miR-497-5p
CTNNB1	hsa-miR-148b-5p
CTSB	hsa-miR-34c-5p
CX3CL1	hsa-miR-497-5p
CXCL12	hsa-miR-221-3p
CXCL16	hsa-miR-34c-5p
DLL4	hsa-miR-497-5p
EDN1	hsa-miR-125b-5p
EFNB1	hsa-miR-34c-5p
EPO	hsa-miR-125b-5p
FCGR3A	hsa-miR-148b-5p
FGF1	hsa-miR-497-5p
FGF2	hsa-miR-497-5p
FOXP3	hsa-miR-34c-5p
IFNG	hsa-miR-125b-5p
IL-13	hsa-miR-125b-5p
IL-15	hsa-miR-148b-5p, hsa-miR-497-5p
IL-20	hsa-miR-497-5p
LIF	hsa-miR-125b-5p
MAPK14	hsa-miR-125b-5p
NRG1	hsa-miR-221-3p
PCSK1	hsa-miR-29a-5p
PDGFA	hsa-miR-221-3p
PGF	hsa-miR-34c-5p
PLA2G6	hsa-miR-34c-5p
PTEN	hsa-miR-497-5p

PTPN1	hsa-miR-125b-5p
SAA1	hsa-miR-125b-5p
SERPINE1	hsa-miR-34c-5p
SIRT1	hsa-miR-34c-5p
SMAD3	hsa-miR-497-5p
SMAD7	hsa-miR-497-5p
STAT3	hsa-miR-125b-5p
TFRC	hsa-miR-497-5p
THBD	hsa-miR-34c-5p
TNFSF13B	hsa-miR-497-5p
TP73	hsa-miR-125b-5p
VEGFA	hsa-miR-497-5p
WDR1	hsa-miR-125b-5p

7.3 VSMC^{PCSK9}-EVs activate ECs and establish a pro-inflammatory milieu in THP-1 and THP-1 derived macrophages. Before assessing the impact of EVs on recipient cells, whether EVs are internalized by cells was tested. EVs isolated from VSMCs^{WT} and VSMCs^{PCSK9} were labelled with PKH67, a specific cell membrane dye, and then 5x10^{8} EVs/ml were transferred for 24 hours to the recipient cells, THP-1 monocytes. As shown in Fig. 18, the fluorescence of THP-1 exposed to labelled EVs was almost 5-fold higher compared to THP-1 receiving EVs not labelled with PKH67, suggesting that EVs can enter inside the target cells to mediate their effects.

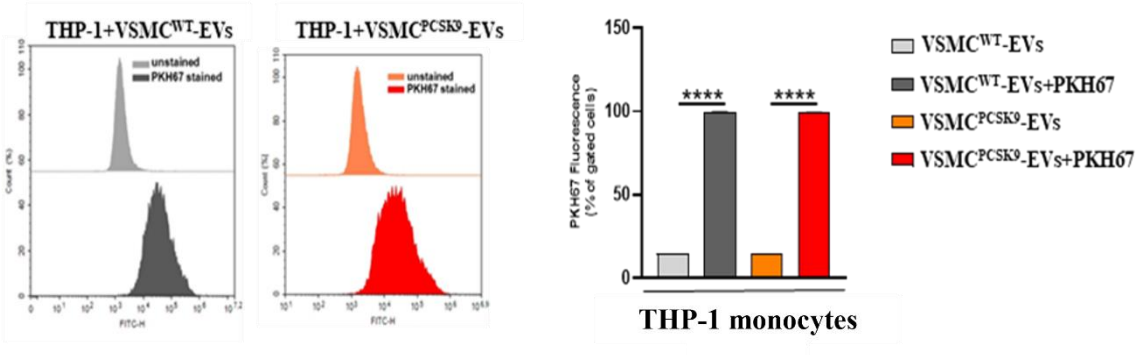

Figure 18. *Plots and bar graphs show the uptake of VSMC^{PCSK9}-EVs and VSMC^{WT}-EVs by target cells (THP-1) assessed by FC. Results are expressed relative to the normal control and represent the means of 3 independent experiments ± SD. Differences between groups have been assessed by t-test. ****p < 0.0001 vs control.*

We initially tested the expression of adhesion molecules and pro-inflammatory markers in EA.hy926 ECs upon exposure to VSMC^{PCSK9}-EVs. A significant rise in gene expression of IL-6, VCAM-1, endothelin 1 (ET-1), ICAM-1 and E-selectin was found in EA.hy926 cells exposed to VSMC^{PCSK9}-EVs compared to those exposed to VSMC^{WT}-EVs (Fig. 19).

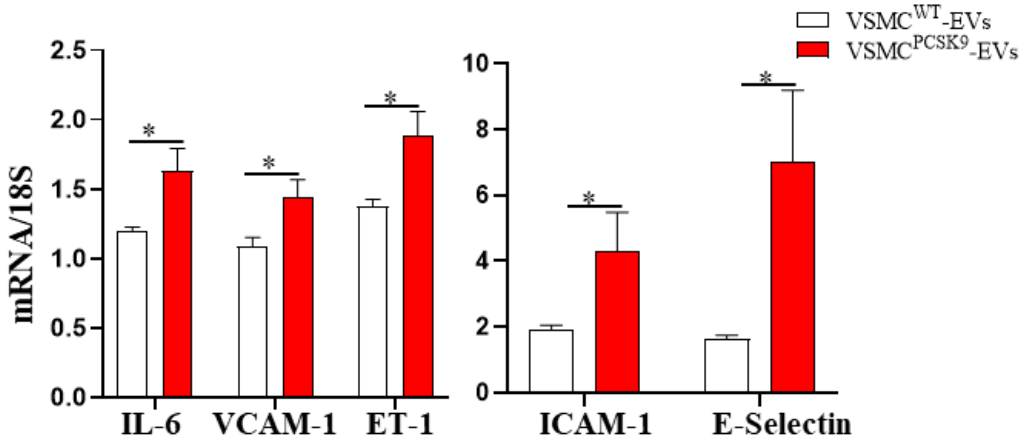

Figure 19. *Gene expression of pro-inflammatory cytokine IL-6 and cell adhesion molecules (VCAM-1, ET-1, ICAM-1 and E-selectin) in EA.hy926 cells. 18S was used as reference gene. Red bar represents cells exposed to VSMC^{PCSK9}-EVs; white bar represents cells exposed to VSMC^{WT}-EVs. Results are expressed relative to the normal control and represent the means of 3 independent experiments ± SD. Differences between groups have been assessed by t-test. *p < 0.05 vs control.*

Additionally, we evaluated whether VSMC^{PCSK9}-EVs could fuel the inflammatory milieu and we have found that 24-hour-exposure of THP-1 and THP-1-derived macrophages to VSMC^{PCSK9}-EVs dramatically increased the gene expression of CCL2, IL-1α, IL-1β, IL-6, and IL-8 (Fig. 20).

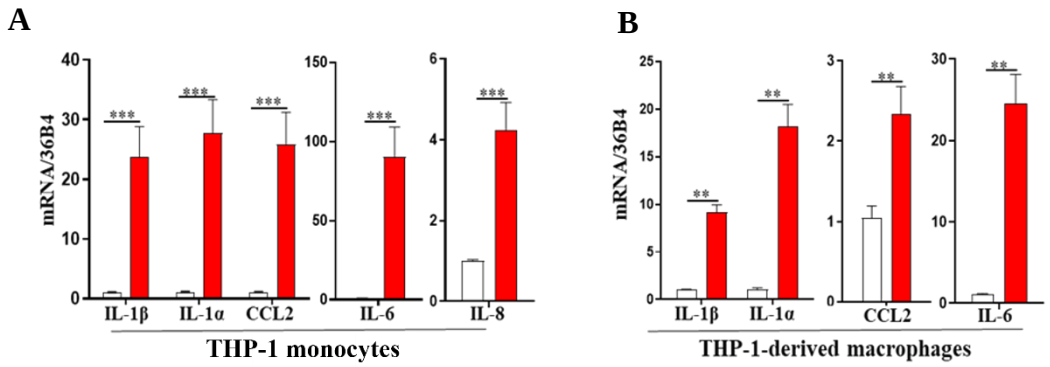

Figure 20. *Gene expression of pro-inflammatory cytokines and chemokines (IL-1β, IL-1α, IL-6, IL-8 and CCL2) in THP-1 monocytes* **(A)** *and in THP-1 derived macrophages* **(B)** *after treatment with VSMC^{PCSK9}-EVs and VSMC^{WT}-EVs. 36B4 was used as reference genes. Red bar represents cells exposed to VSMC^{PCSK9}-EVs; white bar represents cells exposed to VSMC^{WT}-EVs. Results are expressed relative to the normal control and represent the means of 3 independent experiments ± SD. Differences between groups have been assessed by t-test. **p < 0.01, ***p<0.001 vs control.*

The establishment of the inflammatory milieu was further confirmed by measuring the protein expression of phosphorylated form of STAT3 (signal transducer and activator of transcription 3) and SOCS3 (suppressor of cytokine signaling-3), two well-known cell signalling pathways involved in atherosclerosis. In both THP-1 monocytes and THP-1-derived macrophages, only VSMC^{PCSK9}-EVs significantly raised the phosphorylation levels of STAT3 with a subsequent down regulation of SOCS3 (Fig. 21).

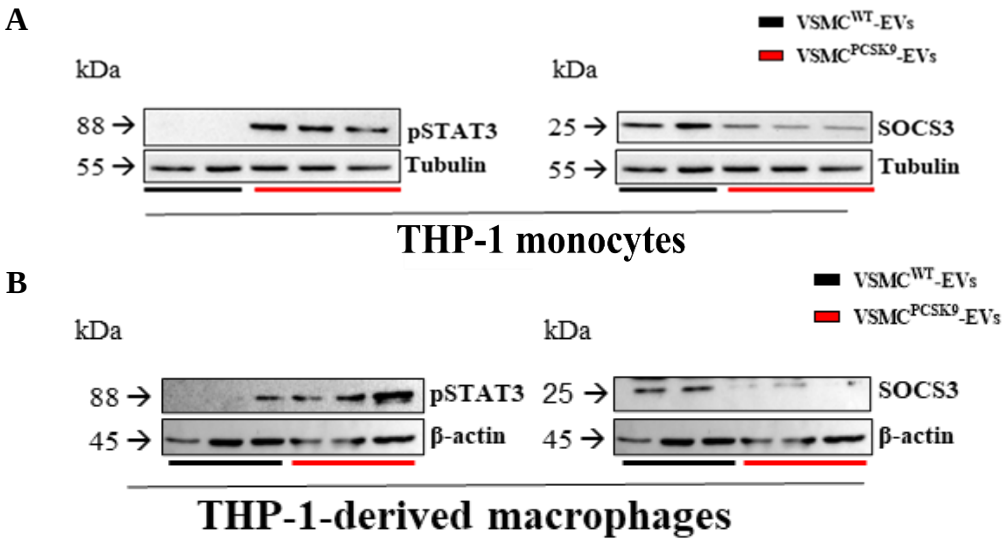

Figure 21. *Protein expression of pSTAT3 and SOCS3 as assessed by WB analysis in THP-1 monocytes (A) and THP-1 derived macrophages (B). Tubulin (A) and β-actin (B) were used as housekeeping proteins.*

A label-free mass spectrometry-based approach was then applied to analyse the secretome of THP-1 exposed to EVs (Table 6). Specifically, GO analysis showed that the exposure to VSMC^{PCSK9}-EVs increase pathway involved in immune response, immune effector process, response to stress and cellular response to cytokines (Fig. 22).

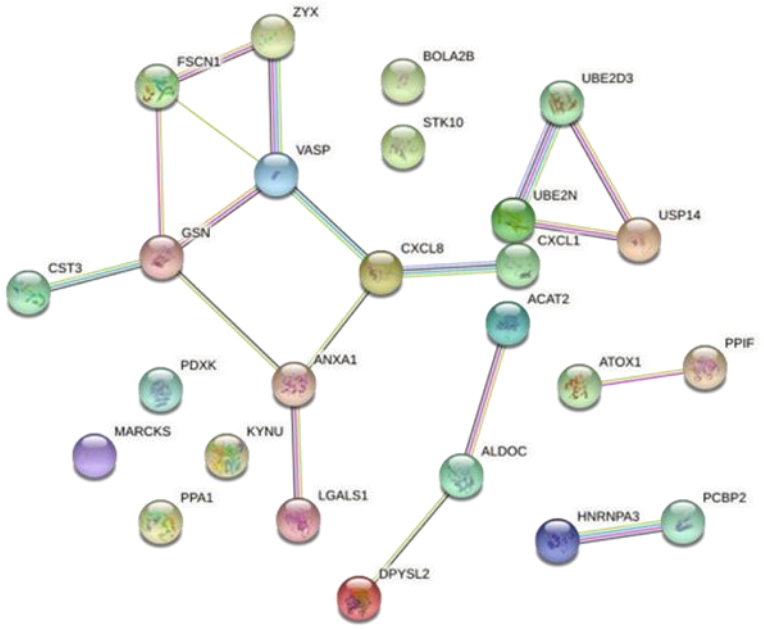

Figure 22. *Proteomic and GO analysis of secreted proteins from THP-1 cells incubated with VSMC^{PCSK9}-EVs.*

Table 6. List of differentially expressed proteins in the secretome of THP-1 exposed to VSMC^{PCSK9}-EVs.

Accession	*Description*	*Peptide count*	*Unique peptides*	*Confidence score*	*p value*	*Max fold change*
P50552	Vasodilator-stimulated phosphoprotein	7	6	44.2	8.76E-07	2.00
P10145	Interleukin-8	4	4	48.8	6.19E-04	1.64
P09972	Fructose-bisphosphate aldolase C	9	4	108.1	1.08E-05	1.54
O94804	Serine/threonine-protein kinase 10	3	2	16.8	1.88E-02	1.54
P09341	Growth-regulated alpha protein	4	3	30.9	2.04E-03	1.54
P29966	Myristoylated alanine-rich C-kinase substrate	12	10	102.4	6.43E-03	1.52
Q9H3K6	BolA-like protein 2	2	2	14.4	5.25E-04	1.47
P30405	Peptidyl-prolyl cis-trans isomerase F mitochondrial	4	2	29.4	2.00E-04	1.46
P04083	Annexin A1	5	5	43.4	2.90E-03	1.46
O00764	Pyridoxal kinase	5	5	50.2	3.67E-03	1.36
P61077	Ubiquitin-conjugating enzyme E2 D3	3	3	21.3	4.93E-03	1.32
Q15942	Zyxin	5	5	34.2	7.03E-04	1.31
P51991	Heterogeneous nuclear ribonucleoprotein A3	10	6	85.6	1.05E-04	1.30
Q15366	Poly(rC)-binding protein 2	4	2	29.4	1.15E-03	1.29
Q9BWD1	Acetyl-CoA acetyltransferase cytosolic	9	8	58.5	7.76E-04	1.27

Q16658	*Fascin*	25	24	259.6	3.50E-03	1.26
P01034	*Cystatin-C*	9	8	109.4	3.78E-05	1.26
Q16719	*Kynureninase*	8	7	65.1	2.94E-03	1.26
P06396	*Gelsolin*	31	12	303.7	1.50E-02	1.26
P09382	*Galectin-1*	9	9	110.6	8.36E-03	1.24
P54578	*Ubiquitin carboxyl-terminal hydrolase 14*	2	2	10.9	8.39E-03	1.24
O00244	*Copper transport protein Atox1*	2	2	22.7	1.06E-02	1.24
P61088	*Ubiquitin-conjugating enzyme E2 N*	6	5	55.1	1.15E-03	1.24
Q15181	*Inorganic pyrophosphatase*	12	11	108.3	8.68E-04	1.23
Q16555	*Dihydropyrimidinase-related protein 2*	17	13	146.8	1.29E-02	1.20

7.4 Effect of EVs on cell migration, oxLDL uptake and mitochondrial functionality in recipient cells. A further step of our experimental design was to evaluate the impact of EVs on the migration capacity of the THP-1 monocytes and J774 macrophages.

Twenty-four hour-exposure of THP-1 cells to VSMC^{PCSK9}-EVs led to a raise in their migratory capacity towards a gradient of 10 ng/ml CCL2. After 10 hours of migration, 6.3% of THP-1 exposed to VSMC^{PCSK9}-EVs migrated from the upper part of the transwell to the bottom of the chamber vs 3.5% of THP-1 monocytes exposed to VSMC^{WT}- EVs (Fig. 23A), which correspondents to a +97,9% compared to their counterpart. On the contrary, VSMC^{PCSK9}-EVs decreases the migratory capacity by 54% compared to J774 exposed to VSMC^{WT}-EVs (Fig. 23B).

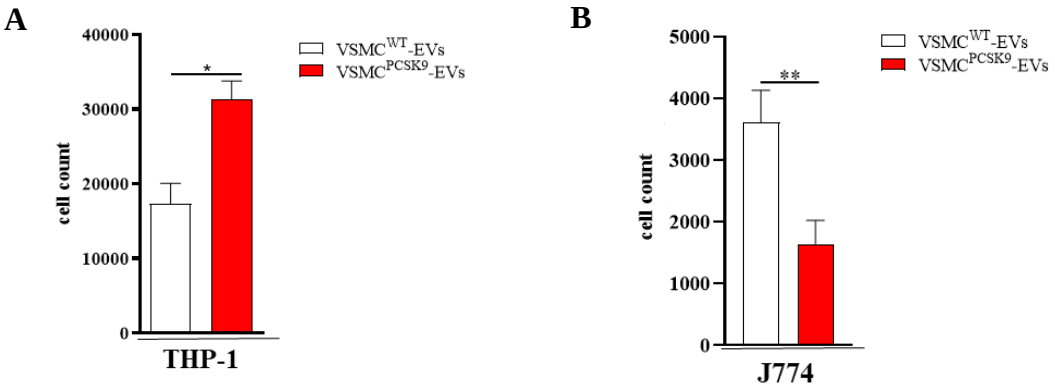

Figure 23. *Migration of THP-1 monocytes **(A)** and J774 macrophages **(B)** upon exposure to EVs. Red bar represents THP-1 exposed to VSMC^{PCSK9}-EVs; white bar represents THP-1 exposed to VSMC^{WT}-EVs. Results are expressed relative to the normal control and represent the means of 3 independent experiments ± SD. Differences between groups have been assessed by t-test. *p< 0.05, **p < 0.01, versus control.*

As a further confirmation of the proatherogenic phenotype carried by VSMC^{PCSK9}-EVs, we demonstrated a 22% rise in the uptake of oxLDL-derived cholesterol by THP-1-derived macrophages compared to VSMC^{WT}-EVs (Fig. 24).

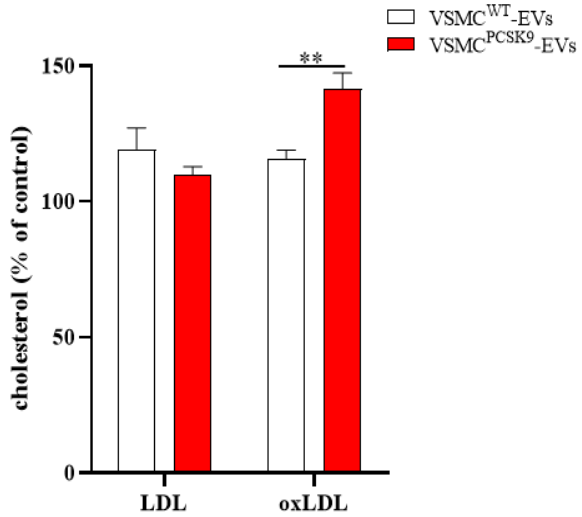

Figure 24. *Uptake of oxLDL-derived cholesterol in THP-1 cells treated with EVs. Red bar represents THP-1 exposed to VSMC^{PCSK9}-EVs; white bar represents THP-1 exposed to VSMC^{WT}-EVs. Results are expressed relative to the normal control and represent the means of 3 independent experiments ± SD. Differences between groups have been assessed by t-test. **p < 0.01, versus control.*

Besides LDLR, PCSK9 has other targets such as the scavenger receptor CD36 which is involved in the uptake of oxLDL. For this reason, we checked for its expression. We found that the protein expression of CD36 was modestly but significantly upregulated in response to VSMC^{PCSK9}-EVs compared to VSMC^{WT}-EVs (Fig. 25).

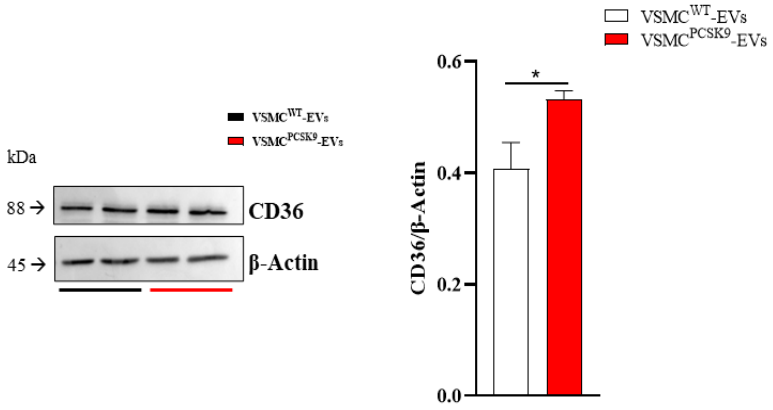

Figure 25. *CD36 protein expression in THP-1-derived macrophages after exposure to VSMC^{PCSK9}-EVs compared with VSMC^{WT}-EVs as assessed by WB. β-Actin was used as housekeeping. Results are expressed relative to the normal control and represent the means of 3 independent experiments ± SD. Differences between groups have been assessed by t-test. *p < 0.05, versus control.*

Since accumulating evidence confirms the involvement of mitochondria in atherosclerosis[74], the direct measurement of the oxygen consumption rate was tested in THP-1 recipient cells. VSMC^{PCSK9}-EVs significantly reduced basal and maximal respiration by 17% and 45%, respectively, compared to VSMC^{WT}-EVs (Fig. 26A). In line with this evidence, we found that VSMC^{PCSK9}-EVs increased the percentage of glycolytic proton efflux rate (PER) (+6%) with a decrement (-17%) in the ratio between mitochondrial oxygen consumption rate (mitoOCR) and glycolytic proton efflux rate (glycoPER) (Fig. 26B). Collectively, the drop in the oxidative phosphorylation and the rise in glycolytic activity, portend to an inflamed cellular phenotype.

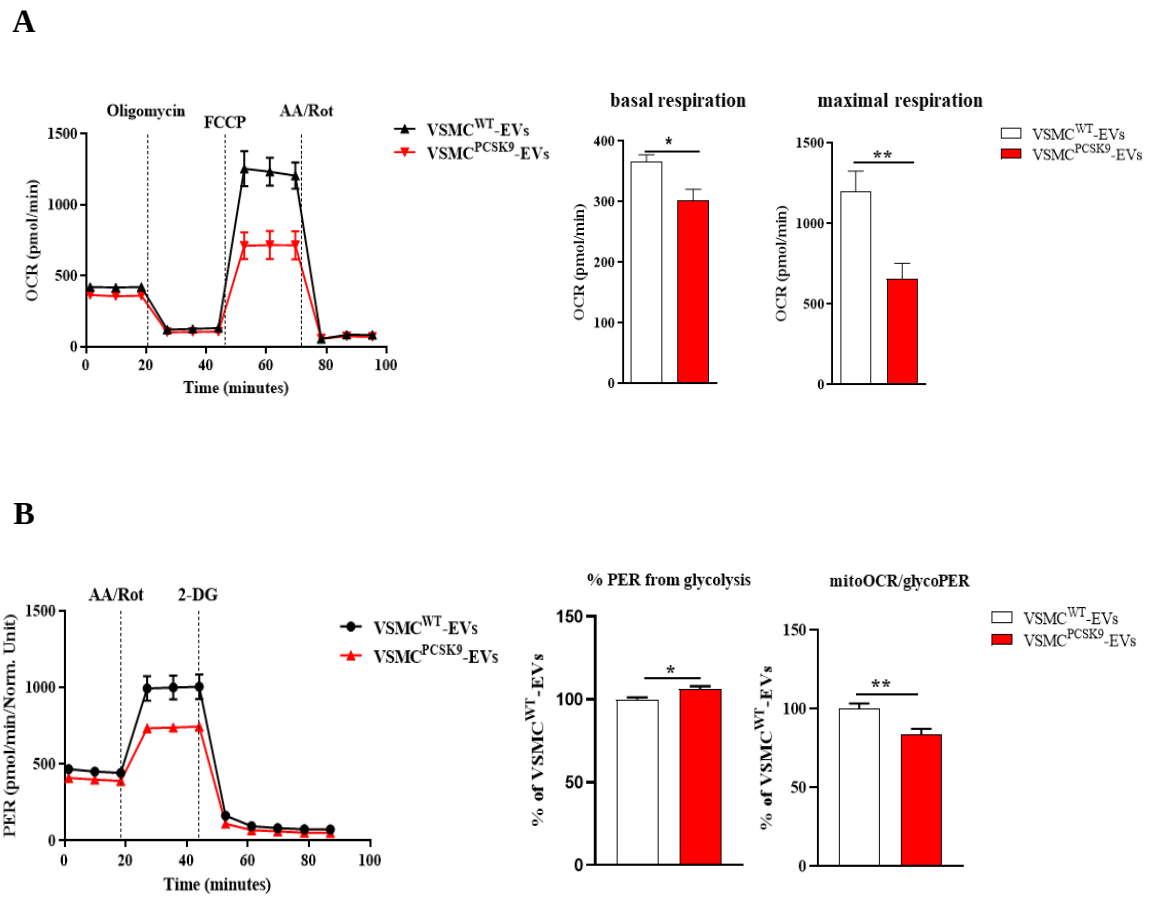

Figure 26. *Mitochondrial respiration function was assessed by Seahorse XFe24 analyser. Mitostress analysis* **(A)** *and glycolytic rate assay* **(B)** *were performed. Red line and bar represent THP-1 exposed to VSMC^{PCSK9}-EVs; black line and white bar represent THP-1 exposed to VSMC^{WT}-EVs. Results are expressed relative to the normal control and represent the means of 3 independent experiments ± SD. Differences between groups have been assessed by t-test. *p < 0.05, **p < 0.01, versus control.*

In vivo study

7.5 VSMC^{PCSK9}-EVs mediate a pro-inflammatory phenotype in zebrafish. Zebrafish represents a very useful *in vivo* experimental model to study inflammation [75]. To generate a systemic delivery, EVs were microinjected into the duct of Cuvier of 48 hpf embryos. Twenty hours post injection (hpi), VSMC^{PCSK9}-EVs elicited a significant increase in the gene expression level of two pro-inflammatory cytokines, IL-1β and IL-8, in comparison to VSMC^{WT}-EVs (Fig. 27).

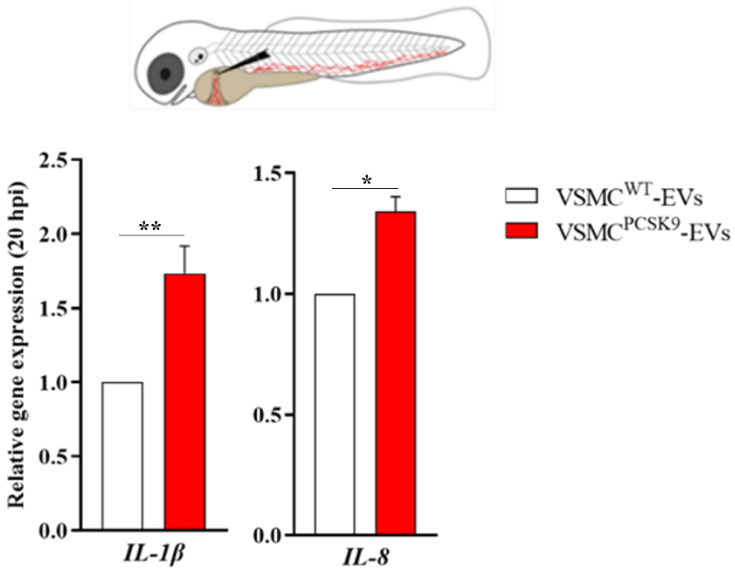

Figure 27. *Gene expression of IL-1β and IL-8 evaluated 20 hpi of EVs in embryos. Red bar represents THP-1 exposed to VSMC^{PCSK9}-EVs; white bar represents THP-1 exposed to VSMC^{WT}-EVs. Statistical significance was assessed by t test; *p < 0.05, ** p<0.001 vs control.*

To better elucidate the contribution of macrophages as mediators of the pro-inflammatory state, we assessed the effect of VSMC^{PCSK9}-EVs on the macrophage migratory capacity. Embryos at 3 dpf were subjected to two types of local injection: in the close cavity of the hindbrain ventricle (Fig. 28) and intramuscularly (Fig. 29) [67]. In both cases, the injection of VSMC^{PCSK9}-EVs increased the recruitment of macrophages toward the local injection site at 6 hpi in comparison to the same amount of VSMC^{WT}-EVs (>27-30% macrophage recruitment on average), as observed through *l-plastin* immunostaining assay.

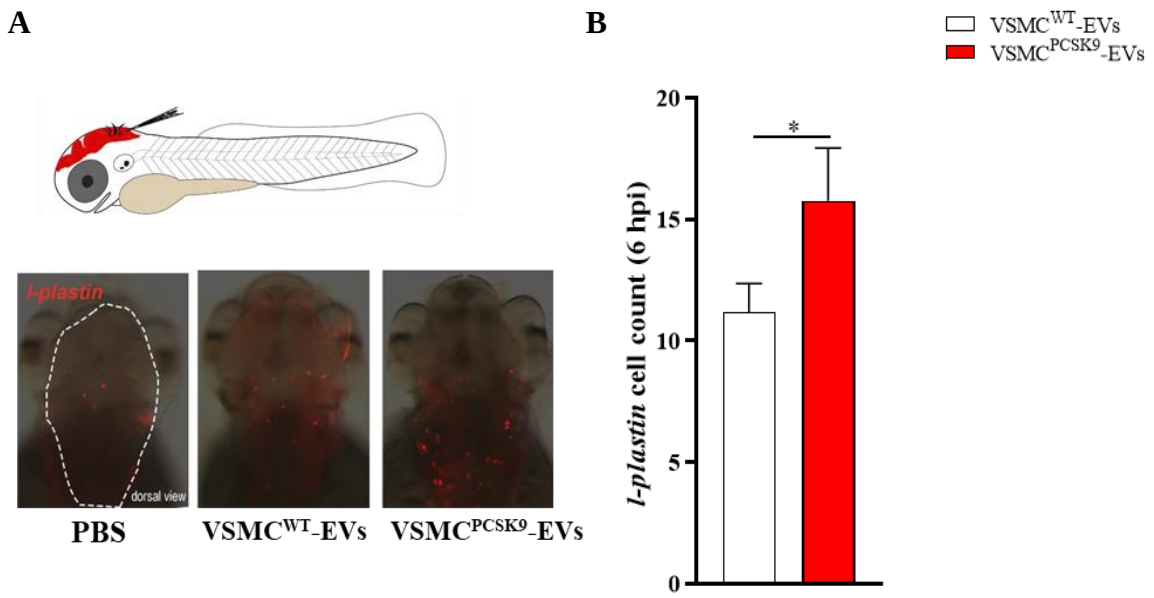

Figure 28. *Immunodetection assay (anti-l-plastin) in brain ventricle area of embryos treated with EVs. A scheme of injection strategy is reported.* **(A)** *Representative fluorescence overlaid with brightfield images shows macrophages recruitment (red) at injection site (dashed line) 6 hpi.* **(B)** *Macrophage quantification (l-plastin positive cells); the mean number of cells per embryo ± SEM are indicated. Red bar represents the injection of VSMC^{PCSK9}-EVs; white bar represents the injection with VSMC^{WT}-EVs. Statistical significance was assessed by t test; scale bar 300 µm. *p < 0.05, versus control.*

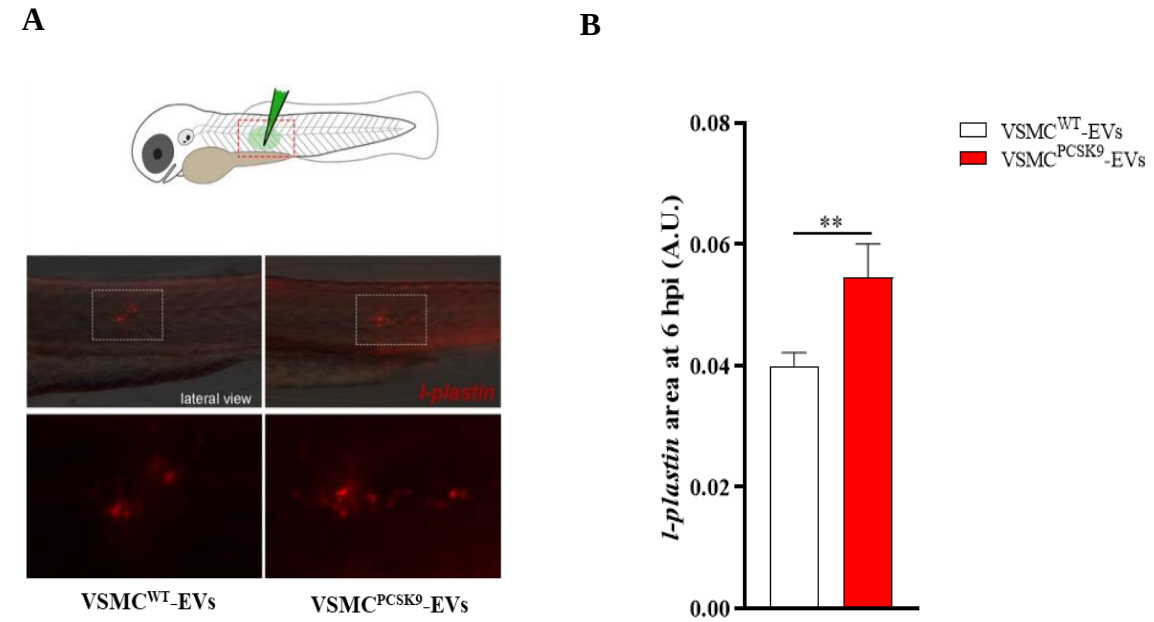

Figure 29. *Immuno-detection assay (anti-l-plastin) in trunk area of embryos treated with EVs. A scheme of injection strategy is reported.* **(A)** *Representative fluorescence overlaid with brightfield images shows macrophages recruitment (red) at injection site (dashed box) 6 hpi;* **(B)** *Macrophage quantification (l-plastin positive signal area) in dashed line area at 6 hpi; the mean values of l-plastin positive signal area per embryo ± SEM are indicated. Red bar represents the injection of VSMC^{PCSK9}-EVs; white bar represents the injection with VSMC^{WT}-EVs. Statistical significance was assessed by t test; scale bar 300 µm. **p < 0.01, vs control.*

To better understand the biodistribution of EVs, they were stained with CFSE and a representative fluorescence overlaid with brightfield images of trunk (lateral view) of 3 dpf embryos treated with CFSE-stained EVs (green) is shown in Fig. 30.

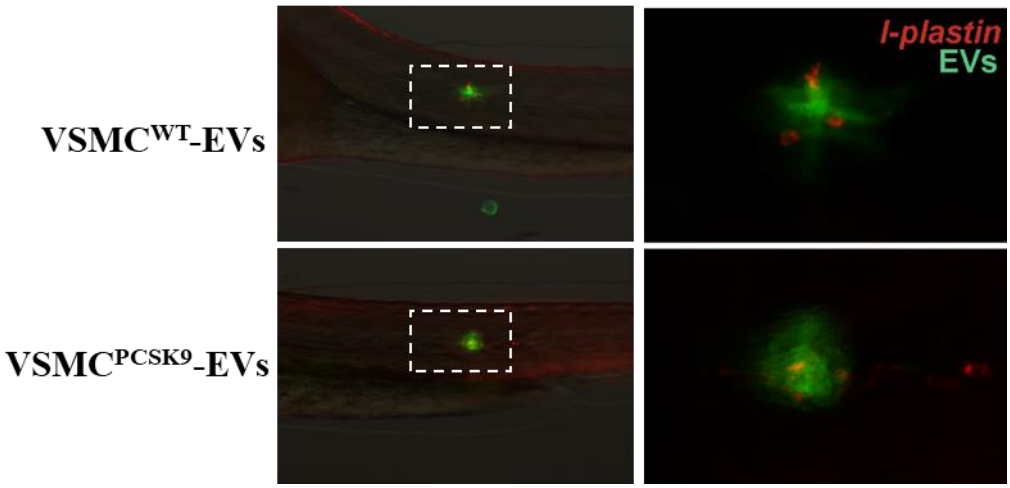

Figure 30. *Immuno-detection assay (anti-l-plastin) in trunk area (lateral view) of embryos treated with CFSE-stained EVs. Representative fluorescence overlaid with brightfield images shows macrophages (red) and EVs (green) recruitment at injection site (dashed line) 6 hpi.*

In human studies

7.6 Characteristics of the study population. The present study included 936 individuals with obesity (BMI= 33.6 ± 5.6 Kg/m^2). The description of study participants is reported in Table 7. In particular, 24.7% men and 75.3% women with a mean age of 52.4 ± 14 years, 47.8% never smoked, 35.4% were former smokers, and 16.0% current smokers. 45.7% of participants were on hypertensive medications and 12.3% of participants were taking statins. Mean values of total cholesterol (TC), LDL-C, and non-high-density cholesterol (non-HDL-C) were in the upper range of normality (TC = 207.4 ± 40.6 mg/dL, LDL-C = 131.6 ± 36.4 mg/dL, and non-HDL-C = 148.4 ± 40.9 mg/dL). HDL-C and TG levels were also in the normal range: 58.5 ± 15.0 and 119.2 ± 76.2 mg/dL, respectively. Glycemia and glycated hemoglobin were in the high range (99.8 ± 22.2 mg/dL and 39.4 ± 8.4 mmol/mol, respectively). Overall, cut-offs of normality have been chosen according to the most recent

guidelines [76],[77]. PCSK9 levels were normally distributed, with a mean level of 283.3 ± 96.3 ng/mL. Since we previously reported the effect of PM10 exposure on EVs release, this variable was used as a covariate in the model. Subjects mean exposure in the day before the blood sampling was equal to 37.9 ± 22.2 μg/m^3 and the apparent temperature was equal to 12.5 ± 8.2◦C [70].

Table 7. Demographic and clinical characteristics of the study participants (N = 936).

Characteristics	
Age, years	52.4 ± 14.0
Gender	231 (24.7%)
Males	705 (75.3%)
Females	33.3 ± 5.6
BMI kg/m^2	
Smoking status	
Never smoker	447 (47.8%)
Former smoker	331 (35.4%)
Current smoker	150 (16.0%)
Na	8 (0.8%)
Blood pressure, mmHg	
Sistolic	126.4 ± 14.9
Diastolic	79.1 ± 8.56
Antihypertensive medications	
Yes	427 (45.7%)
No	509 (54.3%)
Statin medications	
Yes	115 (12.3%)
No	821 (87.7%)
Total cholesterol, mg/ dL	207 ± 40.6
HDL-C, mg/ dL	58.5 ± 15
LDL-C, mg/dL	131.6 ± 36.4
non-HDL-C, mg/ dL	148.4 ± 40.9
Triglyceride, mg/ dL	119 ± 76.2
PCSK9, ng/mL	283.3 ± 96.3
Glucose, mg/dL	99.8 ± 22.2
Glycated hemoglobin, mmol/mol	39.4 ± 8.4
Insulin, U/mL	15.8 ± 14.1
HOMA-IR	3.1 (1.9;4.9)
QUICKI	0.14 ± 0.01
Hemochrome, 10^3 cell/μL	
White blood cells	6.78 ± 1.73
Red blood cells	4.73 ± 0.44
Hemoglobin	13.6 ± 1.4
Hematocrit	40 ± 3.5
Platelets	252 ± 60.8

BMI, body mass index; HDL-C, high-density lipoprotein cholesterol; HOMA-IR, homeostasis model assessment-insulin resistance; LDL-C, low-density lipoprotein cholesterol; PCSK9, proprotein convertase subtilisin/kexin type 9; QUICKI, quantitative insulin-sensitivity check index. For normal distribution, values are expressed as mean ± SD or as median. Discrete variables are expressed as counts (%). NA, not available.

7.7 Association between PCSK9 levels and EVs. We have investigated the association between PCSK9 levels and EVs count for each subject. First of all, we have measured their concentration and size by NTA analysis and we have found that plasma EV median concentration was 1,912 x 10^6/ml of plasma, EVs average size was 212 nm, and EV mode was 155 nm. In Figure 31 is described the Incidence Rate Ratio (IRR) of the association between PCSK9 levels and plasmatic EV concentration. For each EV size (between 30 and 700 nm), the percentage of variation in EV concentration (IRR) associated with every 10 ng/mL increment of PCSK9 levels is reported (Fig. 31A). The lower part of the plot (Fig. 31B) shows the P-values and FDR p-values obtained from negative binomial regression models adjusted for age, gender, BMI, smoking habit, statin use, PM10, and apparent temperature recorded in the day before the blood draw. The effect of PCSK9 on EV count was negative and significant ($p < 0.05$) for EVs in the range of 150 nm and 400 nm. Taken the different EV sizes as a whole (Table 8), PCSK9 was associated with a decreasing number of EVs (IRR = 0.996; 95% CI 0.992–0.999, p = 0.0377).

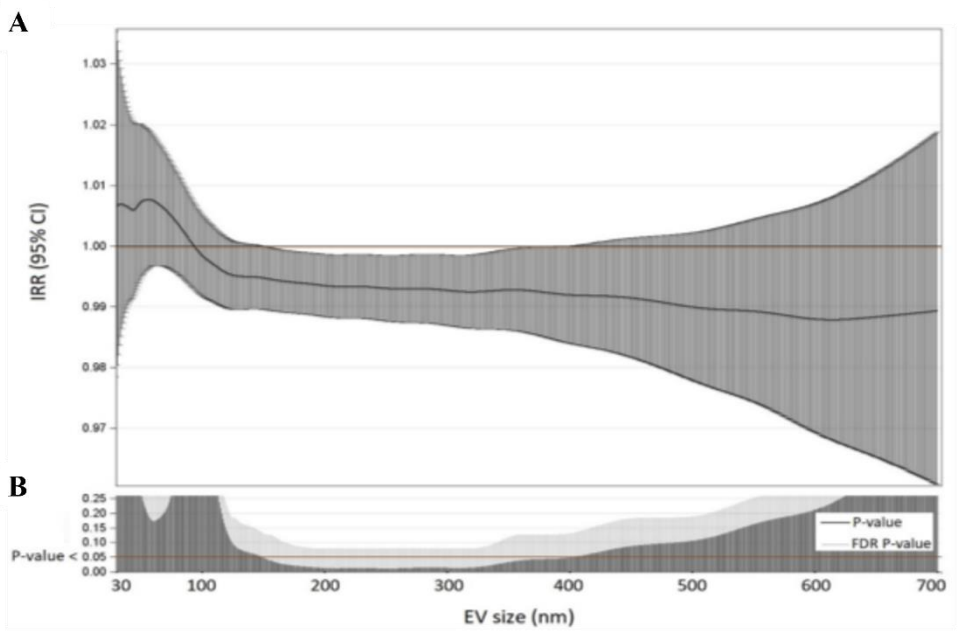

Figure 31. (A) *For each EV size (nm) IRR and 95% CI of associations between PCSK9 levels and EV concentrations were reported. IRR represents the percent variation in EVs concentration for 10 ng/mL increase in PCSK9 levels.* **(B)** *For each size, p-value and False Discovery Rate from negative binomial regression models adjusted for age, gender, BMI, smoking habit, statin use, PM10, and apparent temperature at the day before the blood draw were reported.*

We have evaluated the cellular source of EVs by flow cytometry and we analyzed enriched platelet-derived EVs ($CD61^+$ EVs), enriched monocyte/macrophage-derived EVs ($CD14^+$ EVs), enriched endothelial-derived EVs ($CD105^+$ EVs), and enriched neutrophil-derived EVs ($CD66^+$ EVs). In table 8 the associations between PCSK9 and EVs released from each cell type is described.

Table 8. Associations among PCSK9 levels (ng/mL) and different classes of EVs.

	IRR	**95% CI**	**p-value**
EV total count	0.996	0.992-0.999	0.0377
EV $_{CD14+}$ (macrophages/monocytes)	0.990	0.984-0.997	0.0063
EV $_{CD105+}$ (endothelium)	0.994	0.988-0.999	0.0270
EV $_{CD66b+}$ (neutrophils)	0.990	0.983-0.996	0.0023
EV $_{CD61+}$ (platelets)	0.999	0.991-1.007	0.8740

*All negative binomial regression models were adjusted for age, gender, BMI, smoking habit, statin use, PM10, and apparent temperature at the day before the blood draw. For $CD61^+$ EV, the model was also corrected for platelets; for $CD66^+$, the model was also adjusted for percentage of neutrophils; for $CD14^+$ EV, the model was also adjusted for percentage of monocytes. IRR stands for Incidence Rate Ratios and represents the percent decrease [(1 –IRR)*100] in EV concentration for 10 ng/mL increase in PCSK9 levels.*

A significant decrease was observed for $CD105^+$ EVs (IRR = 0.994; 95% CI 0.988–0.999, p = 0.027), CD14+ EVs (IRR = 0.990; 95% CI 0.984–0.997, p = 0.0063), and CD66+ EVs (IRR = 0.990; 95% CI 0.983–0.996, p = 0.0023). Further, we found that blood cell count and inflammation were modifiers on the above-reported associations. Specifically, the effect of PCSK9 on EVs derived from platelets was modified by platelet count (Fig. 32A). While in subjects with a lower platelet count (mean – SD: 191 × 103 platelets/μL), PCSK9 was associated with a rise in the number of $CD61^+$ EVs (IRR = 1.012; 95% CI 1.001–1.024, p = 0.046), the opposite (IRR = 0.988; 95% CI 0.977–0.999, p = 0.043) was found in individuals with a higher platelet count (mean + SD: 312 × 103 platelets/μl). Using a similar statistical approach, the effect of PCSK9 on macrophages/monocytes-derived EVs ($CD14^+$) was

modified by monocyte count (Fig. 32B). The negative effect was mainly driven by subjects with a higher monocyte count (IRR = 0.983; 95% CI 0.973–0.992, p = 0.0005).

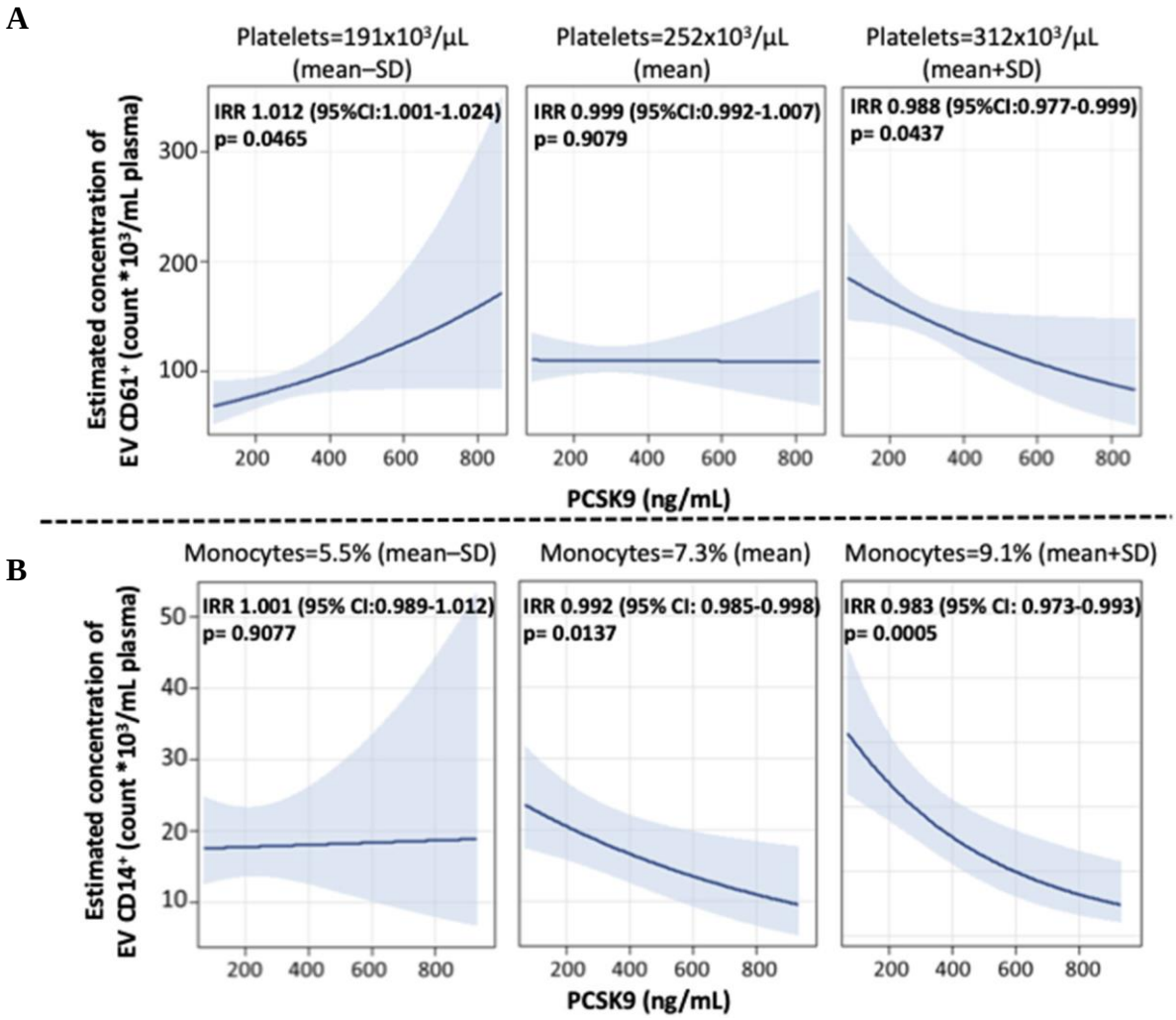

Figure 32. (A) *Association between PCSK9 and EV CD61⁺ at three selected levels of platelets (mean-standard deviation (SD), mean, and mean + SD value).* **(B)** *Adjusted IRR were reported for a 10 ng/mL increase in PCSK9 concentration, at each level of monocytes. The negative binomial regression model was adjusted for age, gender, BMI, smoking habit, statin use, PM10, and apparent temperature measured on the day before the blood draw. P-value of interaction term PCSK9*CD61⁺ was 0.0166* **(A)** *and PCSK9*CD14⁺ was 0.0322* **(B)**.

The effect of PCSK9 on endothelial-derived-EVs ($CD105^+$) was modified by plasmatic IL-8 (Fig. 33), as the effect was larger for subjects with a high concentration of IL-8 (IRR =

0.989; 95% CI 0.980–0.999, p = 0.024). Finally, the interaction between PCSK9 and neutrophils derived- EVs ($CD66^+$) was not modified by neutrophils count (p = 0.7683).

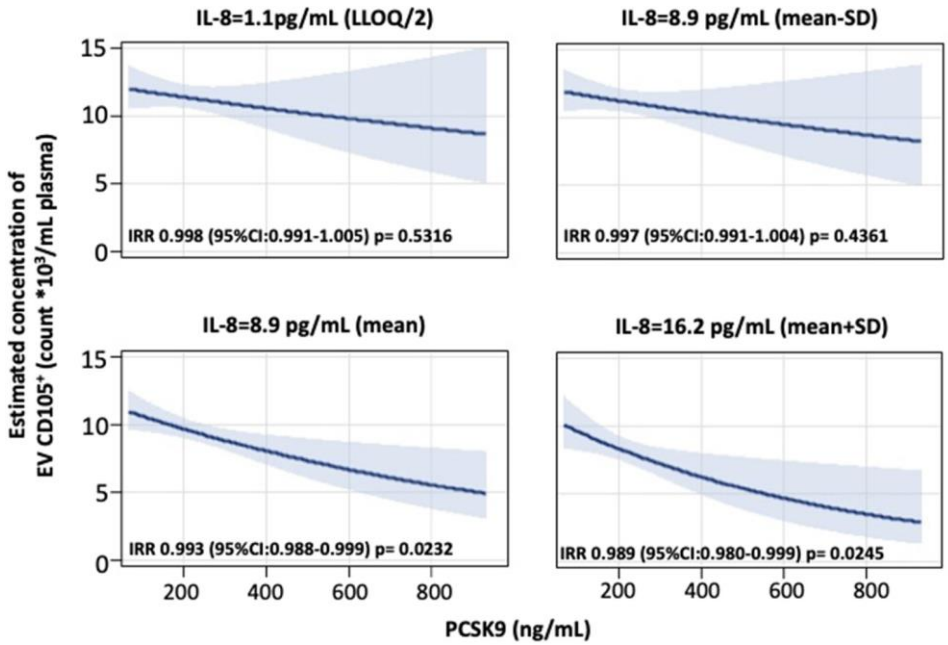

Figure 33. *Association between PCSK9 levels and EV $CD105^+$ concentrations at four selected levels of IL-8 [lower limit of quantification (LLOQ)/2, mean – standard deviation (SD), mean, and mean + SD value]. p-value of interaction term PCSK9*$CD105^+$ was 0.1532. IRR were reported for a 10 ng/mL increase in PCSK9 concentration, at each level of IL-8. The negative binomial regression model was adjusted for age, gender, BMI, smoking habit, statin use, PM10, and apparent temperature measured on the daybefore the blood draw.*

7.8 Association between PCSK9 levels and miRNA related to atherosclerosis. To assess the possible role of PCSK9 in modulating miRNA EV content, an OpenArray technology was used. After data cleaning, 527 miRNAs were expressed in at least one subject. In a model adjusted for age, gender, BMI, smoking habit, use of statin, PM10, and apparent temperature measured the day before the blood draw, PCSK9 levels were associated with a significant increase of 35 miRNAs and a significant decrease of 29 miRNAs. After FDR adjustment for multiple comparisons (FDR P < 0.1), PCSK9 levels were positively associated with hsa-miR-362-5p (1% 3.069; 95%CI 1.6, 4.6; p = 0.0298), hsa-miR-150 (1%

5.238; 95% CI 2.5, 8.0; p = 0.0298), and hsa-miR-1244 (1% 1.661; 95% CI 0.8, 2.5; p = 0.0298), and negatively with hsa-miR-520b-3p (1% −3.776; 95% CI −5.9, −1.6; p = 0.0919) and hsa-miR-638 (1% −4.530; 95% CI −7.1, −1.9; p = 0.0919). For each of the five miRNAs, we considered genes predicted by at least two of the four evaluated algorithms to be bona fide target genes. The number of predicted target genes were 3,599 (for hsa-miR-362-5p), 7,032 (for hsa-miR- 150), 2,812 (for hsa-miR-1244), 4,539 (for hsa-miR-520b-3p), and 1,882 (for hsa-miR-638). To elucidate the mechanisms through which the five EV-derived-miRNAs could impact on atherosclerosis, a miRNA-target interaction analysis was performed and these genes were compared to those found in the atherosclerosis gene network built using the disgenet2r package of R software. Fifty-nine genes were associated with atherosclerosis. Among them, 29 atherosclerosis-related genes were the predicted targets of at least one of the five EV-derived miRNAs. For the genes targeted by these miRNAs, we draw a Venn diagram showing common targets (Fig. 34). Two genes were in common between all the 5 miRNAs [toll-like receptor 4 (TLR4) and estrogen receptor 1 (ERS1)], whereas the LDLR was the target of 4.

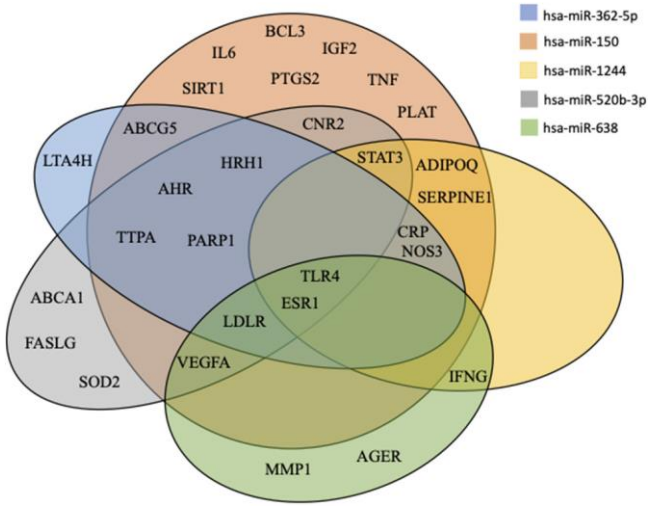

Figure 34. *Venn diagram of miRNAs targets. All predicted genes for the differentially expressed miRNAs were filtered according to their relation with atherosclerosis and were selected for checking gene targets overlap. Results show the miRNAs target common genes.*

7.9 Association between the four miRNAs targeting LDLR in silico, and LDLR mRNA.

We evaluated the mRNA expression of LDLR extracted from circulating leukocytes and we associated them with the levels of hsa-miR-362-5p, hsa-miR-150, hsa-miR- 520b-3p, and hsa-miR-638, as these four miRNAs were found to target LDLR in silico. The sum of the four miRNAs was negatively associated to LDLR gene expression (b=−0.041; 95%CI−0.078, −0.004; p = 0.0296). The effect seems exclusively driven by has-miR-150 (Table 9), which was negatively associated with the gene expression of LDLR in a multivariable model considering all the four miRNAs (bmiR−150 = −0.050; 95% CI −0.092, −0.008; p = 0.0193). Finally, considering that we were not able to validate these findings in atherosclerotic cardiovascular disease patients, we further subdivided our cohort according to the LDL-C risk threshold of 116 mg/dL [77]. A positive association was found between PCSK9 and LDL-C (b = 0.41; SE = 0.10, p < 0.0001), with higher levels of PCSK9 in the group with LDL-C > 116 mg/dL. According to this stratification, the negative association between hsa-miR-150 and LDLR was present only in the group with LDL-C > 116 mg/dL and higher levels of PCSK9 (bmiR−150 = −0.065; 95% CI −0.118, −0-011, p = 0.0182).

Table 9. Association between miRNA levels (RQ) and LDLR (RQ) with multivariable linear regression models.

	IRR	**95% CI**	**p-value**
hsa-miR-362-5p + hsa-miR-150 + hsa-miR-520b-3p + hsa-miR-638	-0.041	-0.078; -0.004	0.0296
Multivariable model:			
hsa-miR-362-5p +	0.021	-0.022; 0.063	0.3444
hsa-miR-150 +	-0.050	-0.092; -0.008	0.0193
hsa-miR-520b-3p +	-0.016	-0.053; 0.021	0.3924
hsa-miR-638	-0.005	-0.042; 0.032	0.8014

All linear regression models were adjusted for age, gender, BMI. β regression coefficients were reported for one SD increment (SD_sum_of_four = 2425.44; SD_ hsa-miR-362-5p = 1.96; SD_ hsa-miR-150 = 2424.43; SD_ hsa-miR-638= 6.93; SD_ hsa-miR-520b-3p= 10.55).

8. Discussion

In the pathogenesis of atherosclerosis, the mechanisms involved in cell-to-cell communication remain largely to be explored. In this field, a growing body of evidence has described a role for EVs. These phospholipid bilayer particles can promote and regulate the initiation of atherosclerosis and the lesion progression [78], [79].

The results of the present thesis of doctorate pointed out the cholesterol-independent role played by PCSK9 in atheroma formation. In particular, we explored the intertwined relationship between PCSK9 and inflammatory milieu by means of EVs. We demonstrated that by influencing the content of EVs released from VSMCs, PCSK9 favours a proinflammatory phenotype in both *in vitro* models of endothelial cells, monocytes and macrophages as well as in *in vivo* model of zebrafish embryos. The possible link between PCSK9 and the phenotypic features of EVs has been also explored in a human cohort. Specifically, the circulating levels of PCSK9 were associated with expression of EV-derived has-miR-150, which regulates the expression of LDLR.

The hypothesis that PCSK9 is directly involved in the atherosclerotic process is supported by the findings that PCSK9 (i) is present in ECs, macrophages and mostly in VSMCs [80]; (ii) the absence of PCSK9 is associated with reduced neointimal formation; (iii) silencing PCSK9 in macrophages determines a lower gene and protein expressions of TNF-α and IL-1β [81], [82].

Since VSMCs play critical roles in multiple vascular diseases, including atherosclerosis, and represent the major sources of extracellular matrix [83], in this project VSMCs have been used as a proxy because they express significant levels of PCSK9 [84], [85], that become particularly higher under pro-inflammatory stimuli [86] and in regions at low shear stress (3-6 dyn/cm^2) [87]. In addition, PCSK9 endogenously present in VSMCs is able to downregulate the expression of LDLR expression in macrophages [87] and monocytes [86].

VSMCs isolated from Pcsk9$^{-/-}$ mice, compared to those of Pcsk9$^{+/+}$ mice, have a reduced proliferation rate and a suppressed migratory capacity [88], [89]. Indeed, PCSK9 mediates a switch towards a pro-calcific phenotype of VSMCs [90] determining a higher proliferation rate and a higher migratory capacity. Moreover, in a synthetic or proliferative non-contractile state, VSMCs exhibit an increased production of EVs [91]. EVs originate from different cells and are released into the extracellular space where they can act as signal complexes or directly stimulate target cells transferring their biomolecular cargo (including lipids, proteins, and nucleic acids) [38]. The composition and the effects of EVs on target cells depend on the donor cell and on the stimuli that triggers their release; indeed, each cell can release different EVs based on their physiological state.

To evaluate whether PCSK9 can affect EVs biological properties, we have taken advantage of an *in vitro* model of VSMCs that stably overexpresses PCSK9. Firstly, we have characterized the phenotype of VSMCs, finding out that PCSK9 favoured a phenotypic switch of human VSMCs towards a synthetic phenotype. This evidence is in line with previous observations reporting that PCSK9 induces cell proliferation in mouse- or rat-derived smooth muscles [88],[92]. Although the different phenotype between VSMCs^{WT} and VSMCs^{PCSK9}, there were no differences in the size, concentration and shape between VSMC^{PCSK9}-EVs and VSMC^{WT}-EVs. However, according to changes in the phenotype of VSMCs, differences have been found in their cargo. VSMC^{PCSK9}-EVs carried a different cargo of proteins (n= 14) and miRNAs (n= 6) compared to VSMC^{WT}-EVs. GO analysis found an enrichment in extracellular matrix structural constituent that is involved in all aspects of vascular pathobiology. This network regulates the biomechanical properties of blood vessels and the phenotype of the cells that reside in them, such as ECs, VSMCs, adventitial fibroblasts and infiltrating immune cells from the circulation.

Although many studies support the direct effect of PCSK9 on atherosclerosis beyond its effect on cholesterol levels, the direct mechanism of involvement is still unknown, driving a gap in the knowledge to such a predominant player in cardiovascular disease [93]. In line with this evidence, $VSMC^{PCSK9}$-EV-miRNAs targeted 54 genes which were associated with both atherosclerosis and inflammation. miRNAs play important roles in various biological processes regulating the expression of genes at the transcriptional levels in recipient cells. EVs can exert their role in the pathophysiology of atherosclerosis via the transport of miRNAs that regulates atherosclerosis-prone genes. Indeed, by affecting the level of synthesized proteins within cells, they may be significant in driving the dysregulation that affects ECs, VSMCs, and leukocytes, which initiates and augments the growth of an atherosclerotic plaque [94].

The communication between VSMCs and ECs is essential to the development and to the homeostasis of mature blood vessel. Indeed, vascular injury arising from atherosclerosis is manifested by disruptions in endothelial cell-smooth muscle cell signalling [95], [96]. In addition, monocytes trapped in the subendothelial space may bind to VSMCs and undergo survival and differentiation through key signalling pathways and soluble and insoluble factors, *e.g.,* those released by VSMCs [97]. VSMCs in atherosclerotic lesion may affect other cellular components of the atheroma formation via EVs.

In particular, EA.hy926 exposed to $VSMC^{PCSK9}$-EVs had a raised expression of adhesion molecules (*e.g.,* VCAM-1, ICAM-1, E-selectin), all features that drive vascular inflammation and atherosclerosis initiation and progression [98]. Indeed, once activated, ECs recruit circulating monocytes from the blood into the intima, where they differentiate into macrophages and internalize modified lipoproteins to become foam cells [99]. Even PCSK9 directly facilitates inflammation in atherosclerotic lesions via the recruitment of monocytes, whereas PCSK9 inhibition ameliorates inflammation by reducing the CCR2-

related migratory ability of monocytes [100]. In line with this knowledge, VSMC^{PCSK9}-EVs enhanced migratory capacity of THP-1 monocytes. Moreover, exposure of THP-1 to VSMC^{PCSK9}-EVs increased the gene expression of inflammatory cytokines as well as raised levels of the phosphorylated form of STAT3. In line with findings showing that STAT3 phosphorylation is markedly increased in atherosclerotic lesions, silencing STAT3 pathway prevents atherosclerotic lesion formation at least in murine models [101]. Consistently, the expression of SOCS3, a protein which plays negative feedback on STAT3, in THP-1 exposed to VSMC^{PCSK9}-EVs was abrogated [102] On this matter, PCSK9 seems intertwined with inflammation with implications in the atherosclerotic process [80], [103], [104].

Once into the subendothelial space, monocytes differentiate in macrophages. Macrophages contribute to the maintenance of the local inflammatory response by secreting proinflammatory cytokines and chemokines. VSMC^{PCSK9}-EVs favoured a pro-inflammatory milieu in macrophages. The role of PCSK9 in increasing human inflammatory signalling is supported by the observation that PCSK9 treatment induces a pro-inflammatory response in macrophages [105]. In line with these findings, the internalization of PCSK9 in macrophages increased the production of reactive oxygen species and that of pro-inflammatory cytokines through a TLR4-dependent mechanism [106].

In this complex scenario, VSMC^{PCSK9}-EVs reduced the migratory capacity of J774 macrophages. Overall, macrophages that accumulate in atherosclerotic plaques have a reduced migratory capacity, hampering their ability to resolve inflammation and thus contributing to the formation of advanced and complex plaques [107]. Moreover, atherosclerosis is characterized by the retention of modified LDL (*e.g.*, oxLDL) within the arterial wall, a burden initiated by the intramural retention of atherogenic lipoproteins. This process activates resident macrophages and the recruitment of monocyte-derived cells. However, although native LDL can be taken up by macrophages by macropinocytosis,

especially when LDL is elevated, it is difficult to be demonstrated this process *in vitro*. For this reason, we used also oxLDL in our *in vitro* experiments. Macrophages engulf accumulated modified lipoproteins through SRs [108] determining the formation of foam cells. In line with these findings, the exposure of THP-1 macrophages to $VSMC^{PCSK9}$-EVs increased the uptake of oxLDL with a concomitant upregulation of CD36, a multifunctional receptor whose expression is significantly increased in macrophages in human carotid atherosclerotic tissue, particularly in advanced stages of atherosclerosis [109].

Another important player in CVD is represented by mitochondrial dysfunction. Indeed, it has been recognized that mitochondria are integrated into the cell signalling circuitry, and a modulation of these cellular pathways is at the basis of many inflammatory diseases such as atherosclerosis [110], [111]. Specifically, $VSMC^{PCSK9}$-EVs impaired the mitochondrial function of THP-1 decreasing both their basal and maximal respiration and rising their glycolytic activity.

These data have been confirmed in *in vivo* model of zebrafish embryos, a useful *in vivo* experimental model for the study of atherosclerosis. The innate immune system of zebrafish shares several features with the human one, recapitulating molecular pathways and immune cell-cell type present in humans [112]. The systemically injection of $VSMC^{PCSK9}$-EVs increased the gene expression of pro-inflammatory cytokines as well as the recruitment of macrophages in the site of injection compared to $VSMC^{WT}$-EVs. This effect may be the confirmation that $VSMC^{PCSK9}$-EVs carry an inflammatory chemoattractant feature. By using a human cohort of 936 individuals in which PCSK9 levels have been evaluated, we found that PCSK9 was associated with the release of EVs derived from atherosclerotic components (i.e., platelets, endothelium, monocytes/macrophages, and neutrophils) as well as with EV-derived miRNA linked to atherosclerosis (hsa-miR-362, hsa-miR-150, hsa-miR-1244, hsa-miR-520b-3p, and hsa-miR-638) and their related targeted genes (*e.g.*, LDLR, TLR4, and

ESR1). These miRNAs play a role in atherosclerosis: hsa-miR-150 enhances inflammatory responses by upregulating endothelial cell proliferation and migration, as well as intravascular environmental homeostasis. On the contrary, has-miR-362 inhibits the proliferation and migration of VSMCs in atherosclerosis [113] supporting the ambivalent nature of EVs in this context. miR-520b-3p suppresses endothelial inflammation and block the cross-talk between monocytes and ECs [114]. Thus, the fact that hsa-miR-520b-3p was downregulated, suggests a possible pro-inflammatory effect. hsa-miR-638 is a key molecule in regulating human VSMC proliferation and migration [115]. Interestingly, taking the network of target genes impacted by these miRNAs as a whole, it is suggestive to note that, besides LDLR, the majority of targets are related to inflammatory pathways (*e.g.*, TLR4, STAT3, CRP, IL6, IFN-g, TNF-a, etc.) pointing out that the role of PCSK9 on atherosclerosis has to be thought also in the context of an inflammatory autocrine/paracrine loop [116].

9. Conclusions

The results of my PhD project showed a new indirect role played by PCSK9 in the atheroma formation by providing new evidence to the hypothesis that PCSK9 is involved in the pathogenesis of cardiovascular disease independently of its role on LDL metabolism. We have demonstrated that PCSK9 influences the cargo of EVs released from VSMCs, favouring a pro-inflammatory milieu among cell components of atheroma formation.

Overall, these data support the evidence that PCSK9 plays a feed-forward inflammatory loop in the context of atheroma formation, highlighting a potential role of PCSK9 on the complex intercellular communication routes involving a network of cells and their EVs-derived miRNAs and proteins.

However, to further corroborate the association between PCSK9 and EVs in the context of atheroma formation, future studies (also epidemiological) are needed to evaluate the impact of PCSK9 inhibitors on the EVs release and cargo, specifically those of VSMCs origin.

Bibliography

[1] P. Wolf, “The Nature and Significance of Platelet Products in Human Plasma,” 1967.

[2] C. Bağcı, M. Sever-Bahcekapili, N. Belder, A. P. S. Bennett, Ş. E. Erdener, and T. Dalkara, “Overview of extracellular vesicle characterization techniques and introduction to combined reflectance and fluorescence confocal microscopy to distinguish extracellular vesicle subpopulations,” *Neurophotonics*, vol. 9, no. 02, Apr. 2022, doi: 10.1117/1.nph.9.2.021903.

[3] R. Suades, M. F. Greco, T. Padró, and L. Badimon, “Extracellular Vesicles as Drivers of Immunoinflammation in Atherothrombosis,” *Cells*, vol. 11, no. 11, p. 1845, Jun. 2022, doi: 10.3390/cells11111845.

[4] M. Colombo, G. Raposo, and C. Théry, “Biogenesis, secretion, and intercellular interactions of exosomes and other extracellular vesicles,” *Annual review of cell and developmental biology*, vol. 30. pp. 255–289, 2014. doi: 10.1146/annurev-cellbio-101512-122326.

[5] G. van Niel, G. D’Angelo, and G. Raposo, “Shedding light on the cell biology of extracellular vesicles,” *Nature Reviews Molecular Cell Biology*, vol. 19, no. 4. Nature Publishing Group, pp. 213–228, Apr. 01, 2018. doi: 10.1038/nrm.2017.125.

[6] C. D. Sherman, S. Lodha, and S. Sahoo, “Ev cargo sorting in therapeutic development for cardiovascular disease,” *Cells*, vol. 10, no. 6. MDPI, Jun. 01, 2021. doi: 10.3390/cells10061500.

[7] A. Hafiane and S. S. Daskalopoulou, “Extracellular vesicles characteristics and emerging roles in atherosclerotic cardiovascular disease,” *Metabolism: Clinical and Experimental*, vol. 85. W.B. Saunders, pp. 213–222, Aug. 01, 2018. doi: 10.1016/j.metabol.2018.04.008.

[8] M. Yáñez-Mó *et al.*, “Biological properties of extracellular vesicles and their physiological functions,” *Journal of Extracellular Vesicles*, vol. 4, no. 2015. Co-Action Publishing, pp. 1–60, 2015. doi: 10.3402/jev.v4.27066.

[9] R. J. Simpson, H. Kalra, and S. Mathivanan, “Exocarta as a resource for exosomal research,” *J Extracell Vesicles*, vol. 1, no. 1, 2012, doi: 10.3402/jev.v1i0.18374.

[10] H. Kalra *et al.*, “Vesiclepedia: A Compendium for Extracellular Vesicles with Continuous Community Annotation,” *PLoS Biol*, vol. 10, no. 12, Dec. 2012, doi: 10.1371/journal.pbio.1001450.

[11] D. K. Kim *et al.*, “EVpedia: An integrated database of high-throughput data for systemic analyses of extracellular vesicles,” *J Extracell Vesicles*, vol. 2, no. 1, 2013, doi: 10.3402/jev.v2i0.20384.

[12] S. W. Ferguson and J. Nguyen, “Exosomes as therapeutics: The implications of molecular composition and exosomal heterogeneity,” *Journal of Controlled Release*, vol. 228. Elsevier B.V., pp. 179–190, Apr. 28, 2016. doi: 10.1016/j.jconrel.2016.02.037.

[13] S. Mezouar, R. Darbousset, F. Dignat-George, L. Panicot-Dubois, and C. Dubois, “Inhibition of platelet activation prevents the P-selectin and integrin-dependent accumulation of cancer cell microparticles and reduces tumor growth and metastasis in vivo,” *Int J Cancer*, vol. 136, no. 2, pp. 462–475, Jan. 2015, doi: 10.1002/ijc.28997.

[14] C. Théry *et al.*, “Journal of Extracellular Vesicles Minimal information for studies of extracellular vesicles 2018 (MISEV2018): a position statement of the International Society for Extracellular Vesicles and update of the MISEV2014 guidelines”, [Online]. Available: https://www.tandfonline.com/loi/zjev20

[15] P. Libby *et al.*, “Atherosclerosis,” *Nat Rev Dis Primers*, vol. 5, no. 1, Dec. 2019, doi: 10.1038/s41572-019-0106-z.

[16] M. Focke, W. Hemmer, R. Bracun, F. Wolf, F. Wantke, and M. Götz, “Characterisation of oilseed rape allergens,” 1997. [Online]. Available: www.bmj.com

[17] P. Raggi *et al.*, “Role of inflammation in the pathogenesis of atherosclerosis and therapeutic interventions,” *Atherosclerosis*, vol. 276. Elsevier Ireland Ltd, pp. 98–108, Sep. 01, 2018. doi: 10.1016/j.atherosclerosis.2018.07.014.

[18] K. Theodorou and R. A. Boon, “Endothelial cell metabolism in atherosclerosis,” *Frontiers in Cell and Developmental Biology*, vol. 6, no. AUG. Frontiers Media S.A., Aug. 07, 2018. doi: 10.3389/fcell.2018.00082.

[19] M. A. Gimbrone and G. García-Cardeña, “Endothelial Cell Dysfunction and the Pathobiology of Atherosclerosis,” *Circ Res*, vol. 118, no. 4, pp. 620–636, Feb. 2016, doi: 10.1161/CIRCRESAHA.115.306301.

[20] T. J. Barrett, “Macrophages in Atherosclerosis Regression,” *Arteriosclerosis, thrombosis, and vascular biology*, vol. 40, no. 1. NLM (Medline), pp. 20–33, Jan. 01, 2020. doi: 10.1161/ATVBAHA.119.312802.

[21] K. J. Moore, F. J. Sheedy, and E. A. Fisher, “Macrophages in atherosclerosis: A dynamic balance,” *Nature Reviews Immunology*, vol. 13, no. 10. pp. 709–721, Oct. 2013. doi: 10.1038/nri3520.

[22] J. L. M. Björkegren and A. J. Lusis, “Atherosclerosis: Recent developments,” *Cell*, vol. 185, no. 10. Elsevier B.V., pp. 1630–1645, May 12, 2022. doi: 10.1016/j.cell.2022.04.004.

[23] I. Tabas and K. E. Bornfeldt, “Macrophage Phenotype and Function in Different Stages of Atherosclerosis,” *Circ Res*, vol. 118, no. 4, pp. 653–667, Feb. 2016, doi: 10.1161/CIRCRESAHA.115.306256.

[24] E. Latz and P. Duewell, “NLRP3 inflammasome activation in inflammaging,” *Seminars in Immunology*, vol. 40. Academic Press, pp. 61–73, Dec. 01, 2018. doi: 10.1016/j.smim.2018.09.001.

[25] G. L. Basatemur, H. F. Jørgensen, M. C. H. Clarke, M. R. Bennett, and Z. Mallat, “Vascular smooth muscle cells in atherosclerosis,” *Nature Reviews Cardiology*, vol. 16, no. 12. Nature Publishing Group, pp. 727–744, Dec. 01, 2019. doi: 10.1038/s41569-019-0227-9.

[26] M. R. Bennett, S. Sinha, and G. K. Owens, “Vascular Smooth Muscle Cells in Atherosclerosis,” *Circ Res*, vol. 118, no. 4, pp. 692–702, Feb. 2016, doi: 10.1161/CIRCRESAHA.115.306361.

[27] L. S. Shankman *et al.*, “KLF4-dependent phenotypic modulation of smooth muscle cells has a key role in atherosclerotic plaque pathogenesis,” *Nat Med*, vol. 21, no. 6, pp. 628–637, Jun. 2015, doi: 10.1038/nm.3866.

[28] M. O. J. Grootaert and M. R. Bennett, “Vascular smooth muscle cells in atherosclerosis: Time for a re-assessment,” *Cardiovascular Research*, vol. 117, no. 11. Oxford University Press, pp. 2326–2339, Oct. 01, 2021. doi: 10.1093/cvr/cvab046.

[29] N. G. Seidah *et al.*, “The secretory proprotein convertase neural apoptosis-regulated convertase 1 (NARC-1): Liver regeneration and neuronal differentiation.” [Online]. Available: www.ncbi.nlm.nih.govBLAST

[30] M. Abifadel *et al.*, “Mutations in PCSK9 cause autosomal dominant hypercholesterolemia,” *Nat Genet*, vol. 34, no. 2, pp. 154–156, Jun. 2003, doi: 10.1038/ng1161.

[31] C. Macchi, N. Ferri, C. R. Sirtori, A. Corsini, M. Banach, and M. Ruscica, “Proprotein Convertase Subtilisin/Kexin Type 9: A View beyond the Canonical Cholesterol-Lowering Impact,” *American Journal of Pathology*, vol. 191, no. 8. Elsevier Inc., pp. 1385–1397, Aug. 01, 2021. doi: 10.1016/j.ajpath.2021.04.016.

[32] N. G. Seidah and A. Prat, “The Multifaceted Biology of PCSK9,” *Endocr Rev*, vol. 43, no. 3, pp. 558–582, Jun. 2022, doi: 10.1210/endrev/bnab035.

[33] S. Liu *et al.*, “Blood flow patterns regulate pcsk9 secretion viamyd88-mediated pro-inflammatory cytokines,” *Cardiovasc Res*, vol. 116, no. 10, pp. 1721–1732, Aug. 2020, doi: 10.1093/cvr/cvz262.

[34] J. M. Cheng *et al.*, “PCSK9 in relation to coronary plaque inflammation: Results of the ATHEROREMO-IVUS study,” *Atherosclerosis*, vol. 248, pp. 117–122, May 2016, doi: 10.1016/j.atherosclerosis.2016.03.010.

[35] N. G. Seidah and A. Prat, “The Multifaceted Biology of PCSK9,” *Endocr Rev*, vol. 43, no. 3, pp. 558–582, Jun. 2022, doi: 10.1210/endrev/bnab035.

[36] P. E. Rautou *et al.*, “Microparticles from human atherosclerotic plaques promote endothelial ICAM-1-dependent monocyte adhesion and transendothelial migration,” *Circ Res*, vol. 108, no. 3, pp. 335–343, Feb. 2011, doi: 10.1161/CIRCRESAHA.110.237420.

[37] M. Brambilla *et al.*, “Different Contribution of Monocyte-and Platelet-Derived Microvesicles to Endothelial Behavior,” *Int J Mol Sci*, vol. 23, no. 9, May 2022, doi: 10.3390/ijms23094811.

[38] R. Suades, M. F. Greco, T. Padró, and L. Badimon, “Extracellular Vesicles as Drivers of Immunoinflammation in Atherothrombosis,” *Cells*, vol. 11, no. 11. MDPI, Jun. 01, 2022. doi: 10.3390/cells11111845.

[39] M. A. Nguyen *et al.*, “Extracellular Vesicles Secreted by Atherogenic Macrophages Transfer MicroRNA to Inhibit Cell Migration,” *Arterioscler Thromb Vasc Biol*, vol. 38, no. 1, pp. 49–63, Jan. 2018, doi: 10.1161/ATVBAHA.117.309795.

[40] C. Niu *et al.*, “Macrophage foam cell-derived extracellular vesicles promote vascular smooth muscle cell migration and adhesion,” *J Am Heart Assoc*, vol. 5, no. 10, Oct. 2016, doi: 10.1161/JAHA.116.004099.

[41] A. Hafiane and S. S. Daskalopoulou, “Extracellular vesicles characteristics and emerging roles in atherosclerotic cardiovascular disease,” *Metabolism: Clinical and Experimental*, vol. 85. W.B. Saunders, pp. 213–222, Aug. 01, 2018. doi: 10.1016/j.metabol.2018.04.008.

[42] D. Tsiantoulas *et al.*, “Circulating microparticles carry oxidation-specific epitopes and are recognized by natural IgM antibodies,” *J Lipid Res*, vol. 56, no. 2, pp. 440–448, Feb. 2015, doi: 10.1194/jlr.P054569.

[43] R. Suades *et al.*, “Circulating microparticle signature in coronary and peripheral blood of ST elevation myocardial infarction patients in relation to pain-to-PCI elapsed time,” *Int J Cardiol*, vol. 202, pp. 378–387, Jan. 2016, doi: 10.1016/j.ijcard.2015.09.011.

[44] N. Amabile and C. M. Boulanger, “Circulating microparticle levels in patients with coronary artery disease: A new indicator of vulnerability?,” *European Heart Journal*, vol. 32, no. 16. pp. 1958–1960, Aug. 2011. doi: 10.1093/eurheartj/ehr055.

[45] R. Suades, T. Padró, R. Alonso, J. López-Miranda, P. Mata, and L. Badimon, “Circulating CD45+/CD3+ lymphocyte-derived microparticles map lipid-rich atherosclerotic plaques in familial hypercholesterolaemia patients,” *Thromb Haemost*, vol. 111, no. 1, pp. 111–121, Oct. 2013, doi: 10.1160/TH13-07-0612.

[46] R. Suades *et al.*, “Liquid Biopsy of Extracellular Microvesicles Predicts Future Major Ischemic Events in Genetically Characterized Familial Hypercholesterolemia

Patients," *Arterioscler Thromb Vasc Biol*, vol. 39, no. 6, pp. 1172–1181, Jun. 2019, doi: 10.1161/ATVBAHA.119.312420.

[47] M. Zarà *et al.*, "Biology and role of extracellular vesicles (Evs) in the pathogenesis of thrombosis," *International Journal of Molecular Sciences*, vol. 20, no. 11. MDPI AG, Jun. 01, 2019. doi: 10.3390/ijms20112840.

[48] M. Camera *et al.*, "Association of Microvesicles With Graft Patency in Patients Undergoing CABG Surgery," *J Am Coll Cardiol*, vol. 75, no. 22, pp. 2819–2832, Jun. 2020, doi: 10.1016/j.jacc.2020.03.073.

[49] T. Ueba *et al.*, "Plasma Level of Platelet-Derived Microparticles Is Associated with Coronary Heart Disease Risk Score in Healthy Men," 2010.

[50] C. D. Sherman, S. Lodha, and S. Sahoo, "Ev cargo sorting in therapeutic development for cardiovascular disease," *Cells*, vol. 10, no. 6. MDPI, Jun. 01, 2021. doi: 10.3390/cells10061500.

[51] P. Vader, E. A. Mol, G. Pasterkamp, and R. M. Schiffelers, "Extracellular vesicles for drug delivery," *Advanced Drug Delivery Reviews*, vol. 106. Elsevier B.V., pp. 148–156, Nov. 15, 2016. doi: 10.1016/j.addr.2016.02.006.

[52] V. Chatterjee, X. Yang, Y. Ma, M. H. Wu, and S. Y. Yuan, "Downloaded from journals.physiology.org/journal/ajpheart," 2020.

[53] L. Badimon, T. Padro, G, Arderiu, G. Vilahur, M. Borrell-Pages, R. Suades, Extracellular vesicles in atherothrombosis: From biomarkers and precision medicine to therapeutic targets. *Immunol Rev*. 2022 Nov;312(1):6-19. doi: 10.1111/imr.13127

[54] O. Giró, A. Jiménez, A. Pané, L. Badimon, E. Ortega, and G. Chiva-Blanch, "Extracellular vesicles in atherothrombosis and cardiovascular disease: Friends and foes," *Atherosclerosis*, vol. 330. Elsevier Ireland Ltd, pp. 61–75, Aug. 01, 2021. doi: 10.1016/j.atherosclerosis.2021.07.002.

[55] N. Ferri *et al.*, "Proprotein convertase subtilisin kexin type 9 (PCSK9) secreted by cultured smooth muscle cells reduces macrophages LDLR levels," *Atherosclerosis*, vol. 220, no. 2, pp. 381–386, Feb. 2012, doi: 10.1016/j.atherosclerosis.2011.11.026.

[56] N. Ferri, G. Colombo, C. Ferrandi, E. W. Raines, B. Levkau, and A. Corsini, "Simvastatin reduces MMP1 expression in human smooth muscle cells cultured on polymerized collagen by inhibiting Rac1 activation," *Arterioscler Thromb Vasc Biol*, vol. 27, no. 5, pp. 1043–1049, May 2007, doi: 10.1161/ATVBAHA.107.139881.

[57] D. Vigetti and A. D. Theocharis, "The Extracellular Matrix Methods and Protocols Methods in Molecular Biology 1952." [Online]. Available: http://www.springer.com/series/7651

[58] K. W. Witwer *et al.*, “Standardization of sample collection, isolation and analysis methods in extracellular vesicle research,” *J Extracell Vesicles*, vol. 2, no. 1, 2013, doi: 10.3402/jev.v2i0.20360.

[59] K. J. Livak and T. D. Schmittgen, “Analysis of relative gene expression data using real-time quantitative PCR and the 2-ΔΔCT method,” *Methods*, vol. 25, no. 4, pp. 402–408, 2001, doi: 10.1006/meth.2001.1262.

[60] E. Favari *et al.*, “Impaired ATP-binding cassette transporter A1-mediated sterol efflux from oxidized LDL-loaded macrophages,” *FEBS Lett*, vol. 579, no. 29, pp. 6537–6542, Dec. 2005, doi: 10.1016/j.febslet.2005.10.042.

[61] L. Kritharides, W. Jessup, E. L. Mander, and R. T. Dean, “Apolipoprotein A-I-Mediated Efflux of Sterols From Oxidized LDL-Loaded Macrophages,” 1995. [Online]. Available: http://ahajournals.org

[62] M. Brioschi, S. Lento, E. Tremoli, and C. Banfi, “Proteomic analysis of endothelial cell secretome: A means of studying the pleiotropic effects of Hmg-CoA reductase inhibitors,” *J Proteomics*, vol. 78, pp. 346–361, Jan. 2013, doi: 10.1016/j.jprot.2012.10.003.

[63] U. Distler, J. Kuharev, P. Navarro, and S. Tenzer, “Label-free quantification in ion mobility-enhanced data-independent acquisition proteomics,” *Nat Protoc*, vol. 11, no. 4, pp. 795–812, Apr. 2016, doi: 10.1038/nprot.2016.042.

[64] P. Amadio *et al.*, “Brain-Derived Neurotrophic Factor and Extracellular Vesicle-Derived miRNAs in an Italian Cohort of Individuals With Obesity: A Key to Explain the Link Between Depression and Atherothrombosis,” *Front Cardiovasc Med*, vol. 9, Jul. 2022, doi: 10.3389/fcvm.2022.906483.

[65] C. B. Kimmel, W. W. Ballard, S. R. Kimmel, B. Ullmann, and T. F. Schilling, “Stages of Embryonic Development of the Zebrafish,” 1995.

[66] M. Cafora, M. Hoxha, L. Cantone, V. Bollati, A. Pistocchi, and L. Ferrari, “Assessment of innate immune response activation following the injection of extracellular vesicles isolated from human cell cultures in zebrafish embryos,” in *Methods in Enzymology*, vol. 645, Academic Press Inc., 2020, pp. 277–295. doi: 10.1016/bs.mie.2020.06.004.

[67] M. Nguyen-Chi, Q. T. Phan, C. Gonzalez, J. F. Dubremetz, J. P. Levraud, and G. Lutfalla, “Transient infection of the zebrafish notochord with E. coli induces chronic inflammation,” *DMM Disease Models and Mechanisms*, vol. 7, no. 7, pp. 871–882, 2014, doi: 10.1242/dmm.014498.

[68] M. Spreafico *et al.*, “HDAC8: A Promising Therapeutic Target for Acute Myeloid Leukemia,” *Front Cell Dev Biol*, vol. 8, Sep. 2020, doi: 10.3389/fcell.2020.00844.

[69] V. Bollati *et al.*, “Susceptibility to particle health effects, miRNA and exosomes: Rationale and study protocol of the SPHERE study,” *BMC Public Health*, vol. 14, no. 1, 2014, doi: 10.1186/1471-2458-14-1137.

[70] C. Macchi *et al.*, “Associations Among PCSK9 Levels, Atherosclerosis-Derived Extracellular Vesicles, and Their miRNA Content in Adults With Obesity,” *Front Cardiovasc Med*, vol. 8, Jan. 2022, doi: 10.3389/fcvm.2021.785250.

[71] J. Piñero *et al.*, “The DisGeNET knowledge platform for disease genomics: 2019 update,” *Nucleic Acids Res*, vol. 48, no. D1, pp. D845–D855, Jan. 2020, doi: 10.1093/nar/gkz1021.

[72] H. Dweep and N. Gretz, “MiRWalk2.0: A comprehensive atlas of microRNA-target interactions,” *Nature Methods*, vol. 12, no. 8. Nature Publishing Group, p. 697, Jul. 30, 2015. doi: 10.1038/nmeth.3485.

[73] N, Ferri, S. Marchianò, G. Tibolla, R. Baetta, A. Dhyani, M. Ruscica, P. Uboldi, AL. Catapano, A. Corsini, PCSK9 knock-out mice are protected from neointimal formation in response to perivascular carotid collar placement. *Atherosclerosis. 2016* Oct;253:214-224. doi: 10.1016/j.atherosclerosis.2016.07.910.

[74] Y. Luan, K.-D. Ren, Y. Luan, X. Chen, and Y. Yang, “Mitochondrial Dynamics: Pathogenesis and Therapeutic Targets of Vascular Diseases,” *Front Cardiovasc Med*, vol. 8, Dec. 2021, doi: 10.3389/fcvm.2021.770574.

[75] T. F. Robertson and A. Huttenlocher, “Real-time imaging of inflammation and its resolution: It’s apparent because it’s transparent*,” *Immunological Reviews*, vol. 306, no. 1. John Wiley and Sons Inc, pp. 258–270, Mar. 01, 2022. doi: 10.1111/imr.13061.

[76] N. A. Elsayed *et al.*, “6. Glycemic Targets: Standards of Care in Diabetes—2023,” *Diabetes Care*, vol. 46, pp. S97–S110, Jan. 2023, doi: 10.2337/dc23-S006.

[77] F. Mach *et al.*, “2019 ESC/EAS Guidelines for the management of dyslipidaemias: Lipid modification to reduce cardiovascular risk,” *European Heart Journal*, vol. 41, no. 1. Oxford University Press, pp. 111–188, Jan. 01, 2020. doi: 10.1093/eurheartj/ehz455.

[78] A. Konkoth *et al.*, “Multifaceted role of extracellular vesicles in atherosclerosis,” *Atherosclerosis*, vol. 319. Elsevier Ireland Ltd, pp. 121–131, Feb. 01, 2021. doi: 10.1016/j.atherosclerosis.2020.11.006.

[79] X. Loyer, A. C. Vion, A. Tedgui, and C. M. Boulanger, “Microvesicles as cell-cell messengers in cardiovascular diseases,” *Circulation Research*, vol. 114, no. 2. Lippincott Williams and Wilkins, pp. 345–353, 2014. doi: 10.1161/CIRCRESAHA.113.300858.

[80] Z. Ding, N. V. K. Pothineni, A. Goel, T. F. Lüscher, and J. L. Mehta, “PCSK9 and inflammation: Role of shear stress, pro-inflammatory cytokines, and LOX-1,”

Cardiovascular Research, vol. 116, no. 5. Oxford University Press, pp. 908–915, Apr. 01, 2020. doi: 10.1093/cvr/cvz313.

[81] N. Ferri *et al.*, "PCSK9 knock-out mice are protected from neointimal formation in response to perivascular carotid collar placement," *Atherosclerosis*, vol. 253, pp. 214–224, Oct. 2016, doi: 10.1016/j.atherosclerosis.2016.07.910.

[82] L. Badimon, A. Luquero, J. Crespo, E. Peña, and M. Borrell-Pages, "PCSK9 and LRP5 in macrophage lipid internalization and inflammation," *Cardiovasc Res*, vol. 117, no. 9, pp. 2054–2068, Aug. 2021, doi: 10.1093/cvr/cvaa254.

[83] C. Gialeli, A. Shami, and I. Gonçalves, "Extracellular matrix: paving the way to the newest trends in atherosclerosis," *Current opinion in lipidology*, vol. 32, no. 5. NLM (Medline), pp. 277–285, Oct. 01, 2021. doi: 10.1097/MOL.0000000000000775.

[84] Y. Guo *et al.*, "PCSK9 (Proprotein Convertase Subtilisin/Kexin Type 9) Triggers Vascular Smooth Muscle Cell Senescence and Apoptosis: Implication of Its Direct Role in Degenerative Vascular Disease," *Arterioscler Thromb Vasc Biol*, vol. 42, no. 1, pp. 67–86, Jan. 2022, doi: 10.1161/ATVBAHA.121.316902.

[85] Z. Ding *et al.*, "Cross-Talk between LOX-1 and PCSK9 in vascular tissues," *Cardiovasc Res*, vol. 107, no. 4, pp. 556–567, Sep. 2015, doi: 10.1093/cvr/cvv178.

[86] J. Grune *et al.*, "PCSK9 regulates the chemokine receptor CCR2 on monocytes," *Biochem Biophys Res Commun*, vol. 485, no. 2, pp. 312–318, Apr. 2017, doi: 10.1016/j.bbrc.2017.02.085.

[87] N. Ferri *et al.*, "Proprotein convertase subtilisin kexin type 9 (PCSK9) secreted by cultured smooth muscle cells reduces macrophages LDLR levels," *Atherosclerosis*, vol. 220, no. 2, pp. 381–386, Feb. 2012, doi: 10.1016/j.atherosclerosis.2011.11.026.

[88] Y. Zou *et al.*, "Targeting PCSK9 Ameliorates Graft Vascular Disease in Mice by Inhibiting NLRP3 Inflammasome Activation in Vascular Smooth Muscle Cells," *Front Immunol*, vol. 13, May 2022, doi: 10.3389/fimmu.2022.894789.

[89] N. Ferri *et al.*, "PCSK9 knock-out mice are protected from neointimal formation in response to perivascular carotid collar placement," *Atherosclerosis*, vol. 253, pp. 214–224, Oct. 2016, doi: 10.1016/j.atherosclerosis.2016.07.910.

[90] M. G. Lupo *et al.*, "PCSK9 promotes arterial medial calcification," *Atherosclerosis*, vol. 346, pp. 86–97, Apr. 2022, doi: 10.1016/j.atherosclerosis.2022.01.015.

[91] L. J. Schurgers, A. C. Akbulut, D. M. Kaczor, M. Halder, R. R. Koenen, and R. Kramann, "Initiation and Propagation of Vascular Calcification Is Regulated by a Concert of Platelet- and Smooth Muscle Cell-Derived Extracellular Vesicles," *Frontiers in Cardiovascular Medicine*, vol. 5. Frontiers Media S.A., Apr. 06, 2018. doi: 10.3389/fcvm.2018.00036.

[92] M. G. Lupo *et al.*, “Pcsk9 induces rat smooth muscle cell proliferation and counteracts the pleiotropic effects of simvastatin,” *Int J Mol Sci*, vol. 22, no. 8, Apr. 2021, doi: 10.3390/ijms22084114.

[93] E. Punch, J. Klein, P. Diaba-Nuhoho, H. Morawietz, and M. Garelnabi, “Effects of PCSK9 Targeting: Alleviating Oxidation, Inflammation, and Atherosclerosis,” *Journal of the American Heart Association*, vol. 11, no. 3. American Heart Association Inc., Feb. 01, 2022. doi: 10.1161/JAHA.121.023328.

[94] Y. Lu, T. Thavarajah, W. Gu, J. Cai, and Q. Xu, “The Impact of microRNA in Atherosclerosis”, doi: 10.1161/ATVBAHA.

[95] M. A. Gimbrone and G. García-Cardeña, “Endothelial Cell Dysfunction and the Pathobiology of Atherosclerosis,” *Circ Res*, vol. 118, no. 4, pp. 620–636, Feb. 2016, doi: 10.1161/CIRCRESAHA.115.306301.

[96] M. Li, M. Qian, K. Kyler, and J. Xu, “Endothelial–Vascular Smooth Muscle Cells Interactions in Atherosclerosis,” *Frontiers in Cardiovascular Medicine*, vol. 5. Frontiers Media S.A., Oct. 23, 2018. doi: 10.3389/fcvm.2018.00151.

[97] Q. Cai, L. Lanting, and R. Natarajan, “Interaction of monocytes with vascular smooth muscle cells regulates monocyte survival and differentiation through distinct pathways,” *Arterioscler Thromb Vasc Biol*, vol. 24, no. 12, pp. 2263–2270, Dec. 2004, doi: 10.1161/01.ATV.0000146552.16943.5e.

[98] Y. Alexander *et al.*, “Endothelial function in cardiovascular medicine: A consensus paper of the European Society of Cardiology Working Groups on Atherosclerosis and Vascular Biology, Aorta and Peripheral Vascular Diseases, Coronary Pathophysiology and Microcirculation, and Thrombosis,” *Cardiovascular Research*, vol. 117, no. 1. Oxford University Press, pp. 29–42, Jan. 01, 2021. doi: 10.1093/cvr/cvaa085.

[99] R. Ross, “The pathogenesis of atherosclerosis: a perspective for the 1990s,” 1993.

[100] M. Nahrendorf and F. K. Swirski, “Cholesterol, CCR2, and monocyte phenotypes in atherosclerosis,” *Eur Heart J*, vol. 38, no. 20, pp. 1594–1596, May 2017, doi: 10.1093/eurheartj/ehx098.

[101] J. Dutzmann, J. M. Daniel, J. Bauersachs, D. Hilfiker-Kleiner, and D. G. Sedding, “Emerging translational approaches to target STAT3 signalling and its impact on vascular disease,” *Cardiovascular Research*, vol. 106, no. 3. Oxford University Press, pp. 365–374, Jun. 01, 2015. doi: 10.1093/cvr/cvv103.

[102] J. J. Babon *et al.*, “Suppression of Cytokine Signaling by SOCS3: Characterization of the Mode of Inhibition and the Basis of Its Specificity,” *Immunity*, vol. 36, no. 2, pp. 239–250, Feb. 2012, doi: 10.1016/j.immuni.2011.12.015.

[103] E. Punch, J. Klein, P. Diaba-Nuhoho, H. Morawietz, and M. Garelnabi, “Effects of PCSK9 Targeting: Alleviating Oxidation, Inflammation, and Atherosclerosis,” *Journal of the American Heart Association*, vol. 11, no. 3. American Heart Association Inc., Feb. 01, 2022. doi: 10.1161/JAHA.121.023328.

[104] Z. Ding *et al.*, “NLRP3 inflammasome via IL-1β regulates PCSK9 secretion,” *Theranostics*, vol. 10, no. 16, pp. 7100–7110, 2020, doi: 10.7150/thno.45939.

[105] C. Ricci *et al.*, “PCSK9 induces a pro-inflammatory response in macrophages,” *Sci Rep*, vol. 8, no. 1, Dec. 2018, doi: 10.1038/s41598-018-20425-x.

[106] R. I. Jaén *et al.*, “Functional Crosstalk between PCSK9 Internalization and Pro-Inflammatory Activation in Human Macrophages: Role of Reactive Oxygen Species Release,” *Int J Mol Sci*, vol. 23, no. 16, Aug. 2022, doi: 10.3390/ijms23169114.

[107] K. J. Moore *et al.*, “Macrophage Trafficking, Inflammatory Resolution, and Genomics in Atherosclerosis: JACC Macrophage in CVD Series (Part 2),” *Journal of the American College of Cardiology*, vol. 72, no. 18. Elsevier USA, pp. 2181–2197, Oct. 30, 2018. doi: 10.1016/j.jacc.2018.08.2147.

[108] J. Kzhyshkowska, C. Neyen, and S. Gordon, “Role of macrophage scavenger receptors in atherosclerosis,” *Immunobiology*, vol. 217, no. 5, pp. 492–502, May 2012, doi: 10.1016/j.imbio.2012.02.015.

[109] H. Shu, Y. Peng, W. Hang, J. Nie, N. Zhou, and D. W. Wang, “The role of CD36 in cardiovascular disease,” *Cardiovascular Research*, vol. 118, no. 1. Oxford University Press, pp. 115–129, Jan. 01, 2022. doi: 10.1093/cvr/cvaa319.

[110] E. Murphy *et al.*, “Mitochondrial Function, Biology, and Role in Disease: A Scientific Statement from the American Heart Association,” *Circ Res*, vol. 118, no. 12, pp. 1960–1991, Jun. 2016, doi: 10.1161/RES.0000000000000104.

[111] A. Dumont, M. K. Lee, T. Barouillet, A. Murphy, and L. Yvan-Charvet, “Mitochondria orchestrate macrophage effector functions in atherosclerosis,” *Mol Aspects Med*, vol. 77, Feb. 2021, doi: 10.1016/j.mam.2020.100922.

[112] B. Novoa and A. Figueras, “Zebrafish: Model for the study of inflammation and the innate immune response to infectious diseases,” *Adv Exp Med Biol*, vol. 946, pp. 253–275, 2012, doi: 10.1007/978-1-4614-0106-3_15.

[113] M. Li, Q. Liu, J. Lei, X. Wang, X. Chen, and Y. Ding, “MiR-362-3p inhibits the proliferation and migration of vascular smooth muscle cells in atherosclerosis by targeting ADAMTS1,” *Biochem Biophys Res Commun*, vol. 493, no. 1, pp. 270–276, Nov. 2017, doi: 10.1016/j.bbrc.2017.09.031.

[114] B. Yang *et al.*, “MiR-520b inhibits endothelial activation by targeting NF-κB p65-VCAM1 axis,” *Biochem Pharmacol*, vol. 188, Jun. 2021, doi: 10.1016/j.bcp.2021.114540.

[115] P. Li *et al.*, “MicroRNA-638 is highly expressed in human vascular smooth muscle cells and inhibits PDGF-BB-induced cell proliferation and migration through targeting orphan nuclear receptor NOR1,” *Cardiovasc Res*, vol. 99, no. 1, pp. 185–193, Jul. 2013, doi: 10.1093/cvr/cvt082.

[116] Z. H. Tang *et al.*, “New role of PCSK9 in atherosclerotic inflammation promotion involving the TLR4/NF-κB pathway,” *Atherosclerosis*, vol. 262, pp. 113–122, Jul. 2017, doi: 10.1016/j.atherosclerosis.2017.04.023.

[117] S. el Andaloussi, I. Mäger, X. O. Breakefield, and M. J. A. Wood, “Extracellular vesicles: Biology and emerging therapeutic opportunities,” *Nature Reviews Drug Discovery*, vol. 12, no. 5. pp. 347–357, May 2013. doi: 10.1038/nrd3978.

[118] R. Kalluri and V. S. LeBleu, “The biology, function, and biomedical applications of exosomes,” *Science*, vol. 367, no. 6478. American Association for the Advancement of Science, Feb. 07, 2020. doi: 10.1126/science.aau6977.

[119] C. Macchi, N. Ferri, C. R. Sirtori, A. Corsini, M. Banach, and M. Ruscica, “Proprotein Convertase Subtilisin/Kexin Type 9: A View beyond the Canonical Cholesterol-Lowering Impact,” *American Journal of Pathology*, vol. 191, no. 8. Elsevier Inc., pp. 1385–1397, Aug. 01, 2021. doi: 10.1016/j.ajpath.2021.04.016.

[120] R. T. Dadu and C. M. Ballantyne, “Lipid lowering with PCSK9 inhibitors,” *Nature Reviews Cardiology*, vol. 11, no. 10. Nature Publishing Group, pp. 563–575, Jan. 01, 2014. doi: 10.1038/nrcardio.2014.84.

[121] E. Yurtseven, D. Ural, K. Baysal, and L. Tokgözoğlu, “An update on the role of PCSK9 in atherosclerosis,” *Journal of Atherosclerosis and Thrombosis*, vol. 27, no. 9. Japan Atherosclerosis Society, pp. 909–918, 2020. doi: 10.5551/jat.55400.